Partons in phase space

David A. Brown* and Paweł Danielewicz†
National Superconducting Cyclotron Laboratory and Department of Physics and Astronomy, Michigan State University, East Lansing, Michigan 48824

(Received 6 February 1998; published 14 September 1998)

Within QED, we examine several issues related to constructing a parton-model-based QCD transport theory. We rewrite the QED analog of the parton model, the Weizsäcker-Williams approximation, entirely in terms of phase-space quantities and we study the phase-space photon and electron densities created by a classical point charge. We find that the densities take a distinctive ''source-propagator'' form. This form does not arise in a conventional derivation of the semiclassical transport equations because of the overuse of the gradient approximation. We do not apply the gradient approximation and so derive the phase-space analog of the generalized fluctuation-dissipation theorem. Together, this theorem and the expression for the phase-space particle self-energies give a set of coupled phase-space evolution equations. We illustrate how these evolution equations can be used perturbatively or to derive semiclassical transport equations. Our work relies on phase-space propagators and sources, so we describe them in detail when calculating the photon and electron phase-space densities. We use these tools to discuss the shape of a nucleon's parton cloud. [S0556-2821(98)08019-9]

PACS number(s): 24.10.Cn, 12.38.Mh, 25.75.−q

I. INTRODUCTION

Primary hadronic collisions in a typical nuclear reaction at the BNL Relativistic Heavy Ion Collider (RHIC) will occur at $\sqrt{s}\sim 200A$ GeV. Such a collision is so violent that the partons, i.e. the quarks and gluons, comprising the hadrons will become deconfined. With hadronic densities exceeding the inverse volume of a typical hadron, the partons will remain deconfined and are expected to form a quark-gluon plasma (QGP) [1–3]. Since transport theory descriptions of nuclear collisions have proven successful at lower energies, it is natural to attempt to describe the time evolution of the QGP using a transport model derived from QCD. A transport model would describe the time evolution of the parton phase-space[1] densities throughout the collision. The procedures for deriving semiclassical transport equations using time-ordered nonequilibrium methods are well developed [5–9]. In fact, there have been several attempts at constructing a QCD transport model based on these procedures [10–12], but each of them have their problems. Chief among these problems is that one either treats the soft long-range phenomena (in the case of [12]) or one treats the hard short-distance phenomena (in the case of [10]), but never both in the same framework. Normally when one discusses transport, one assumes a separation between the interaction and the kinetic length scales. This assumption allows one to apply the gradient approximation, simplifying the form of transport equations. However, the trade-off of making this approximation is that one throws out the structure of the densities on one length scale in favor of the structure at another length scale. If one relaxes this assumption then one may be able to treat *both* hard and soft modes on equal footing. We have not done this for QCD, but we have made several steps toward doing the analogous thing in QED. Our techniques also allow for a simple connection with the QCD parton model. This paper consists of three parts, each one using QED and the partons of QED (i.e. photons and electrons) to describe different aspects of the problem of constructing a QCD-based partonic transport theory. In the end, we use our accumulated insight to discuss the shape of the parton cloud of a nucleon.

Before outlining the paper, we must say a few words about our formalism. In the first two sections, we use Feynman's formulation of perturbation theory. In Feynman perturbation theory, one specifies the initial and final states of a reaction and calculates the probability of going from the initial to final state. Thus, it is the appropriate tool for calculating observables for simple processes (such as exclusive cross sections). For this reason, we use Feynman perturbation theory to illustrate how the phase-space sources and propagators work and to calculate the reaction probabilities for some simple processes. We show that, in Feynman perturbation theory, the particle phase-space densities have a ''source-propagator'' form. Namely, the densities are a convolution of the probability[2] to create a particle (the source) with the probability to propagate from the creation point to the observation point (the propagator). We are not the first to consider writing transition probabilities in phase-space: Remler [13] discusses simulating many-particle systems in phase-space. Remler's work is not immediately applicable to partons because it only applies to particles with large mass. For more complicated processes, i.e. when we only know the initial conditions, we must resort to time-ordered nonequilibrium methods. In the last two sections we use time-ordered

*Email address: dbrown@nscl.msu.edu
†Email address: danielewicz@nscl.msu.edu

[1]By phase-space, we mean in space, time, momentum and energy (or invariant mass) simultaneously.

[2]Strictly speaking, neither the phase-space sources nor propagators are probabilities as they can be negative. As with any other Wigner transformed quantities, they must be smoothed over small phase-space volumes to render them positive definite.

 © 1998 The American Physical Society

methods to derive the phase-space evolution equations, to derive the generalized fluctuation-dissipation theorem and to discuss the parton distributions of a nucleon. The generalized fluctuation-dissipation theorem shows that, in time-ordered field theory, the particle densities also have a ''source-propagator'' form. It should come as no surprise that we find similar forms for the particle phase-space densities since both formalisms are equivalent descriptions of elementary processes. For simple tree-type processes in the energy-momentum representation, the moduli of the Feynman and retarded (or advanced) single particle propagators are the same, so one can rewrite the reaction probability in terms of either [17]. In fact, both sets of Feynman rules are special cases of the contour Feynman rules in Appendix A.

In the QCD parton model, a cross section is a folding of the parton distribution function (PDF) with the cross section for the partonic subprocess. The QED analog of the parton model is the Weizsäcker-Williams approximation [18,19] since a cross section in the Weizsäcker-Williams approximation is a folding of the effective photon distribution with the cross section for the photon absorption subprocess [14–16]. In Sec. II, we write the Weizsäcker-Williams approximation in phase-space in several steps. First, we write the reaction rate density for our ''partonic subprocess,'' namely the reaction rate for absorbing a free photon. By writing this rate in phase-space, we also illustrate how we do our momentum-space to phase-space conversions. Next, we write the reaction probability for photon exchange in phase-space. Comparing the full reaction probability with the reaction rate density for absorbing a photon, we identify the effective phase-space photon distribution. This photon distribution is the effective photon number density in phase-space and it has the form of a phase-space source folded with a phase-space propagator. We calculate the photon number density surrounding a classical point charge and explain how the photon's phase-space propagator and phase-space source work. Finally, we comment on the implications of this section for the QCD parton model. We will find that we understand how partons propagate and have an idea how to make the gluon distribution gauge invariant, but since our photon source is point-like we do not learn anything about QCD parton sources.

To find the parton distribution functions, one can solve the parton evolution equations or equivalently one can sum up a class of parton ladder diagrams. The simplest parton ladder has one rung corresponding to a single partonic splitting. In Sec. III, we study the QED analog of this process: a virtual photon splitting into a virtual electron and on-shell positron. We start our analysis by generalizing the phase-space Weizsäcker-Williams approximation to include electrons and writing down the effective electron distribution. This effective electron distribution takes the ''source-propagator'' form. While this ''partonic'' splitting leads to a complicated form of the electron source, the shape of the source is mostly determined by the underlying photon (the ''parent parton'') distribution. We calculate the electron distribution explicitly for a classical point charge and discuss how the electron propagates from the source to the observation point. We have another reason for studying electrons: we can discuss a simple case where the ''source-propagator'' picture breaks down. This is the case of two virtual photons colliding to produce an electron positron pair. The ''source-propagator'' picture breaks down because the photon fields interfere on the length scale of the electron-positron creation region. Nevertheless, discussing the process in phase-space gives us insight into the reaction dynamics. Finally, we comment on the implications of the results from this section for QCD parton densities.

In Feynman perturbation theory, both the photon and electron phase-space densities have a ''source-propagator'' form. This form does not usually arise when one uses time-ordered nonequilibrium methods because one usually derives transport theory only after making the gradient approximation. The gradient approximation amounts to ignoring small-scale structure of the particle phase-space densities, resulting in much simpler collision integrals [5,9]. In Sec. IV, we follow essentially the standard semiclassical transport equation derivation, but never make the gradient approximation. Thus, we arrive at the generalized fluctuation-dissipation theorem which codifies the ''source-propagator'' picture of the particle densities. Crucial inputs to the theorem are the phase-space sources; we will discuss how to calculate them. With the sources and the generalized fluctuation-dissipation theorem, we derive a set of phase-space evolution equations. These evolution equations describe the evolution of the system in phase-space from the distant past to the present, including all ''partonic'' splittings, recombinations and scatterings. Furthermore, we can expand these evolution equations to get the lowest order contributions to the particle densities or we can differentiate the evolution equations to get transport equations.

As a practical application of this study, in Sec. V we examine the coordinate space structure of the parton cloud of a nucleon. In principle, one should Wigner transform the quark or gluon wavefunctions of a nucleon. Since we do not know the quark or gluon wavefunctions of a nucleon, such a specification is not possible and we must result to model-building. One might envision constructing a model phase-space parton density of a nucleon by multiplying the momentum space density (the parton distribution function) and the coordinate space density of the partons [21]. This approximation neglects correlations between the momentum and position in the parton density which are present in the phase-space density [22,23]. One might insert these correlations using uncertainty principle based arguments [20,21]. This has intuitive appeal, but such a prescription is *ad hoc* at best. We can approach this problem in a more systematic manner using some physical insight from the momentum-space renormalization-group improved parton model. In this model, one calculates the parton densities by evolving the densities in virtuality (Q^2) and in longitudinal momentum fraction (x). This evolution is equivalent to evaluating a certain class of ladder diagrams and these diagrams can be recast in the form of the phase-space generalized fluctuation-dissipation theorem. Thus, we can discuss the parton phase-space densities of a hadron in the large-Q^2 limit or in the small-x limit. We argue that neither large-Q^2 partons nor small-x partons extend beyond the nucleon bag in the trans-

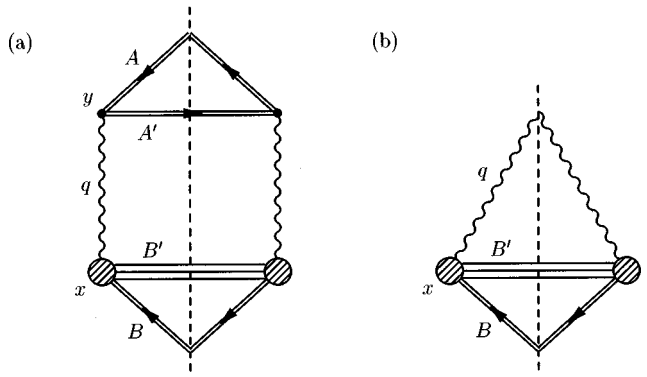

FIG. 1. (a) Cut diagram for current A to exchange a photon with current B. (b) Cut diagram for current B to absorb a free photon. In both figures, the photon/current B interaction is unspecified and is represented with a blob.

verse direction. However, we also argue that the large-Q^2 partons extend out an additional[3] $\hbar c/xP_L$ from the bag surface in the longitudinal direction. This is in line with what others have estimated [20,21]. Furthermore, we estimate that the small-x partons extend at least an additional $\hbar c\sqrt{-q^2}$ from the bag so the small-x parton cloud is substantially larger than the large-Q^2 cloud.

Throughout this paper we use natural units ($\hbar=c=1$) when convenient, but we insert factors of $\hbar c$ whenever directly comparing a length to an inverse momentum. The signature of the metric tensor is $(+,-,-,-)$.

II. THE PHASE-SPACE PHOTON DENSITY

One calculates a QCD parton-model cross-section by folding a parton distribution function (PDF) with the cross section for the partonic subprocess. One follows a similar procedure for calculating the cross-section in the Weizsäcker-Williams approximation [14–16]: one folds the effective photon distribution with the cross section for absorbing the photon [shown in Fig. 1(b)] to obtain the full cross section [shown in Fig. 1(a)]. We recast the Weizsäcker-Williams approximation in phase-space and, in the process, define the phase-space effective photon distribution. This phase-space photon density has the form of a phase-space source convoluted with a phase-space propagator.

Let us outline this section. First we will compute the photon-current B reaction rate in phase-space. This is simply the probability for the probe particle, B, to interact with a free photon. This calculation is simple so we use it to illustrate how we rewrite quantities in phase-space. Second, we will calculate the reaction probability for one-photon exchange. In the Weizsäcker-Williams approximation, the reaction rate is the effective photon distribution folded with the photon-current B reaction rate. So, we can identify the phase-space effective photon distribution. The effective photon distribution is a gauge-independent effective number density of photons. Next, we calculate the phase-space photon density surrounding a classical point charge. This calculation will highlight how the photon source and the propagator function in phase-space. Finally, we conclude this section with a brief discussion of the implications for a phase-space version of the QCD parton model.

In all of our calculations, we find the reaction probability. Mapping our results to cross sections is trivial and is outlined in Appendix B. Since we are finding reaction probabilities, we work in Feynman perturbation theory.

A. Photon-current B reaction rate

We start this subsection by finding the photon-current B reaction rate, $\mathcal{W}_{\gamma \mathrm{B}\to \mathrm{B}'}(x,q)$. This reaction rate plays the role of the ''partonic'' subprocess cross section in a QCD parton model calculation. Our derivation demonstrates how to rewrite the reaction probability completely in terms of phase-space quantities. The high point in this calculation occurs in Eq. (2.1) when we identify the Wigner transforms of B's current and of the photon field. This type of identification lets us rewrite the reaction probabilities in phase-space.

To find $\mathcal{W}_{\gamma \mathrm{B}\to \mathrm{B}'}(x,q)$ we write the S-matrix for the process in Fig. 1(b):

$$S_{\gamma B\to B'} = \int d^4x \langle 0|A^\mu(x)|\vec{q},\lambda\rangle\langle B'|j_\mu(x)|B\rangle = \int d^4x \frac{d^4k}{(2\pi)^4} e^{-ik\cdot x}\langle 0|A^\mu(x)|\vec{q},\lambda\rangle\langle B'|j_\mu(k)|B\rangle.$$

Here $\langle 0|A^\mu(x)|\vec{q},\lambda\rangle=\sqrt{4\pi/2|q_0|V}\epsilon^\mu(\lambda)e^{iq\cdot x}$ is the free photon wave function (with $q^2=0$) and j_μ is the current operator for the probe particle B. We leave both the initial and final states of B unspecified so the final state may be a single particle or several particles [as in Fig. 1(b)].

We now square the S-matrix and average over photon polarizations:

$$|S_{\gamma \mathrm{B}\to \mathrm{B}'}|^2 = \int d^4x d^4x' \frac{d^4k}{(2\pi)^4}\frac{d^4k'}{(2\pi)^4} e^{-i(k\cdot x-k'\cdot x')}\frac{1}{2} \times \sum_{\lambda=\pm}\langle 0|A^\mu(x)|\vec{q},\lambda\rangle\langle\vec{q},\lambda|A^{*\nu}(x')|0\rangle \times\langle B'|j_\mu(k)|B\rangle\langle B|j^\dagger_\nu(k')|B'\rangle.$$

On writing the coordinates and momenta in terms of the relative and average quantities [i.e. $\tilde{k}=k-k'$ and $K=\frac{1}{2}(k+k')$], and taking advantage of the momentum conserving delta functions in the current matrix elements, $|S_{\gamma \mathrm{B}\to \mathrm{B}'}|^2$ becomes

$$|S_{\gamma \mathrm{B}\to \mathrm{B}'}|^2 = \int d^4X d^4\tilde{x}\,\frac{d^4K}{(2\pi)^4}\frac{d^4\tilde{k}}{(2\pi)^4} e^{-i(K\cdot\tilde{x}+\tilde{k}\cdot X)}$$

[3]The nucleon has 4-momentum $P_\mu=(P_0,P_L,\vec{0}_T)$.

$$\times\frac{1}{2}\sum_{\lambda=\pm}\langle 0|A^{\mu}(X+\tilde{x}/2)|\vec{q},\lambda\rangle$$
$$\times\langle\vec{q},\lambda|A^{*\nu}(X-\tilde{x}/2)|0\rangle$$
$$\times\langle B'|j_{\mu}(K+\tilde{k}/2)|B\rangle\langle B|j_{\nu}^{\dagger}(K-\tilde{k}/2)|B'\rangle. \tag{2.1}$$

There are two Wigner transforms in this equation: the Wigner transform of the photon field (the $\tilde{x}$ integral) and the Wigner transform of B's current (the $\tilde{k}$ integral).

Now we rewrite the S-matrix in terms of the phase-space quantities and define the reaction rate density:

$$|S_{\gamma B\to B'}|^2=\int d^4x\,\frac{d^4k}{(2\pi)^4}\,\frac{\pi}{V|q_0|}\sum_{\lambda=\pm}\epsilon_{\mu}(\lambda)\epsilon_{\nu}^{*}(\lambda)$$
$$\times(2\pi)^4\delta^4(q-k)J_{\mathrm{B}}^{\mu\nu}(x,k)$$
$$\equiv\int d^4x\mathcal{W}_{\gamma B\to B'}(x,q). \tag{2.2}$$

We also have defined the Wigner transform of the current:

$$J_{\mathrm{B}}^{\mu\nu}(x,q)\equiv\int\frac{d^4\tilde{q}}{(2\pi)^4}\,e^{-i\tilde{q}\cdot x}\langle B'|j^{\mu}(q+\tilde{q}/2)|B\rangle$$
$$\times\langle B|j^{\dagger\nu}(q-\tilde{q}/2)|B'\rangle. \tag{2.3}$$

Since B's Wigner current is proportional to the reaction rate, it is natural to give them the same physical interpretation: as a ''probability'' density,[4] for absorbing a free photon with momentum q at space-time point x. Now, it may not be clear where the spatial structure of the reaction rate comes from, especially since the incident photon is completely delocalized in space (it is in a momentum eigenstate). To give the reaction rate spatial structure, we must localize either the initial or final states of B with a wavepacket.

B. Photon exchange

In this section, we write the reaction rate for one-photon exchange [see Fig. 1(a)] in phase-space. We do it two different ways: in terms of the Wigner transforms of the currents A and B and the photon propagator and in terms of the Wigner transform of the photon vector potential. The first form of the reaction rate has a clear physical interpretation in terms of photon emission, propagation, and absorption. However, it is the second form which can be brought into the form of a ''partonic'' cross-section.

The S-matrix for Fig. 1(a) is

$$S_{\mathrm{AB}\to\mathrm{A'B'}}=\int d^4xd^4y\langle A'|j^{A\mu}(x)|A\rangle$$
$$D_{\mu\nu}^{\mathrm{c}}(x,y)\langle B'|j^{B\nu}(y)|B\rangle. \tag{2.4}$$

Taking the absolute square of this S-matrix and rewriting it in terms of Wigner transformed currents and propagators, we find

$$|S_{\mathrm{AB}\to\mathrm{A'B'}}|^2=\int d^4yd^4x\,\frac{d^4q}{(2\pi)^4}\,J_{\mathrm{A}}^{\mu\nu}(y,q)$$
$$\times D_{\mu\nu\mu'\nu'}^{\mathrm{c}}(y-x,q)J_{\mathrm{B}}^{\mu'\nu'}(x,q). \tag{2.5}$$

Here, the Wigner transform of the photon propagator is

$$D_{\mu\nu\mu'\nu'}^{\mathrm{c}}(x,q)=\int d^4\tilde{x}e^{i\tilde{x}\cdot q}D_{\mu\nu}^{\mathrm{c}}(x+\tilde{x}/2)$$
$$\times D_{\mu'\nu'}^{\mathrm{c}*}(x-\tilde{x}/2)$$
$$=(4\pi)^2g_{\mu\nu}g_{\mu'\nu'}G^{\mathrm{c}}(x,q)$$

and $G^{\mathrm{c}}(x,q)$ is the Wigner transform of the scalar propagator. We outline the derivation of $G^{c}(x,q)$ in Appendix G. We discuss the Wigner transforms of the propagator and current when we study the photon and electron distributions of a point charge.

Equation (2.5) has an obvious physical meaning: (1) current A makes a photon with momentum q at space-time point y, (2) the photon propagates from y to x with momentum q and (3) current B absorbs the photon at space-time point x. The spatial structure of the integrand of (2.5) can come from localizing either A or B.

Now we take a detour and calculate the Wigner transform of the vector potential of the current A. This detour will lead us to a form of the reaction probability amenable to a parton model-like interpretation. In terms of the current density and propagator, the vector potential is[5] [15]

$$A^{\mu}(x)=\int d^4yD_{\mu\nu}^{c}(x-y)J_{A}^{\nu}(y). \tag{2.6}$$

The Wigner transform of this is

$$A_{\mu\nu}(x,q)=\int d^4\tilde{x}e^{i\tilde{x}\cdot q}A_{\mu}(x+\tilde{x}/2)A_{\nu}^{*}(x-\tilde{x}/2)$$
$$=\int d^4yJ_{\mathrm{A}}^{\mu'\nu'}(y,q)D_{\mu'\nu'\mu\nu}^{\mathrm{c}}(x-y,q). \tag{2.7}$$

The Wigner transform of the vector potential has a ''source-propagator'' form. Current A (the photon source) creates the photon with momentum q at space-time point y and the propagator takes the photon from y to x. Let us put this in Eq. (2.5),

$$|S_{AB\to A'B'}|^2=\int d^4x\,\frac{d^4q}{(2\pi)^4}A_{\mu\nu}(x,q)J_{B}^{\mu\nu}(x,q). \tag{2.8}$$

[4]Because the Wigner current is the Wigner transform of a quantum object, it may not be positive definite [22,23] so it cannot be strictly interpreted as a probability.

[5]Jackson actually uses the retarded propagator to define the vector potential because he discusses classical fields.

Stated this way, the spatial structure of the integrand of this equation comes from either localizing B or from the spatial structure in the Wigner transform of the photon vector potential.

Equation (2.8) is close to the form of a cross section in the QCD parton model because current B is proportional to the photon-current B reaction rate (as discussed in the previous subsection) and the vector potential is proportional to the phase-space effective photon density (as discussed in the next subsection).

C. The Weizsäcker-Williams approximation

The effective photon distribution we derive here is the phase-space analog of Weizsäcker-Williams' effective photon distribution. Thus, it has the interpretation as the number of photons with virtuality q^2 in a unit cell of phase-space. One could use it to calculate the reaction probability in Fig. 1(a) by folding it with the photon-target reaction rate $\mathcal{W}_{\gamma B\to B'}(x,q)$. In QCD parton model terms, we take the parton distribution function (the effective photon distribution) and fold it with the partonic subprocess (the photon-target reaction rate) to get the reaction probability for the entire process.

We will derive the Weizsäcker-Williams approximation in several stages. First we decompose B's Wigner current into photon polarization vectors, allowing us to rewrite $\mathcal{W}_{\gamma B\to B'}(x,q)$ in terms of $J_{\rm B}^{\mu\nu}(x,q)$. Knowing this, we identify the effective photon distribution. In the final subsection we will discuss the gauge independence of our effective photon distribution.

1. Current decomposition

If the photon probing $J_{\rm B}^{\mu\nu}(x,q)$ is sufficiently delocalized in space [i.e. $\partial_\sigma A_{\mu\nu}(x,q)\ll q_\sigma A_{\mu\nu}(x,q)$], the momentum-space cutting rules tell us that we can expand $J_{\rm B}^{\mu\nu}(x,q)$ in terms of the photon polarization vectors [24]:

$$J_{\rm B}^{\mu\nu}(x,q) = \sum_{\lambda=\pm} \epsilon^{\mu}(\lambda)\epsilon^{*\nu}(\lambda) J_{trans}(x,q) + \epsilon^{\mu}(0)\epsilon^{*\nu}(0) J_{scalar}(x,q) + \frac{q^\mu q^\nu}{q^2} J_{long}(x,q). \tag{2.9}$$

Here, $\epsilon_\mu(0)$ is the scalar (i.e. time-like) polarization vector: $\epsilon_\mu(0)=p_{B\mu}-q_\mu q\cdot p_B/q^2$, where p_B is the momentum of B. The transverse polarization vectors, $\epsilon_\mu(\pm)$, span the hyperplane perpendicular to $\epsilon_\mu(0)$ and q_μ. Now, if $A_{\mu\nu}(x,q)$ is not delocalized, then Eq. (2.9) should be modified to include gradients[6] in x. However, if we were to include those gradients here, we may not be able to map $J_{\rm B}^{\mu\nu}(x,q)$ to $\mathcal{W}_{\gamma B\to B'}$.

[6]These gradients come from Wigner transforming terms proportional to the relative photon momentum.

Since $\epsilon^{\mu}(\lambda)\epsilon^{*}_{\mu}(\lambda')=\delta_{\lambda\lambda'}$, it is simple to find the separate currents in (2.9) in terms of $J_{\rm B}^{\mu\nu}(x,q)$:

$$J_{scalar}(x,q)=\epsilon_\mu(0)\epsilon^{*}_{\nu}(0)J_{\rm B}^{\mu\nu}(x,q)$$

and

$$J_{trans}(x,q)=\frac{1}{2}\sum_{\lambda=\pm}\epsilon_\mu(\lambda)\epsilon^{*}_{\nu}(\lambda)J_{\rm B}^{\mu\nu}(x,q).$$

The longitudinal piece, $J_{long}(x,q)$, vanishes due to current conservation.

2. The effective photon distribution

If we insert (2.9) into Eq. (2.5), the reaction probability is a sum of two terms:

$$|S_{\rm AB\to A'B'}|^2 = \int d^4x\,\frac{d^4q}{(2\pi)^4}\,A_{\mu\nu}(x,q) \times\sum_{\lambda=\pm}\epsilon^{\mu}(\lambda)\epsilon^{*\nu}(\lambda)J_{trans}(x,q) + \int d^4x\,\frac{d^4q}{(2\pi)^4}\,A_{\mu\nu}(x,q) \times\epsilon^{\mu}(0)\epsilon^{*\nu}(0)J_{scalar}(x,q). \tag{2.10}$$

The two terms in (2.10) describe transverse and scalar photon exchange between currents A and B, respectively.

Noting that if $J_{trans}(x,q)$ has a weak q^2 dependence,[7] then $J_{trans}(x,q)\propto\mathcal{W}_{\gamma B\to B'}(x,q)$. In other words, $J_{trans}(x,q)$ is proportional to the reaction rate for the ''partonic'' subprocess. Therefore, the transverse term of (2.10) can be written as

$$|S_{\rm AB\to A'B'}|^2=\frac{1}{4\pi}\int d^4x\,\frac{Vd^3q}{(2\pi)^3}\,\frac{dq^2}{2\pi} \times\frac{dn_\gamma(x,q)}{d^3xd^3qdq^2}\,\mathcal{W}_{\gamma B\to B'}(x,q), \tag{2.11}$$

provided we identify the transverse effective photon distribution as[8]

$$\frac{dn_\gamma(x,q)}{d^3xd^3qdq^2}=\sum_{\lambda=\pm}\epsilon^{\mu}(\lambda)\epsilon^{*\nu}(\lambda)A_{\mu\nu}(x,q). \tag{2.12}$$

This effective photon distribution is the spin summed photon Wigner function. In other words, it is the phase-space number density of photons at time x_0 per unit q^2. This effective photon distribution is the QED analog of the phase-space parton distribution function. With Eq. (2.12), we have generalized the Weizsäcker-Williams method to phase-space.

[7]The reader should note here that the reaction rates are for photons with any q^2, while in Sec. II A the reaction rate was for on-shell photons only.

[8]We can make a similar identification with the scalar term.

While classical derivations of the Weizsäcker-Williams method begin with finding the photon power spectra from the Poynting flux [15,14], a quantum mechanical derivation follows along the lines of what we do here [24,16]. Were we to perform the spatial integrals in (2.10), we would find that the exponentials in the Wigner transforms conspire to make several delta functions. The resulting delta function integrations are trivial and we would quickly recover the momentum-space result.

Now, multiplying the photon phase-space density by the projection tensor $\Sigma_{\lambda=\pm}\epsilon^{\mu}(\lambda)\epsilon^{*\nu}(\lambda)$ in (2.12) does *not* render the photon distribution gauge invariant, unlike in momentum space [24], because the photon distribution is not completely delocalized. When $A_{\mu\nu}(x,q)$ undergoes a gauge transformation, terms proportional to q_{μ} are removed but terms proportional to $\partial/\partial x^{\mu}$ are not. A gauge invariant virtual photon distribution is introduced below. This gauge invariant distribution reduces to (2.12) when $A_{\mu\nu}(x,q)$ is sufficiently delocalized.

3. Gauge issues

Parton densities are supposed to be gauge invariant but our effective photon distribution is gauge dependent. In this section, we discuss how $A_{\mu\nu}(x,q)$ transforms under a change of gauge, determine the gauge invariant part of $A_{\mu\nu}(x,q)$, and state how the gauge invariant part of $A_{\mu\nu}(x,q)$ is related to the effective photon phase-space distribution.

In the energy-momentum representation, gauge transforming the photon field adds an arbitrary function in the direction of the photon momentum to the photon vector potential: $A_{\mu}(q)\rightarrow A_{\mu}(q)+q_{\mu}f(q)$. Because components of $A_{\mu}(q)$ in the direction of q_{μ} are gauge dependent, we can write $A_{\mu}(q)$ as a sum of the gauge independent and dependent parts:

$$A_{\mu}(q)=A_{\mu}^{\parallel}(q)+A_{\mu}^{\perp}(q)$$

where $A_{\mu}^{\parallel}(q)=(q_{\mu}q_{\nu}/q^2)A^{\nu}(q)$ is the gauge dependent part of $A_{\mu}(q)$ and $A_{\mu}^{\perp}(q)=A_{\mu}(q)-A_{\mu}^{\parallel}(q)$ is the gauge independent part. Wigner transforming the photon field gives us a term that is gauge independent and terms which are gauge dependent:

$$\begin{aligned}A_{\mu\nu}(x,q)=&\int\frac{d^4\tilde{q}}{(2\pi)^4}\,e^{-ix\cdot\tilde{q}}\\&\times[A_{\mu}^{\parallel}(q+\tilde{q}/2)+A_{\mu}^{\perp}(q+\tilde{q}/2)]\\&\times[A_{\nu}^{\parallel}(q-\tilde{q}/2)+A_{\nu}^{\perp}(q-\tilde{q}/2)]^*\\\equiv&A_{\mu\nu}^{\perp\perp}(x,q)+A_{\mu\nu}^{\perp\parallel}(x,q)\\&+A_{\mu\nu}^{\parallel\perp}(x,q)+A_{\mu\nu}^{\parallel\parallel}(x,q).\end{aligned}\tag{2.13}$$

The only gauge independent piece of $A_{\mu\nu}(x,q)$ is $A_{\mu\nu}^{\perp\perp}(x,q)$. We do the integrals in (2.13) and identify the tensor that projects off the gauge dependent part of $A_{\sigma\rho}(x,q)$:

$$\begin{aligned}A_{\mu\nu}^{\perp\perp}(x,q)&=(g_{\mu\sigma}-h_{\mu\sigma}^{+})(g_{\nu\rho}-h_{\nu\rho}^{-})A^{\sigma\rho}(x,q)\\&\equiv\mathcal{P}_{\mu\nu\sigma\rho}A^{\sigma\rho}(x,q)\end{aligned}\tag{2.14}$$

where

$$h_{\mu\nu}^{\pm}=\frac{(q\pm i\partial/2)_{\mu}(q\pm i\partial/2)_{\nu}}{(q\pm i\partial/2)^2}.\tag{2.15}$$

This projector must be understood as a series in q_{μ} and ∂_{μ}, so can only really be used when $\partial_{\sigma}A_{\mu\nu}(x,q)<q_{\sigma}A_{\mu\nu}(x,q)$. Now, the statement of current conservation for a general $J_{\mu\nu}(x,q)$ is

$$(q\pm i\partial/2)^{\mu}J_{\mu\nu}(x,q)=(q\pm i\partial/2)^{\nu}J_{\mu\nu}(x,q)=0.\tag{2.16}$$

So, as expected, current conservation ensures that only the gauge independent part of $A_{\mu\nu}(x,q)$ appears in the reaction probability.

With $A_{\mu\nu}^{\perp\perp}(x,q)$ in hand, we can postulate the gauge invariant photon distribution:

$$\frac{dn_{\gamma}(x,q)}{d^3xd^3qdq^2}=\sum_{\lambda=\pm}\epsilon^{\mu}(\lambda)\epsilon^{*\nu}(\lambda)A_{\mu\nu}^{\perp\perp}(x,q).\tag{2.17}$$

This reduces to (2.12) if the photon field varies slowly in space [i.e. we neglect the gradients $\partial_{\sigma}A_{\mu\nu}(x,q)\ll q_{\sigma}A_{\mu\nu}(x,q)$], as we now show. Neglecting the derivatives in (2.15), the projection tensor in (2.14) reduces to

$$\begin{aligned}\mathcal{P}_{\mu\nu\sigma\rho}&\approx\left(g_{\mu\sigma}-\frac{q_{\mu}q_{\sigma}}{q^2}\right)\left(g_{\nu\rho}-\frac{q_{\nu}q_{\rho}}{q^2}\right)\\&=\left(\sum_{\lambda=\pm,0}\epsilon_{\mu}(\lambda)\epsilon_{\sigma}^{*}(\lambda)\right)^*\\&\quad\times\left(\sum_{\lambda'=\pm,0}\epsilon_{\nu}(\lambda')\epsilon_{\rho}^{*}(\lambda')\right).\end{aligned}\tag{2.18}$$

Since the polarization vectors form a complete basis in Minkowski space, i.e. $\Sigma_{\lambda=\pm,0}\epsilon_{\mu}(\lambda)\epsilon_{\nu}^{*}(\lambda)+(q_{\mu}q_{\nu}/q^2)=g_{\mu\nu}$. Putting (2.18) in Eq. (2.17), we arrive back at the effective photon distribution in (2.12).

The tactic of projecting out the gauge dependent parts of the photon distribution works mainly because of the simple form of the U(1) gauge transformation. Nevertheless, a variant of this technique may possibly be applied to the gluon field.

D. Photon phase-space density of classical point charge

We now calculate the density for the simple case of a classical point charge radiating photons. If we localize the source's wavepacket and view it on a length scale larger than its localization scale, we can treat its density as a delta function. Thus, the shape of the photon distribution is determined the photon propagation and we can use this calculation to illustrate how partons propagate in phase-space. We explain that, despite our use of Feynman perturbation theory, we can describe photon propagation via the Wigner transform of the

retarded (time-ordered) propagator. As such, the photon propagates a distance of roughly $R_{\|}\sim 1/|q_L|$ in the direction parallel to the photon 3-momentum and $R_{\perp}\sim 1/\sqrt{|q^2|}$ in the direction perpendicular to the photon 3-momentum. We demonstrate this behavior by plotting the coordinate-space distribution of photons with $q^2 \ll q_0^2$ (making the photons collinear with the source) and with $q^2 \sim q_0^2$. In Appendix E we examine the additional case of a static point charge (i.e. $\vec{v}=0$). This case is not relevant for QCD partons since a QCD parton source must be taken in the limit $|\vec{v}|\to c$.

1. Classical current

For our source current, we assume the source particle's wavepacket is localized on the length scales that our photons can resolve so we can replace its current with the current of a point particle (we discuss when this replacement is valid in Appendix D). The source particle follows a classical trajectory $x_\mu = x_0 v_\mu$ with four-velocity $v_\mu = (1, v_L, \vec{0}_T)$, $v_L \approx c$ and $\gamma = 1/(1-v_L^2) \gg 1$. Ignoring the recoil caused by photon emission, the current of the point charge is [15]

$$j_\mu(x) = e v_\mu \delta^3(\vec{x} - x_0 \vec{v}).$$

The Wigner transform of this is the classical Wigner current:

$$J^{\mu\nu}_{\text{classical}}(x,q) = \int d^4\tilde{x} e^{iq\cdot\tilde{x}} j_\mu(x+\tilde{x}/2) j^\dagger_\nu(x-\tilde{x}/2)$$
$$= 2\pi \alpha_{em} v_\mu v_\nu \delta(q\cdot v)\delta^3(\vec{x} - x_0\vec{v}). \tag{2.19}$$

Here $e^2 = \alpha_{em}$ is the QED coupling constant.

The current has several easy to interpret features. The first delta function sets $q\cdot v = 0$. This ensures that the emitted photons are space-like and that current is conserved. It also insures that, when $q^2 \to 0$, the photons become collinear with the emitting particle ($q_0 = v_L q_L \approx q_L$ making $q^2 \approx \vec{q}_T^{\,2} \approx 0$). This delta function arises because we neglect the recoil of the point charge as it emits a photon. The second delta function insures that the source is point-like and follows its classical trajectory.

This source has one other feature of note: it allows for emission of both positive and negative energy photons. In the following work, we consider creating only positive energy photons so we insert a factor of $2\theta(q_0)$ in (2.19). This amounts to constraining the source's initial energy to be greater than its final energy.

2. Retarded propagator

For our phase-space propagator, we take the Wigner transform of the retarded propagator instead of the Wigner transform of the Feynman propagator. This replacement is legal since the reaction probability may be expressed in terms of either propagator, provided one uses the same asymptotic states in both cases. Both propagators will give different particle densities at intermediate stages but the final state particle densities converge as time goes to $\pm\infty$. We use the retarded propagator here because it leads to a more transparent interpretation of the particle densities. We discuss the Feynman propagator in our discussion of the electron distribution of the point charge.

The Wigner transform of the retarded propagator gives the weight for a particle with four-momentum q_μ to propagate across the space-time separation $\Delta x_\mu = x_\mu - y_\mu$. In the Lorentz gauge, the retarded photon propagator, $D^+_{\mu\nu\mu'\nu'}(\Delta x, q)$, is proportional to the retarded scalar propagator $G^+(\Delta x, q)$:

$$D^+_{\mu\nu\mu'\nu'}(\Delta x, q) = g_{\mu\nu} g_{\mu'\nu'} G^+(\Delta x, q). \tag{2.20}$$

The retarded scalar propagator is

$$G^+(\Delta x, q) = \frac{1}{\pi}\theta(\Delta x_0)\,\theta(\Delta x^2)\,\theta(\lambda^2)\frac{\sin(2\sqrt{\lambda^2})}{\sqrt{\lambda^2}}$$

and it is derived in Appendix G. In this expression, the Lorentz invariant λ^2 is $\lambda^2 = (\Delta x\cdot q)^2 - q^2\Delta x^2$.

Let us now estimate how far the retarded propagator can send a particle with the momentum $q_\mu = (q_0, q_L, \vec{0})$. First, the retarded propagator has two theta functions, one that enforces causality and one that forces propagation inside the light cone. The rest of the interesting features of the propagator are tied up in the dependence on λ^2. Since $G^+(\Delta x, q) \propto \theta(\lambda^2)\sin(\sqrt{\lambda^2})/\sqrt{\lambda^2}$, the particle does not propagate much farther than the inequalities $0 \leqslant \sqrt{\lambda^2} \lesssim 1$ allow. To see what these constraints mean, we investigate the $q^2 > 0$, $q^2 < 0$, and $q^2 = 0$ cases separately.

To study the $q^2 > 0$ case, we position ourselves in the frame where $q'_\mu = (q'_0, \vec{0})$. In this frame, the λ^2 constraint translates into a restriction on the spatial distance a particle can propagate:

$$0 \leqslant q_0'^2 \Delta\vec{x}'^2 \lesssim 1.$$

Combined with the light-cone constraint, $\Delta\vec{x}'$ is constrained to

$$|\Delta\vec{x}'| \lesssim \begin{cases} \Delta x'_0 & \text{for small } \Delta x'_0 < 1/|q'_0|, \\ 1/|q'_0| & \text{for large } \Delta x'_0 > 1/|q'_0|. \end{cases} \tag{2.21a}$$

To find a cutoff for $\Delta x'_0$, we realize that, for a given q'_μ, the propagator gives the ''probability'' distribution for propagating across the space-time displacement $\Delta x'_\mu$. Thus, we can integrate $G^+(\Delta x', q')$ over all space and over time up to some cutoff time τ, giving us the total ''probability'' for propagating to time τ. We find that the propagation probability becomes unimportant for $\tau \gtrsim 1/|q'_0|$ and this sets a cutoff in $\Delta x'_0$:

$$\Delta x'_0 \lesssim 1/|q'_0|. \tag{2.21b}$$

Together, these three constraints define the space-time region where the particle can propagate. When we move back to the

frame with $q_\mu=(q_0,q_L,\vec{0}_T)$, the region contracts in the temporal and longitudinal directions. From Eq. (2.21), the limits of the propagation region are

$$|\Delta\vec{x}_T|\lesssim R_\perp=\frac{1}{\sqrt{|q^2|}} \tag{2.22a}$$

$$|\Delta x_L|\lesssim R_\parallel=\frac{1}{|q_L|} \tag{2.22b}$$

$$|\Delta x_0|\lesssim R_0=\frac{1}{|q_0|}. \tag{2.22c}$$

We study the $q^2<0$ case in a similar manner. In the frame with $q'_\mu=(0,q'_L,\vec{0}_T)$, the λ^2 constraint implies

$$0\lesssim q'^2_L(\Delta x'^2_0-\Delta x'^2_T)\lesssim 1.$$

Combining this with the light-cone constraint immediately gives us a limit on $\Delta x'_L$:

$$|\Delta x'_L|\lesssim\frac{1}{|q'_L|}. \tag{2.23a}$$

As with the $q^2>0$ case, we can integrate the propagator to find the total ''probability'' for propagating to the time τ. In this case, the propagation probability is important only for $\tau\lesssim 1/|q'_L|$, giving us a limit in $\Delta x'_0$ of

$$|\Delta x'_0|\lesssim\frac{1}{|q'_L|}. \tag{2.23b}$$

The limit on $|\Delta\vec{x}'_T|$ then follows directly from the light-cone constraint:

$$|\Delta\vec{x}'_T|\lesssim\frac{1}{|q'_L|}. \tag{2.23c}$$

Again, these constraints define a space-time region where the particle can propagate. Boosting back to the frame with $q_\mu=(q_0,q_L,\vec{0}_T)$, again the longitudinal and temporal spread gets Lorentz contracted:

$$|\Delta\vec{x}_T|\lesssim R_\perp=\frac{1}{\sqrt{|q^2|}} \tag{2.24a}$$

$$|\Delta x_L|\lesssim R_\parallel=\frac{1}{|q_0|} \tag{2.24b}$$

$$|\Delta x_0|\lesssim R_0=\frac{1}{|q_L|}. \tag{2.24c}$$

Now we study the $q^2=0$ case. With $q^2=0$, λ^2 becomes

$$\lambda^2=|\Delta x\cdot q|=|q_0||\Delta\vec{x}\cdot\hat{q}-\Delta x_0|\lesssim 1. \tag{2.25}$$

In other words, high energy particles tend to follow their classical path while low energy particles can deviate from their classical path. Expression (2.25) then gives a measure of the deviation from the classical path.

3. Phase-space effective photon distribution

Now we put these elements together into the photon density. We concentrate our efforts on $A_{\mu\nu}(x,q)$ because all of the spatial dependence of the photon distribution is tied up in the Wigner transform of the vector potential. Inserting the classical current and the retarded photon propagator in the Lorentz gauge into (2.7), we find

$$A_{\mu\nu}(x,q)=4\pi\alpha_{em}v_\mu v_\nu\theta(q_0)\,\delta(q\cdot v)\times\int d^4y G^+(x-y,q)\,\delta^3(\vec{y}-y_0\vec{v}). \tag{2.26}$$

The delta function integrals in Eq. (2.26) are trivial, however the remaining proper time integral cannot be done analytically. We find

$$A_{\mu\nu}(x,q)=\frac{(8\pi)^2\alpha_{em}\gamma\theta(q_0)\,\delta(q\cdot v)}{\sqrt{-q^2}}v_\mu v_\nu\mathcal{A}(2|x\cdot q|,2\sqrt{-q^2\gamma^2((x\cdot v)^2-x^2v^2)-(x\cdot q)^2}), \tag{2.27}$$

where the dimensionless function $\mathcal{A}(a,b)$ is given by

$$\mathcal{A}(a,b)=\int_a^\infty d\tau\frac{\sin\,\tau}{\sqrt{b^2+\tau^2}}. \tag{2.28}$$

There are two interesting cases that are easy to explore: that of photons nearly collinear to the source particle (i.e. $q_0\approx q_L\gg|\vec{q}_T|$), and that of photons with a large transverse momentum (i.e. $|\vec{q}_T|\sim q_0,q_L$). Since there is a $1/\sqrt{-q^2}$ singularity in the photon density and nearly on-shell photons (i.e. $q^2\to 0$) are collinear, there will be many more collinear photons than any other kind.

Two plots, representative of collinear photons and high $\vec{q}_T$ photons, are shown in Fig. 2. The left is a plot of the dimensionless function $\mathcal{A}(a,b)$ for collinear photons with $q_\mu=(m_e,m_e/v_L,\vec{0}_T)$. On the right is a plot of photons with transverse momentum comparable to their transverse momentum and energy, $q_\mu=(m_e,m_e/v_L,0.56\ \mathrm{MeV}/c,0)$. The characteristic energy scale of QED is m_e, so we choose this scale for the momenta to plot. In both plots, we chose $v_L=0.9c$ to illustrate the Lorentz contraction of the distribu-

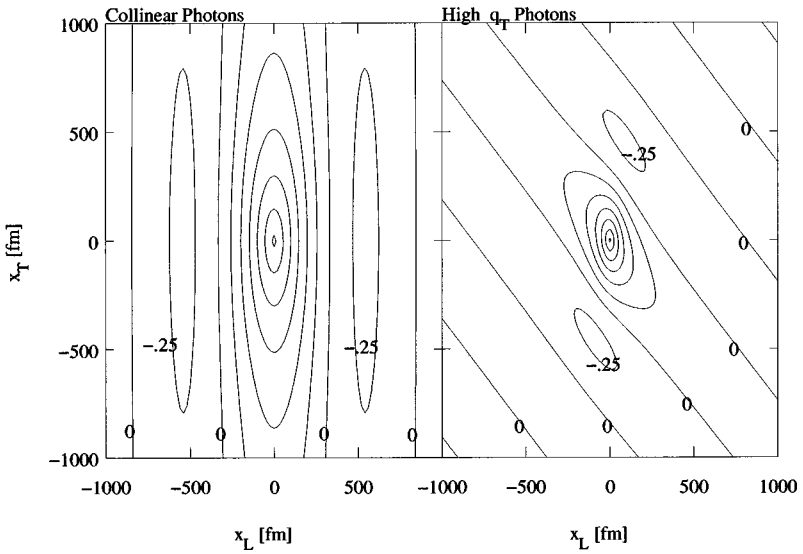

FIG. 2. Both figures are plots of the dimensionless function $\mathcal{A}$ corresponding to the effective photon distribution of a point charge with 3-velocity $\vec{v}=(v_L,\vec{0}_T)$ with $v_L=0.9c$. The photons in these slices of the phase-space distribution have $q_\mu=(m_e,m_e/v_L,\vec{0}_T)$ (left) and $q_\mu=(m_e,m_e/v_L,0.56\ \mathrm{MeV}/c,0)$ (right). In both plots, only the negative and zero contours are labeled. The positive contours increase in increments of 0.25.

tion. The oscillations exhibited by both photon distributions are expected for a Wigner transformed density [22,23]. To obtain an equivalent classical distribution, one should smear this distribution over a unit volume of phase-space.

Both cuts through the photon distribution show Lorentz contraction. For the collinear photons, this contraction occurs in the longitudinal direction. We can account for the contraction with the behavior of the retarded propagator. We expect that the width will be $\sim R_\parallel=\hbar c/|q_0|$ parallel to $\vec{q}$ and $\sim R_\perp=\hbar c/\sqrt{|q^2|}$ perpendicular to $\vec{q}$. For the collinear photons, $\vec{q}$ is in the longitudinal direction and $q_0=\gamma\sqrt{|q^2|}$ so $\sim R_L=\hbar c/\gamma\sqrt{|q^2|}$. In other words, the collinear photon distribution is a ''Lorentz contracted onion'' centered on the moving point source. The inner layers of this ''onion'' correspond to higher $|q^2|$ photons. However, we must emphasize that the contraction is *not* due to the movement of the source, but rather due to kinematics of the photon's creation and the propagation of the photon. To illustrate this point, one only needs to look at the high transverse momentum photons: their distribution is tilted. In the case plotted on the right in Fig. 2, the photon momentum points 45° to the longitudinal direction, coinciding with the tilt of the distribution. Furthermore, the width of the distribution is $\sim R_\parallel=\hbar c/|q_0|$ along this tilted axis and $\sim R_\perp=\hbar c/\sqrt{|q^2|}$ perpendicular to this tilted axis.

4. Comment on the gauge dependence of the effective photon distribution of a point charge

Now, $A_{\mu\nu}(x,q)$ is a gauge dependent object and the physically interesting object, the effective photon distribution, is gauge invariant. One might ask whether the interesting features of $A_{\mu\nu}(x,q)$ disappear under a gauge transform. To see whether this happens, one must insert $A_{\mu\nu}(x,q)$ into Eq. (2.17); the only things in (2.17) that could significantly alter shape of the distribution (2.27) are the gradients. Now because the photon source is extremely localized (it is a delta function), the shape of the photon distribution comes solely from the propagator. Since the propagator varies significantly on length scale comparable to $1/q_\mu$, derivatives of $A_{\mu\nu}(x,q)$ are always comparable in size to q_μ and any expansion of the gauge projector in Eq. (2.14) will not converge. So, we must conclude that our photon distribution cannot be made gauge invariant using this technique and that we cannot tell what features of the photon density survive a general gauge transform. Now, had we *not* used a point source for our photons, the integration over the source could smooth the photon distribution so that it varies slower in space. In that case, our distribution could be rendered gauge invariant.

E. What the photons tell us about QCD partons

QCD parton model cross sections can be written in phase-space as a folding of the phase-space parton distribution function with the reaction rate for the partonic sub-process. The phase-space parton distribution functions are the spatial number density of partons with a certain momentum. The parton distribution functions have a ''source-propagator'' form and can be defined in a gauge invariant manner. If the phase-space parton source produces only positive energy partons or if we use time-ordered field theory then the partons propagate from their source using the Wigner transform of the retarded propagator. This retarded propagator propagates off-shell partons up to roughly $\sim R_\parallel=\hbar c/\min(|q_0|,|\vec{q}|)$ parallel to the parton three-momentum and $\sim R_\perp=\hbar c/\sqrt{|q^2|}$ perpendicular to the parton 3-momentum. Both of these estimates are valid only in frames with $q_0,\vec{q}\neq 0$. When either $q_0=0$ or $\vec{q}=0$, propagation is cut off at

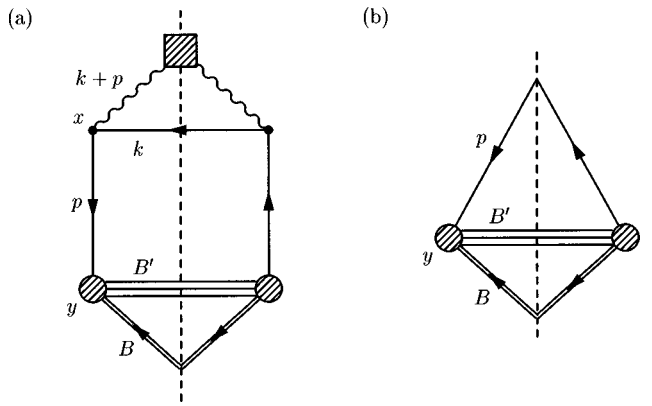

FIG. 3. (a) Cut diagram for creating an electron-positron pair by photon splitting. The electron interacts with the probe particle, B. The square vertex represents the photon source. (b) Cut diagram for a free electron interacting with the probe particle.

$\sim R_{\parallel,\perp}=\hbar c/\sqrt{|q^2|}$. On-shell (i.e. $q^2=0$) partons tend to follow their classical trajectory, with deviations from that trajectory of order $\sim 1/|q_0|$.

Despite what we have learned, we know next to nothing about QCD parton sources in phase-space. We use a point source here while a nucleon has spatial structure on the length scales of interest. Furthermore, QCD partons radiate other partons and this alters the source. We gain more insight into the phase-space sources in the next few sections.

III. PHASE-SPACE ELECTRON DENSITY

In the QCD parton model, the parton distribution functions can be found by summing a class of ladder diagrams and the simplest of these has only one rung, corresponding to a single partonic splitting. One can see the QED analog of the first rung of such a ladder in Fig. 3(a). Probing the electron distribution occurs in three steps: (1) a virtual photon splits into an electron-positron pair with the positron on-shell, (2) the virtual electron propagates from the splitting point toward the probe particle and (3) the electron interacts with the probe. We can give this rate a parton-model like form by associating steps 1 and 2 with the effective electron distribution and step 3 with the electron-probe reaction rate [see Fig. 3(b)].

Let us outline this section. In subsection III A, we demonstrate that the reaction rate for the virtual electron exchange process in Fig. 3(b) factorizes in phase-space, giving the reaction rate a parton model like form. In the process, the electron phase-space density acquires the ''source-propagator'' form. In subsection III B, we calculate the electron distribution of a point charge. The electron source shape is determined mostly by the shape of the parent photon distribution. The electron can equivalently propagate with the retarded or Feynman phase-space propagators. We assume the electrons are massless throughout this section because we only know the form of the propagator for massive particles in the high mass limit ($m_e \gg p_0, |\vec{p}|$). This limit is irrelevant for QCD as $\Lambda_{QCD} \sim m_q \ll p_0, |\vec{p}|$. For completeness, we calculate the electron distribution in the high-mass limit in Appendix F. In subsection III C, we discuss an apparent failure of the ''source-propagator'' picture: lepton pair production in the strong field produced by two point charges. Because the photon fields of the two point charges interfere, it is not possible to clearly isolate the source or probe and we cannot factorize the square S-matrix into an electron distribution and electron-probe interaction. Nevertheless, we can still discuss the process in phase-space, even though we cannot write down the electron distribution. Finally, in subsection III D we discuss the implications of this section. The discussions of splitting, of the massless propagators, and of a failure of factorization are all relevant for QCD partons.

A. Factorization and the effective electron phase-space distribution

First we show that the process in Fig. 3 can be factorized in phase-space, giving a parton model-like form. The S-matrix for the process in Fig. 3(a) is

$$S_{\gamma B\to \bar{e}B'}=\int d^4x d^4y A_\mu(x)\bar{\psi_e}(x,s) \times e\gamma^\mu S^c(x-y)\mathcal{V}_{Be\to B'}(y). \tag{3.1}$$

The spatial structure of the electron source comes from localizing the photon vector potential, $A_\mu(x)$. The spatial structure of the ''partonic'' subprocess comes from $\mathcal{V}_{Be\to B'}(y)$, the electron-probe interaction in Fig. 3(b). In Eq. (3.1), $\bar{\psi_e}(x,s)=\int[d^4k/(2\pi)^4]v(k,s)e^{ik\cdot x}[f^*(k)/\sqrt{2k_0V}]$ is the final positron wavepacket and $S^c(x-y)=\int[d^4p/(2\pi)^4]e^{-ip\cdot(x-y)}[(\not{p}+m_e)/(p^2+m_e^2+i\epsilon)]$ is the electron Feynman propagator.

We square $S_{\gamma B\to \bar{e}B'}$ and write it in terms of phase-space quantities:

$$|S_{\gamma B\to \bar{e}B'}|^2=\alpha_{em}\int d^4x d^4y \frac{d^4p}{(2\pi)^4}\frac{d^4q}{(2\pi)^4}\frac{d^4k}{(2\pi)^4} \times A_{\mu\nu}(x,q)f(x,k)(2\pi)^4\delta^4(k+p-q) \times \mathrm{Tr}\left\{\frac{1}{2}(\not{k}-m)\gamma^\mu S^c(y-x,p) \times \mathcal{V}_{Be\to B'}(y,p)\gamma^\nu\right\}. \tag{3.2}$$

Here, $S^c(y-x,p)$ is the Wigner transform of the electron Feynman propagator and it can be written in terms of the Wigner transform of the scalar Feynman propagator, $G^c(x,q)$:

$$S^c_{\alpha\alpha'\beta\beta'}(x,p) = \int \frac{d^4\tilde{p}}{(2\pi)^4}e^{-i\tilde{p}\cdot x}S^c_{\alpha\beta}(p+\tilde{p}/2)\bar{S}^c_{\alpha'\beta'}(p-\tilde{p}/2) = (\not{p}+i\not{\partial}+m_e)_{\alpha\beta}(\not{p}-i\not{\partial}+m_e)_{\alpha'\beta'}G^c(x,p).$$

Also in Eq. (3.2), $\mathcal{V}_{\mathrm{Be}\to\mathrm{B}'}(y,p)$ is the Wigner transform of the electron-probe interaction and $f(x,k)$ is the phase-space density of final state positrons.

Since the positron rung in Fig. 3 is cut, we sum over the complete set of positron final states by putting the final positron in a momentum eigenstate[9] and summing over the positron final states and spin. Furthermore, we can separate off the spinor structure of the electron propagator and shift the derivatives to act on $\mathcal{V}_{\mathrm{Be}\to\mathrm{B}'}$. In the end we find

$$|S_{\gamma\mathrm{B}\to\bar{e}\mathrm{B}'}|^2=\alpha_{em}\int d^4x d^4y\,\frac{d^4p}{(2\pi)^4}\,\frac{d^4q}{(2\pi)^4}\,\frac{d^3k_f}{2|k_{f0}|(2\pi)^3}$$
$$\times A_{\mu\nu}(x,q)G^c(y-x,p)(2\pi)^4\delta^4(k_f+p-q)$$
$$\times\mathrm{Tr}\left\{\frac{1}{2}(\not{k}_f-m)\gamma^\mu(\not{p}+i\not{\partial}/2+m_e)\right.$$
$$\left.\times\mathcal{V}_{\mathrm{Be}\to\mathrm{B}'}(y,p)(\not{p}-i\not{\partial}/2+m_e)\gamma^\nu\right\}. \tag{3.3}$$

Since $\mathcal{V}_{\mathrm{Be}\to\mathrm{B}'}(y,p)$ is separated from the electron propagator, the reaction probability factorizes. We could explicitly calculate the rate for the ''partonic'' subprocess $eB\to B'$, but we are only interested in the shape of the distribution as a function of electron momentum. We can guess the form of the electron density just by looking at Eq. (3.3), without performing the explicit rate density calculation. The electron density is

$$\frac{dn_{e^-}(y,p)}{d^3y d^3p dp^2}\propto\alpha_{em}\int d^4x G^c(y-x,p)$$
$$\times\int\frac{d^3k}{2|k_0|(2\pi)^3}A_{\mu\nu}(x,k+p)$$
$$\equiv\int d^4x G^c(y-x,p)\Sigma(x,p). \tag{3.4}$$

Here, $G^c(x,p)$ is the Wigner transform of the scalar propagator. Equation (3.4) has the ''source-propagator'' form: the integral of $A_{\mu\nu}(x,k+p)$ over the positron momentum, Σ, plays the role of the ''partonic'' source. Because the emitted positron is in a momentum eigenstate, the spatial structure of the source comes solely from the parent photon's phase-space distribution.

At this stage, we see several important features of the source. First, we note the $d^3k/|k_0|$ in the positron momentum integral. This factor weights positron emission toward small k_0. In a typical QCD parton ladder, ordering momenta to maximize the contribution from this particular singularity leads to the BFKL evolution equations [25,26]. Second, we note that the entire spatial dependence of the electron source comes from the parent photon distribution. These two points are especially important for the partons in Sec. V so they are elaborated on in the next subsection.

B. The effective electron distribution of a classical point charge

Our main interest is with how the ''parton ladder'' (in our case, the source is only one rung of the ladder) shapes the electron distribution. First, we discuss the electron's source and how both the parent photon distribution and the cut positron rung effect it. Second, we discuss the interplay of the electron creation and propagation. Because the electron has positive energy, we can use either the retarded or Feynman phase-space propagator. We choose to use the retarded propagator but, for completeness, we describe the Feynman propagator.

1. The electron source

For our electron source, we choose the photon distribution of Eq. (2.27). This is not a QCD parton-like distribution as the photon source is point-like. Nevertheless, it contains many of the general features that one expects from a QCD parton source. In particular, we discuss the $1/|k_0|$ singularity from the positron rung and we detail both the shape of the source and how this shape depends on the photon distribution.

Up to irrelevant constants, the electron source is

$$\Sigma(x,p)\propto\alpha_{em}\int d^4k\,\theta(-k_0)\,\theta(p_0+k_0)\,\delta(k^2-m_e^2)\,\delta(q\cdot v)\,\frac{\mathcal{A}(a,b)}{\sqrt{-(k+p)^2}} \tag{3.5}$$

where $a=2|x\cdot(k+p)|$ and

$$b=2\sqrt{-(k+p)^2\gamma^2((x\cdot v)^2-x^2v^2)-(x\cdot(k+p))^2}.$$

The longitudinal and temporal positron momentum integrals can be done with the aid of the delta functions, leaving the transverse momentum integrals:

[9]This makes the positron momentum weight-function $f^*(k)\propto\delta^4(k-k_f)$, with $k_f^2=m_e^2$, and the positron phase-space density $f(x,k)=(2V|k_{f0}|)^{-1}(2\pi)^4\delta^4(k-k_f)$.

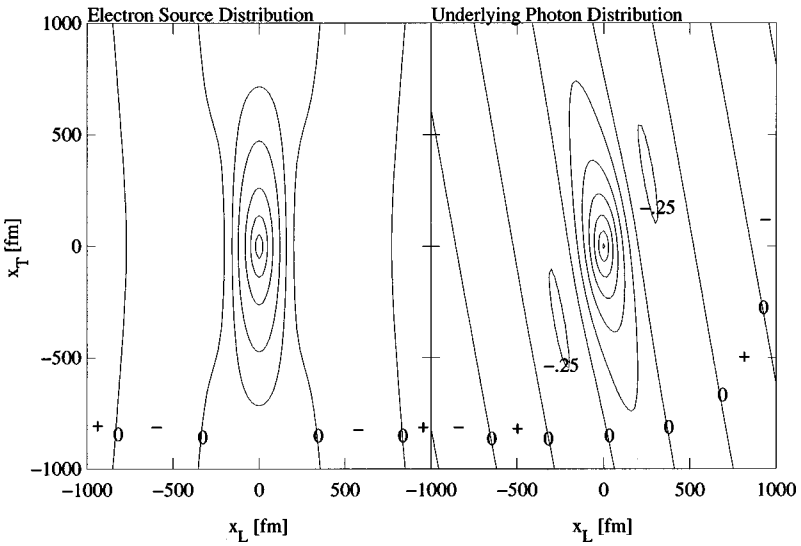

FIG. 4. On the left: the electron source for electrons with momentum $p_\mu=(2.0,2.05,\vec{0}_T)$ MeV/c electrons. In this figure, only the zero contours are labeled. The positive contours are (in arbitrary units) 1.0, 2.5, 5.0, 7.5 and 10.0. On the right: the virtual photon distributions corresponding to one of dominant contributions to electron source. These photons have $\langle q_{+\mu}\rangle=(0.956,1.063,0.045,0.045)$ MeV/c. The other root has similar momentum and a similar distribution. In this figure, only the negative and zero contours are labeled. The positive contours increase in increments of 0.25 (in arbitrary units).

$$\Sigma(x,p)\propto\alpha_{em}\theta(p\cdot v)\int_{|\vec{k}_T|<k_{T\,\max}}\frac{d^2k_T}{\sqrt{k_{T\,\max}^2-k_T^2}}\left\{\frac{\theta(p_0+k_{0+})\mathcal{A}(a_+,b_+)}{\sqrt{-(k_++p)^2}}+\frac{\theta(p_0+k_{0-})\mathcal{A}(a_-,b_-)}{\sqrt{-(k_-+p)^2}}\right\}. \tag{3.6}$$

Here, $k_{T\,\max}^2=\gamma^2(p\cdot v)^2-m_e^2$. The two roots of the positron momentum are given by

$$k_{0\pm}=-\gamma(\gamma p\cdot v\mp v_L\sqrt{k_{T\,\max}^2-\vec{k}_T^2})$$

$$k_{L\pm}=-\gamma(\gamma v_L p\cdot v\mp\sqrt{k_{T\,\max}^2-\vec{k}_T^2}). \tag{3.7}$$

Now, in a QCD parton ladder we expect to find a factor of $d^3k/|k_0|$ for each cut rung. Here is no exception, one can see that $d^4k\,\theta(-k_0)\,\delta(k^2-m_e^2)$ gives us this factor. However, because we neglect the recoil of the source, we have an additional $\delta(q\cdot v)$ and the factor becomes $d^2k/\sqrt{k_{T\,\max}^2-k_T^2}$. Because $|\vec{k}_T|<k_{T\,\max}=\gamma p\cdot v\ll|k_{0\pm}|,|k_{L\pm}|$, this singularity forces the positrons to be anti-collinear with the point charge. Furthermore, because $q^2\approx 0$ (because of the $1/\sqrt{-q^2}$ singularity) the electrons are collinear with the point charge.

As in a QCD parton ladder, the shape of Σ comes from the parent's distribution. In the case at hand, we can actually estimate the $\langle q_\mu\rangle$ that gives the dominant contribution to Σ. Because k_L and k_0 are fixed by the delta functions and $\vec{k}_T$ is bounded by $k_{T\,\max}$, we can estimate the average positron recoil momentum. The average $\vec{k}_T$ is given by $\langle|\vec{k}_T|\rangle\approx(\sqrt{3}/2)k_{T\,\max}$. In general, for $v_L\approx 1$, the average $\langle k_{\mp\mu}\rangle$ is given by

$$\langle k_{\mp\mu}\rangle=\gamma^2(p\cdot v)\left(-1\pm\frac{1}{2},-1\pm\frac{1}{2},\cos(\theta_T)/\gamma,\sin(\theta_T)/\gamma\right).$$

For the purposes of illustration, we choose to emit the positron in the direction $\hat{k}_T\cdot\hat{x}_T=\cos(\theta_T)=1/\sqrt{2}$. By momentum conservation, the dominant photon momentum is $\langle q_{\pm\mu}\rangle=p_\mu+\langle k_{\pm\mu}\rangle$.

On the left in Fig. 4, we plot the electron source for $p_\mu=(2.0,2.05,\vec{0}_T)$ MeV/c electrons from a point charge moving to the right with $v_L=0.9c$. We choose this p_μ because it is both collinear with the point charge and because it is space-like ($p^2<0$). Our source can emit both $p^2>0$ and $p^2\leqslant 0$ electrons, however the typical QCD parton in a parton ladder is either space-like or on-shell. On the right in Fig. 4, we also plot the photon distribution corresponding to the dominant $\langle q_\mu\rangle$. Note that both the source and the photon distribution have approximately the same width in both the longitudinal and transverse directions. The tilt in the photon distribution gets averaged away in the $\vec{k}_T$ integrals in Eq. (3.6).

2. Electron density using the retarded propagator

Now we put elements of the electron distribution together. In Eq. (3.6), we need the Wigner transform of the Feynman propagator. However, since the electrons have positive energy we can replace the Feynman propagator with the retarded propagator. We discuss the retarded propagator in Sec. II D 2 and we describe the phase-space Feynman propagator in the next subsection.

We are interested in electrons that have momenta that are both space-like and collinear with the source (for comparison

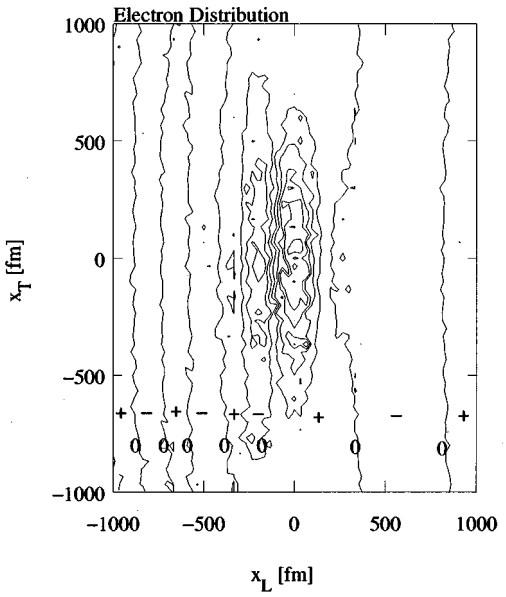

FIG. 5. Coordinate space distribution of $p_\mu=(2.0,2.05,\vec{0})$ MeV/c electrons. Only the negative and zero contours are labeled. The positive contours are in increments of 1.0 (in arbitrary units). The sign of the contours in each region are denoted by $\pm$ signs.

with QCD partons), so we plot the coordinate space distribution of electrons with $p_\mu=(2.0,2.05,\vec{0}_T)$ MeV/c in Fig. 5. The point source is moving to the right with velocity $0.9c$. Both the source and the underlying photon distribution for these electrons are shown in Fig. 4. To perform the four-dimensional spatial integral in Eq. (3.6), we use a Monte Carlo integration scheme [27]. This integration scheme, being probabilistic by nature, returns both the integral at a point and the error on the integral at that point. The nonzero data points never had a relative error greater than 20%, but due to this error, the location of the zero contours is uncertain by ~ 30 fm.

Comparing the electron distribution with the source, we see that the electron distribution is elliptical with longitudinal and transverse widths comparable to what one expects by adding the source width in Fig. 4(a) to our estimates for the propagation length in Eqs. (2.24). Unlike the electron source distribution, the electron distribution is not symmetric about $x_L=0$. This is caused by the positron recoil because, were there no positron recoil, we would have a delta function to insure $p_0=p_L v_L$ (as we found for the photons). Because of the positron recoil, the delta function is widened and the additional spread in energy causes the electron to propagate forward preferentially.

3. The Feynman propagator

Even though we choose situations where we can avoid using the phase-space Feynman propagator, we should describe how it works. While the Feynman propagator propagates a particle with a given momentum [say $p_\mu=(p_0,p_L,\vec{0}_T)$] across a space-time displacement $\Delta x_\mu=(\Delta x_0,\Delta x_L,\Delta\vec{x}_T)$, it does so in a manner very different from the retarded propagator. The Feynman propagator is

$$G^c(\Delta x,p)$$
$$=\frac{1}{4\pi}[\mathrm{sgn}(\Delta x^2)+\mathrm{sgn}(p^2)+2\ \mathrm{sgn}(\Delta x\cdot p)]$$
$$\times\left\{\theta(\lambda^2)\ \frac{\sin(2\sqrt{\lambda^2})}{\sqrt{\lambda^2}}-\theta(-\lambda^2)\ \frac{\exp(-2\sqrt{-\lambda^2})}{\sqrt{-\lambda^2}}\right\}.$$

The combination of the sign functions in the square brackets can be rewritten in a more transparent form:

$$[\cdots]=\begin{cases}4 & \text{if } \Delta x\cdot p,p^2,\Delta x^2>0,\\ -4 & \text{if } \Delta x\cdot p,p^2,\Delta x^2<0,\\ 2\ \mathrm{sgn}(\Delta x\cdot p) & \text{if } p^2,x^2 \text{ have opposite sign.}\end{cases}$$

Thus, particles with time-like momentum tend to travel forward in time and inside the light-cone and particles with space-like momentum tend to travel backwards in time outside the light cone. Also as one might expect, anti-particles with time-like momentum tend to travel backwards in time inside the light-cone and anti-particles with space-like momentum tend to travel forwards in time outside the light-cone.

The rest of the interesting features of the Feynman propagator are tied up in the dependence on the Lorentz invariant $\lambda^2=(\Delta x\cdot p)^2-\Delta x^2p^2$. As with the retarded propagator in subsection II D, we will study the $p^2>0$, $p^2<0$, and $p^2=0$ cases separately.

To study the $p^2>0$ case, we boost to the frame where $p'_\mu=(p'_0,\vec{0})$. In this frame, $\lambda^2=p'^2_0|\Delta\vec{x}'|^2\geqslant 0$, so only the sine term contributes. The sine term is greatest for $\sqrt{\lambda^2}\lesssim 1$ so we have the following limit on the spatial propagation distance:

$$|\Delta\vec{x}'|\lesssim\frac{1}{|p'_0|}. \tag{3.8a}$$

As with the retarded propagator, we can compute the total ''probability'' to propagate to certain time. This calculation gives us the following limit on the temporal propagation distance:

$$|\Delta x_0|\lesssim\frac{1}{|p'_0|}. \tag{3.8b}$$

Boosting the space-time region defined by these constraints back to the frame with $p_\mu=(p_0,p_L,\vec{0}_T)$, we find the following constraints:

$$|\Delta\vec{x}_T|\lesssim R_\perp=\frac{1}{\sqrt{|p^2|}} \tag{3.9a}$$

$$|\Delta x_L|\lesssim R_\parallel=\frac{1}{|p_L|} \tag{3.9b}$$

$$|\Delta x_0|\lesssim R_0=\frac{1}{|p_0|}. \tag{3.9c}$$

These limits are exactly the same as the ones we found for the retarded propagator in subsection II D.

To study the $p<0$ case, we boost to the $p'_\mu=(0,p'_L,\vec{0}_T)$ frame. In this frame, $\lambda^2=p'^2_L(\Delta x'^2_0-\Delta x'^2_T)$. Inside the light-cone, the exponential term disappears and we get a constraint on λ^2:

$$0\geqslant\lambda^2=p'^2_L(\Delta x'^2_0-\Delta x'^2_T)\lesssim 1.$$

We can integrate to find the total ''probability'' to propagate to a certain time, giving us a limit on $\Delta x'_0$:

$$|\Delta x'_0|\lesssim\frac{1}{|p'_L|}. \tag{3.10a}$$

Using the λ^2 and light-cone constraints, we find similar limits on $\Delta\vec{x}'_T$ and $\Delta x'_L$:

$$|\Delta x'_L|\lesssim\frac{1}{|p'_L|} \tag{3.10b}$$

$$|\Delta\vec{x}'_T|\lesssim\frac{1}{|p'_L|}. \tag{3.10c}$$

Boosting back to the $p_\mu=(p_0,p_L,\vec{0}_T)$ frame, we find

$$|\Delta\vec{x}_T|\lesssim R_\perp=\frac{1}{\sqrt{|p^2|}} \tag{3.11a}$$

$$|\Delta x_L|\lesssim R_\parallel=\frac{1}{|p_0|} \tag{3.11b}$$

$$|\Delta x_0|\lesssim R_0=\frac{1}{|p_L|}, \tag{3.11c}$$

which is what we found for the retarded propagator. Now, outside of the light-cone the situation is more complicated and we must integrate the propagator in the various directions to find limits. We find

$$|\Delta x'_0|\lesssim\frac{1}{|p'_L|} \tag{3.12a}$$

$$|\Delta x'_L|\lesssim\frac{1}{|p'_L|} \tag{3.12b}$$

$$|\Delta\vec{x}'_T|\lesssim\frac{1}{|p'_L|}. \tag{3.12c}$$

When we boost back to the frame with $p_\mu=(p_0,p_l,\vec{0}_T)$, we find the result in Eq. (3.11c).

Finally, we investigate the $p^2=0$ case. With $p^2=0$, λ^2 becomes

$$0\lesssim\lambda^2=|\Delta x\cdot p|=|p_0||\Delta\vec{x}\cdot\hat{p}-\Delta x_0|\lesssim 1 \tag{3.13}$$

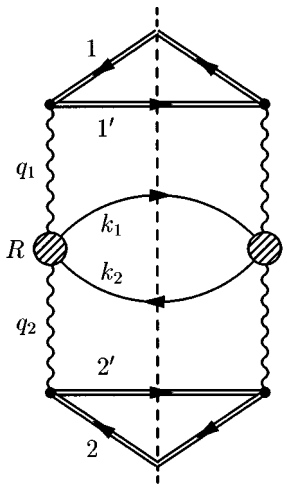

FIG. 6. Cut diagram for lepton pair production from a two photon interaction. R is the space-time point of the center of the collision region.

because the exponential term does not contribute on the light cone. In other words the Feynman propagator functions exactly like the retarded propagator: high energy particles tend to follow their classical path while low energy particles can deviate from their classical path. Expression (3.13) then gives a measure of the deviation from the classical path.

We find that, despite the different boundary conditions on the two propagators, both the Feynman and retarded propagators send particles the same distances. This is probably no surprise since a calculation done using Feynman's formulation of perturbation theory must give the same results as the same calculation done using time-ordered perturbation theory.

C. Failure of factorization and the ''source-propagator'' picture

In this section, we investigate electron-positron pair production in the strong field of two point charges. One might visualize this interaction as a virtual photon from one point charge probing the virtual electron distribution of another point charge. Thus, the electron distribution would appear factorized from the virtual electron-virtual photon collision process. However, we will show that this picture is incorrect because the photon fields interfere with one another on length scales comparable to the size of pair production region. Of course, this also means that our ''source-propagator'' picture fails here. Nevertheless, we can still formulate the problem in phase space and discuss the interplay of the interaction length and particle production length scales.

1. Interference of photon fields

We can write down the S-matrix corresponding to the process in Figs. 6 and 7 using the same procedures used in the previous sections. To lowest order in the coupling strength, we obtain

FIG. 7. The diagrams that contribute, at lowest order, to the $\gamma\gamma\to e\bar{e}$ effective vertex.

$$S_{12\to 1'2'e\bar{e}}=\alpha_{em}\int d^4x_1 d^4x_2\,\frac{d^4k_1}{(2\pi)^4}\frac{d^4k_2}{(2\pi)^4}\frac{d^4p}{(2\pi)^4}\times\frac{f^*(k_1,k_2)}{\sqrt{2k_{1,0}V}\sqrt{2k_{2,0}V}}\times e^{ik_1\cdot x_1+ik_2\cdot x_2+ip\cdot(x_1-x_2)}\Lambda_{\mu\nu}(k_1,s_1,k_2,s_2,p)\times\{A_1^\mu(x_1)A_2^\nu(x_2)+A_2^\mu(x_1)A_1^\nu(x_2)\}. \tag{3.14}$$

Here x_1 and x_2 are the interaction points of the photons and should not be confused with the classical source particles 1 and 2. We have already separated the $\gamma\gamma e\bar{e}$ effective vertex

$$\Lambda_{\mu\nu}(k_1,s_1,k_2,s_2,p)=\bar{u}(k_1,s_1)\gamma_\mu iS^c(p)\gamma_\nu v(k_2,s_2).$$

In $\Lambda_{\mu\nu}(k_1,s_1,k_2,s_2,p)$, $S^c(p)$ is the momentum-space Feynman electron propagator. The final state electron-positron wavepacket is $f^*(k_1,k_2)$ and we will assume the final $e\bar{e}$ pair to be free and use the free wavepacket from Appendix D. The reader should note that we can already see the photons interfering in Eq. (3.14).

As usual, we can rewrite Eq. (3.14) in terms of Wigner transformed quantities. However, due to the photon fields interfering, the structure of the cross terms are complicated. The $|S_{12\to 1'2'e\bar{e}}|^2$ is

$$\begin{aligned}|S_{12\to 1'2'e\bar{e}}|^2&=\alpha_{em}^2\int d^4R d^4r\,\frac{d^4k_1}{(2\pi)^4}\frac{d^4k_2}{(2\pi)^4}\frac{d^4q_1}{(2\pi)^4}\frac{d^4q_2}{(2\pi)^4}\frac{d^4p}{(2\pi)^4}\,f(R-r/2,k_1,R+r/2,k_2)\Lambda_{\mu\mu'\nu\nu'}(k_1,k_2,p,r)(2\pi)^4\delta^4\\&\times(q_1+q_2-k_1-k_2)\Big\{(2\pi)^4\delta^4(q_1-k_1+p)A_1^{\mu\mu'}(R-r/2,q_1)A_2^{\nu\nu'}(R+r/2,q_2)+(2\pi)^4\delta^4(q_1-k_2-p)A_1^{\nu\nu'}\\&\times(R+r/2,q_1)A_2^{\mu\mu'}(R-r/2,q_2)+\int d^4\tilde{r}\,\exp\left[i\tilde{r}\cdot\left(-p+\frac{k_1-k_2}{2}\right)-ir\cdot(q_1-q_2)\right]A_1^{\nu\mu'}(R-\tilde{r}/4,q_1)A_2^{\mu\nu'}(R+\tilde{r}/4,q_2)\\&+\int d^4\tilde{r}\,\exp\left[i\tilde{r}\cdot\left(-p+\frac{k_1-k_2}{2}\right)+ir\cdot(q_1-q_2)\right]A_1^{\mu\nu'}(R+\tilde{r}/4,q_1)A_2^{\nu\mu'}(R-\tilde{r}/4,q_2)\Big\}.\end{aligned} \tag{3.15}$$

This equation could look simpler if, in the interference terms, we Wigner transformed A_1 together with A_2. However then we would have a virtual electron being emitted by some interference field and then reabsorbed by another interference field and the resulting equations would be impossible to interpret using our photon distributions. In Eq. (3.15), we neglect $\tilde{k}$ relative to k in the effective vertex and in the factors of $(2k_0V)$ because the final state wavepackets are sharply peaked in momentum. In Eq. (3.15), R is the center of the interaction points x_1 and x_2 and r is the space-time separation of these points. The final state Wigner density is

$$f(x_1,k_1,x_2,k_2)=\frac{1}{(2k_{1,0}V)}\frac{1}{(2k_{2,0}V)}\int\frac{d^4\tilde{k}_1}{(2\pi)^4}\frac{d^4\tilde{k}_2}{(2\pi)^4}\,e^{-i\tilde{k}_1x_1-i\tilde{k}_2x_2}f^*(k_1+\tilde{k}_1/2,k_2+\tilde{k}_2/2)f(k_1-\tilde{k}_1/2,k_2-\tilde{k}_2/2)$$

and the Wigner transform of the effective vertex is

$$\Lambda_{\mu\mu'\nu\nu'}(k_1,k_2,p,r)=\int\frac{d^4\tilde{p}}{(2\pi)^4}\,e^{i\tilde{p}\cdot r}\Lambda_{\mu\nu}(k_1,k_2,p+\tilde{p}/2)\Lambda^*_{\mu'\nu'}(k_1,k_2,p-\tilde{p}/2).$$

We can write the effective vertex in terms of the scalar Feynman propagator,

$$\begin{aligned}\Lambda_{\mu\mu'\nu\nu'}(k_1,k_2,p,r)&=\bar{u}(k_1,s_1)\gamma_\mu\left(\not{p}+\frac{i}{2}\not{\partial}+m_e\right)\gamma_\nu v(k_2,s_2)\bar{v}(k_2,s_2)\gamma_{\nu'}\left(\not{p}-\frac{i}{2}\not{\partial}+m_e\right)\gamma_{\mu'}u(k_1,s_1)G^c(r,p)\\&\equiv\lambda_{\mu\mu'\nu\nu'}(k_1,k_2,p,r)G^c(r,p).\end{aligned} \tag{3.16}$$

We simplify the reaction probability by summing over the final state electron and positron spins. We simplify things even further by working in the ultrarelativistic limit, namely when $v_1^2\approx v_2^2\approx 0$. Under these approximations, we find

$$|S_{12\to 1'2'e\bar{e}}|^2=\alpha_{em}^2\int d^4Rd^4r\,\frac{d^4k_1}{(2\pi)^4}\frac{d^4k_2}{(2\pi)^4}\frac{d^4q_1}{(2\pi)^4}\frac{d^4q_2}{(2\pi)^4}\frac{d^4p}{(2\pi)^4}\,f(R-r/2,k_1,R+r/2,k_2)\sum_{\text{spins}}\lambda_{\mu\mu'\nu\nu'}(k_1,k_2,p,r)G^c(r,p)$$
$$\times(2\pi)^4\delta^4(q_1+q_2-k_1-k_2)\Big\{(2\pi)^4\delta^4(q_1-k_1+p)A_1^{\mu\mu'}(R-r/2,q_1)A_2^{\nu\nu'}(R+r/2,q_2)+(2\pi)^4\delta^4$$
$$\times(q_1-k_2-p)A_1^{\nu\nu'}(R+r/2,q_1)A_2^{\mu\mu'}(R-r/2,q_2)+2\int d^4\tilde{r}\,\cos\left[\tilde{r}\cdot\left(-p+\frac{k_1-k_2}{2}\right)-r\cdot(q_1-q_2)\right]A_1^{\nu\mu'}$$
$$\times(R-\tilde{r}/4,q_1)A_2^{\mu\nu'}(R+\tilde{r}/4,q_2)\Big\}. \tag{3.17}$$

Given the relatively simple form of this equation, one would think that we could identify the exchanged electron's phase-space density. In fact, if we use free particle distributions for the final state electron and positron and sum over final states, we can identify the virtual electron distribution [Eq. (3.4)] in the direct terms. However, we cannot make the same identification in the interference term and factorization is not possible here. We might find factorization again if we had several point charges as one can envision a situation with many photon sources screening the photons (a plasma for instance). The photon field might then be an incoherent superposition of photon fields. In the absence of photon interference, we might be able to define an effective electron distribution.

2. The $e\bar{e}$ production region vs the interaction region

With Eq. (3.17), we can discuss the various length scales of the problem. First the $e\bar{e}$ production region is set by the shape and size of the photon distributions. Second, the two photon interaction region's size depends on the mass and virtuality of the exchanged electron.

First, take the virtual photon distribution of the classical point charge from Sec. II D. Now, the lowest energy and momentum that each of the interacting photons can have is[10] $q=(m_e,m_e/v_L,\vec{0}_T)$. Because the high energy or far off-shell photons are closer to the point charge then their lower energy and nearly on-shell cousins, photons with the minimum q_μ have the largest distributions. So, the geometrical overlap of the high energy portions of the virtual photon distribution sets the size of the $e\bar{e}$ production region. In Fig. 8 we illustrate this: the two ellipses represent the edge of the photon distribution and the shaded region is the region where the $e\bar{e}$ pairs can be created.

Now, the size of the two photon interaction itself is determined by how far the exchanged electron can travel between the vertices in Fig. 7. For this, we look at the phase-space electron propagator. Assuming massive electrons,[11] we use Remler's causal propagator. Here the phase-space ''probability'' for propagating between two space-time points drops like $e^{-2m_e\tau}$ for space-like electrons and like $\sin 2\tau(\sqrt{p^2}\pm m_e)/(\sqrt{p^2}\pm m_e)$ for time-like electrons. The proper time along the electron 4-momentum is τ. In the direction transverse to the electron four-momentum, the ''probability'' is zero. Thus, the interaction region has a characteristic length scale of $\approx 1/m_e$. This is comparable to the width of the photon distributions, so there is no scale separation. Typically one requires the interaction length scale to be much smaller than the characteristic length scale of the particle density in order to justify the gradient expansions and allow for a transport description. Because our approach does not rely on the gradient expansions, a transport description may still be possible.

D. What the electrons tell us about QCD partons

In this section, we learned several things about the massless QCD parton phase-space densities. First, owing to the fact that the simplest parton ladder contains one rung representing a single partonic splitting, we learned how both the parent parton and cut rung affect the parton distribution. The

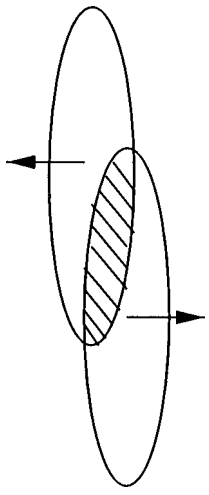

FIG. 8. The ellipses represent the edge of the photon distributions, each with four-momentum $q=(m_e,m_e/v_L,\vec{0}_T)$. The shaded region is the geometrical overlap of the photon distributions and sets the size of the $e\bar{e}$ production region. The arrows point in the direction of the photons' source's 3-momentum.

[10]The distribution of photons with $q=(m_e,m_e/v_L,\vec{0}_T)$ is shown in Fig. 2.

[11]The $m_e=0$ case is uninteresting because the $e\bar{e}$ production region always extends over the two photon interaction region.

shape of the parent parton distribution determines the spatial structure of the parton source. The rung of the parton ladder segment gets cut, putting that parton on shell. The integral over final states of this parton is weighted toward giving it a low k_0. Second, partons propagate to the same distances with the Feynman propagator that we found for the retarded propagator, despite the difference in the boundary conditions of the two propagators. Finally, we learned that the ''source-propagator'' picture of parton densities fails when the source particle and probe particle interact, even through quantum interference. Nevertheless, we can still discuss the process in phase-space with the phase-space sources and propagators, even if the densities have no clear meaning.

IV. QED TRANSPORT THEORY

The ''source-propagator'' picture of particle densities seems both common and physically intuitive. In this section, we see how this picture arises in time-ordered nonequilibrium theory by deriving the generalized fluctuation-dissipation theorem in phase-space. The derivation of this theorem mirrors the steps often used to derive the semiclassical transport equations. Namely, we derive the Kadanoff-Baym equations and formally solve them to get the generalized fluctuation-dissipation theorem. Unlike other derivations of the transport equations, we do not perform the gradient expansion. Instead, we directly Wigner transform the generalized fluctuation-dissipation theorem. If we then insert the Wigner transformed self-energies into the fluctuation-dissipation theorem, we get a set of phase-space evolution equations for the particle densities. These evolution equations describe the complete evolution of the system in phase-space from some time in the distant past to the present, including all parton splittings, recombinations and scatterings. In principle, the equations are nonperturbative, but we can expand them perturbatively. We demonstrate this by recalculating the photon and electron distributions of Secs. II and III. Following this, we derive transport equations from the phase-space evolution equations. Finally, we describe how the results of this section can be applied to QCD parton transport.

For those familiar with the common steps in deriving semiclassical transport equations from the Kadanoff-Baym equations, we suggest skipping past Sec. IV B to Sec. IV C.

A. Green's functions

Our derivations begin with the contour Green's function which we define as

$$iG(x,y)=\langle \tilde{T}\hat{\phi}(x)\hat{\phi}^*(y)\rangle \tag{4.1a}$$

for scalar particles,

$$iD_{\mu\nu}(x,y)=\langle \tilde{T}\hat{A}_\mu(x)\hat{A}_\nu(y)\rangle-\langle \hat{A}_\mu(x)\rangle\langle \hat{A}_\nu(x)\rangle \tag{4.1b}$$

for photons and

$$iS_{\alpha\beta}(x,y)=\langle \tilde{T}\hat{\psi}_\alpha(x)\hat{\bar{\psi}}_\beta(y)\rangle \tag{4.1c}$$

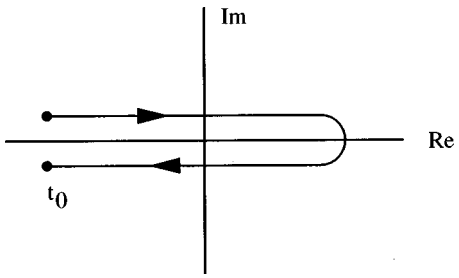

FIG. 9. The contour in the complex time plane used in the evaluation of operator expectation values. The upper branch corresponds to causal ordering and the lower branch to anticausal ordering. The arrows denote the contour ordering enforced by the $\tilde{T}$ operator.

for fermions. The $\langle\cdots\rangle=\mathrm{Tr}(\rho\ldots)/\mathrm{Tr}(\rho)$ is a trace over the system's density matrix, specified at time $t_0\to-\infty$. The field operators are taken in the Heisenberg picture. $\tilde{T}$ denotes ordering along the contour shown in Fig. 9. This ordering can be written as

$$\tilde{T}A(x)B(y)\equiv\theta(x_0,y_0)A(x)B(y)\pm\theta(y_0,x_0)B(y)A(x). \tag{4.2}$$

The upper sign refers to bosons and the lower sign to fermions. The contour theta function is defined as

$$\theta(x_0,y_0)=\begin{cases}1 & \text{if } x_0 \text{ is later on the contour than } y_0\\ 0 & \text{otherwise.}\end{cases}$$

In addition to the contour Green's functions (4.1a)–(4.1c), we define the $>$ and $<$ Green's functions:

$$iG^{>}(x,y)=\langle \hat{\phi}(x)\hat{\phi}^*(y)\rangle \tag{4.3a}$$

$$iD^{>}_{\mu\nu}(x,y)=\langle \hat{A}_\mu(x)\hat{A}_\nu(y)\rangle-\langle \hat{A}_\mu(x)\rangle\langle \hat{A}_\nu(y)\rangle \tag{4.3b}$$

$$iS^{>}_{\alpha\beta}(x,y)=\langle \hat{\psi}_\alpha(x)\hat{\bar{\psi}}_\beta(y)\rangle \tag{4.3c}$$

$$iG^{<}(x,y)=\langle \hat{\phi}^*(y)\hat{\phi}(x)\rangle \tag{4.3d}$$

$$iD^{<}_{\mu\nu}(x,y)=\langle \hat{A}_\nu(y)\hat{A}_\mu(x)\rangle-\langle \hat{A}_\mu(x)\rangle\langle \hat{A}_\nu(y)\rangle \tag{4.3e}$$

$$iS^{<}_{\alpha\beta}(x,y)=-\langle \hat{\bar{\psi}}_\beta(y)\hat{\psi}_\alpha(x)\rangle. \tag{4.3f}$$

These Green's functions are hermitian and contain the complete single-particle information of the system. For example, setting $x=y$ gives us the single particle density matrix. Furthermore, Wigner transforming in the relative coordinate, we find the off-mass shell generalization of the Wigner function for the particles:

$$f(x,p) = iG^<(x,p)$$
$$= \int d^4(x-y) e^{i(x-y)\cdot p} iG^<(x,y)$$
$$= \int d^4(x-y) e^{i(x-y)\cdot p} \langle \hat{\phi}^*(y)\hat{\phi}(x)\rangle .$$

We identify $f(x,p)$ with the number density of particle (or antiparticles) per unit volume in phase-space per unit invariant mass at time x_0:

$$f(x,p) = \frac{dn(x,p)}{d^3x d^3p dp^2}.$$

The off-shell Wigner function is related to the conventional Wigner function, $f_0(x,\vec{p})$, through the invariant mass integration:

$$f_0(x,\vec{p}) = \frac{dn(x_0,\vec{x},\vec{p})}{d^3x d^3p} = \int_{-\infty}^{\infty} dp^2 f(x,p).$$

In terms of the $\gtrless$ Green's functions, the contour Green's function can be written as

$$G(x,y) = \theta(x_0,y_0)G^>(x,y) + \theta(y_0,x_0)G^<(x,y) \quad (4.4)$$

for both fermions and bosons. Furthermore, because of the equal time commutation relations, for both fermions and bosons $G^>(x,y) = G^<(y,x)$ and $G(x,y) = G(y,x)$.

We define several auxiliary Green's functions in terms of the $>$ and $<$ Green's functions: the retarded and advanced Green's functions and the Feynman and anti-Feynman propagators. We write only the equations for the scalar particles. For the retarded and advanced propagators, we have

$$G^{\pm}(x,y) = \pm\,\theta(\pm(x_0-y_0))$$

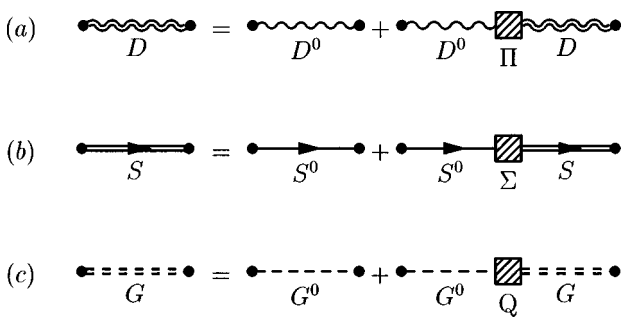

FIG. 10. The Dyson-Schwinger equations of the propagators. Double lines represent the dressed Green's functions and single lines represent the non-interacting Green's functions. The particle self-energies are the large square vertices.

$$(G^>(x,y) - G^<(x,y)). \quad (4.5)$$

For the Feynman and anti-Feynman propagators, we have

$$G^{\mathrm{c}}(x,y) = \theta(x_0-y_0)G^>(x,y) + \theta(y_0-x_0)G^<(x,y), \quad (4.6a)$$

$$G^{\mathrm{a}}(x,y) = \theta(y_0-x_0)G^>(x,y) + \theta(x_0-y_0)G^<(x,y). \quad (4.6b)$$

One can also obtain these Feynman and anti-Feynman propagators by restricting the arguments of the contour propagators to be on one side of the contour in Fig. 9.

B. Conventional transport theory

In this subsection, we follow the standard derivation of the transport equations up to the point where we find the generalized fluctuation-dissipation theorem. The procedure is as follows: (1) find the Dyson-Schwinger equations for the contour Green's functions, (2) apply the free field equations of motion to get the Kadanoff-Baym equations and (3) solve

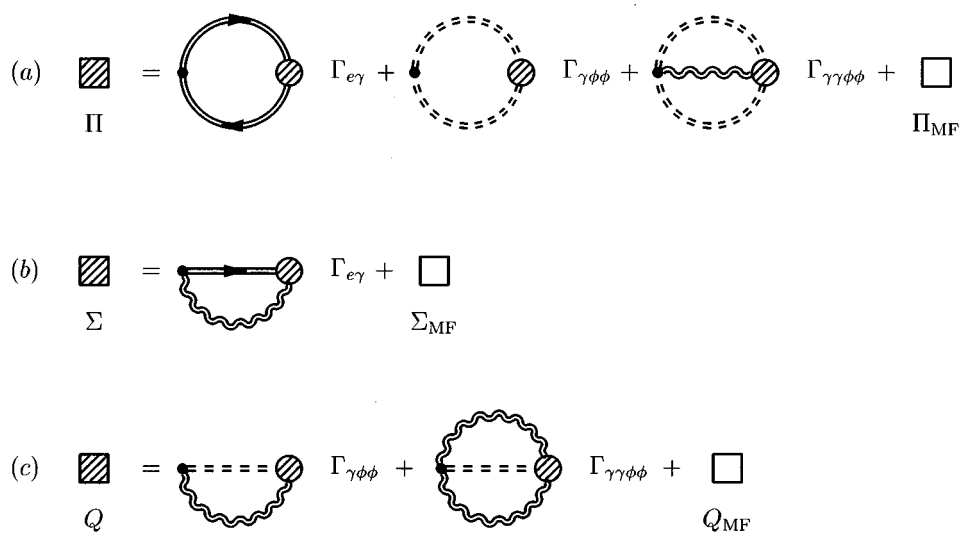

FIG. 11. The scalar and electron self-energies and the photon polarization tensor. Bare vertices are represented by dots and dressed vertices by blobs. The self-energies and the polarization tensor are all represented by large square vertices.

the Kadanoff-Baym equations to get the generalized fluctuation-dissipation theorem.

1. Dyson-Schwinger equations

The Dyson-Schwinger equations encapsulate all of the nonperturbative effects in the field theory that are possible with only two-point functions. We can write the Dyson-Schwinger equations for the photon, electron and scalar contour Green's functions:

$$G(1,1')=G^0(1,1')+\int_{\mathcal{C}} d2d3G^0(1,2)\times Q(2,3)G(3,1') \tag{4.7a}$$

$$D_{\mu\nu}(1,1')=D^0_{\mu\nu}(1,1')+\int_{\mathcal{C}} d2d3D^0_{\mu\mu'}(1,2)\times\Pi^{\mu'\nu'}(2,3)D_{\nu'\nu}(3,1') \tag{4.7b}$$

$$S_{\alpha\beta}(1,1')=S^0_{\alpha\beta}(1,1')+\int_{\mathcal{C}} d2d3S^0_{\alpha\alpha'}(1,2)\times\Sigma^{\alpha'\beta'}(2,3)S_{\beta'\beta}(3,1'). \tag{4.7c}$$

In these equations, we represent the coordinates by their index, i.e. $x_1\rightarrow 1$. We present the corresponding diagrams in Figs. 10(a)–10(c). In Eqs. (4.7a–4.7c), the non-interacting contour Green's functions have a 0 superscript.

The self-energies describe all of the branchings and recombinations possible for the photons, electrons and scalars. The self-energies are

$$Q(1,1')=i(eZ\overleftrightarrow{\partial}^{\mu})\int_{\mathcal{C}} d2d3G(1,3)\Gamma^{\nu}_{\gamma\phi\phi}(2,3,1')D_{\mu\nu}(1,3)+i(2i\alpha_{em}Z^2g^{\mu\nu})\times\int_{\mathcal{C}} d2d3d4G(1,2)\Gamma^{\mu'\nu'}_{\gamma\gamma\phi\phi}(2,3,4,1')D_{\mu\nu'}(1,3)D_{\nu\nu'}(1,4)+Q_{\rm MF}(1)\delta^4(1,1') \tag{4.8a}$$

$$\Pi_{\mu\nu}(1,1')=-i(-ie(\gamma_{\mu})_{\alpha\beta})\int_{\mathcal{C}} d2d3S_{\alpha\alpha'}(1,2)\Gamma^{\alpha'\beta'}_{\gamma e,\nu}(2,3,1')S_{\beta'\beta}(3,1)+i(eZ\overleftrightarrow{\partial}_{\mu})\times\int_{\mathcal{C}} d2d3G(1,2)\Gamma_{\gamma\phi\phi,\nu}(2,3,1')G(3,1)+i(2i\alpha_{em}Z^2g_{\mu\mu'})\times\int_{\mathcal{C}} d2d3d4G(1,2)G(3,1)\Gamma^{\nu'}_{\gamma\gamma\phi\phi,\nu}(2,3,4,1')D_{\mu'\nu'}(1,4)+\Pi_{\rm MF}(1)g_{\mu\nu}\delta^4(1,1') \tag{4.8b}$$

$$\Sigma_{\alpha\beta}(1,1')=i(-ie(\gamma^{\mu})_{\alpha\alpha'})\int_{\mathcal{C}} d2d3S_{\alpha'\beta'}(1,2)\Gamma^{\beta'\beta,\nu}_{\gamma e}(2,3,1')D_{\mu\nu}(1,3)+\Sigma_{\rm MF}(1)\delta_{\alpha\beta}\delta^4(1,1'). \tag{4.8c}$$

In Figs. 11(a)–11(c), we show all the diagrams corresponding to the non-mean-field terms in Eqs. (4.8a)–(4.8c). We define the contour delta function $\delta^4(x,y)$ by

$$\delta^4(x,y)=\begin{cases}\delta^4(x-y) & \text{for } x_0,y_0 \text{ on the upper branch}\\ 0 & \text{for } x_0,y_0 \text{ on different branches}\\ -\delta^4(x-y) & \text{for } x_0,y_0 \text{ on the lower branch.}\end{cases}$$

Finally, there is another set of Dyson-Schwinger equations for the vertex functions. Since we will truncate the vertices at tree level, we will not state the Dyson-Schwinger equations here.

2. Kadanoff-Baym equations

The free-field contour Green's functions satisfy the equations of motion:

$$(\partial_x^2+M^2)G^0(x,y)=\delta^4(x,y) \tag{4.9a}$$

$$\partial_x^2 D^0_{\mu\nu}(x,y)=4\pi g_{\mu\nu}\delta^4(x,y) \tag{4.9b}$$

$$(i\not{\partial}_x-m_e)S^0_{\alpha\beta}(x,y)=\delta_{\alpha\beta}\delta^4(x,y). \tag{4.9c}$$

Combining these with the Dyson-Schwinger equations, we have

$$(\partial_1^2+M^2)G(1,1')=\delta^4(1,1')+\int_{\mathcal{C}}d2Q(1,2)G(2,1') \tag{4.10a}$$

$$\partial_1^2 D_{\mu\nu}(1,1,')=4\pi g_{\mu\nu}\delta^4(1,1') +4\pi\int_{\mathcal{C}}d2\Pi_\mu^{\nu'}(1,2)D_{\nu'\nu}(2,1') \tag{4.10b}$$

$$(i\not\partial_1-m_e)S_{\alpha\beta}(1,1')=\delta_{\alpha\beta}\delta^4(1,1') +\int_{\mathcal{C}}d2\Sigma_{\alpha\beta'}(1,2)S_{\beta',\beta}(2,1'). \tag{4.10c}$$

There is a conjugate set of equations (4.9), (4.10) with the differential operators acting on $1'$.

Restricting t_1 and $t_{1'}$ to lie on different sides of the time contour in Fig. 9, we arrive at the Kadanoff-Baym equations.

$$\begin{aligned}(\partial_1^2+M^2)G^{\gtrless}(1,1') &= \int d^3x_2 Q_{\rm MF}(\vec{x}_1,\vec{x}_2,t_1)G^{\gtrless}(\vec{x}_2,t_1,1') \\ &+\int_{t_0}^{t_1}d2(Q^{>}(1,2)-Q^{<}(1,2))G^{\gtrless}(2,1') \\ &+\int_{t_0}^{t_1'}d2Q^{\gtrless}(1,2)(G^{>}(2,1')-G^{<}(2,1'))\end{aligned} \tag{4.11a}$$

$$\begin{aligned}\frac{1}{4\pi}\partial_1^2 D_{\mu\nu}^{\gtrless}(1,1') &= \int d^3x_2\Pi_{\rm MF}(\vec{x}_1,\vec{x}_2,t_1)D_{\mu\nu}^{\gtrless}(\vec{x}_2,t_1,1') \\ &+\int_{t_0}^{t_1}d2(\Pi_\mu^{>\nu'}(1,2)-\Pi_\mu^{<\nu'}(1,2))D_{\nu'\nu}^{\gtrless}(2,1') \\ &+\int_{t_0}^{t_1'}d2\Pi_\mu^{\gtrless\nu'}(1,2)(D_{\nu'\nu}^{>}(2,1')-D_{\nu'\nu}^{<}(2,1'))\end{aligned} \tag{4.11b}$$

$$\begin{aligned}(i\not\partial_1-m_e)S_{\alpha\beta}^{\gtrless}(1,1') &= \int d^3x_2\Sigma_{\rm MF}(\vec{x}_1,\vec{x}_2,t_1)S_{\alpha\beta}^{\gtrless}(\vec{x}_2,t_1,1') \\ &+\int_{t_0}^{t_1}d2(\Sigma_{\alpha\beta'}^{>}(1,2)-\Sigma_{\alpha\beta'}^{<}(1,2))S_{\beta'\beta}^{\gtrless}(2,1') \\ &+\int_{t_0}^{t_1'}d2\Sigma_{\alpha\beta'}^{\gtrless}(1,2)(S_{\beta'\beta}^{>}(2,1')-S_{\beta'\beta}^{<}(2,1')).\end{aligned} \tag{4.11c}$$

Here the $>$ and $<$ self-energies have the same relation to the contour self-energy that the $>$ and $<$ Green's functions have to the contour Green's functions. Again, there is a set of conjugate equations with the differential operators acting on $1'$.

3. Generalized fluctuation-dissipation theorem

Now we define the retarded and advanced self-energies for scalars:

$$Q^{\pm}(1,2)=Q_{\rm MF}\delta(t_1,t_2)\pm\theta(\pm(t_1-t_2)) \times(Q^{>}(1,2)-Q^{<}(1,2)). \tag{4.12}$$

The photon polarization tensor and electron self-energy are defined in a similar manner.

Using these, we simplify the Kadanoff-Baym equations:

$$(\partial_1^2+M^2)G^{\gtrless}(1,1')=\int_{t_0}^{\infty}d2Q^{+}(1,2)G^{\gtrless}(2,1') \tag{4.13a}$$

$$+\int_{t_0}^{\infty}d2Q^{\gtrless}(1,2)G^{-}(2,1') \tag{4.13b}$$

$$\frac{1}{4\pi}\partial_1^2 D_{\mu\nu}^{\gtrless}(1,1')=\int_{t_0}^{\infty}d2\Pi_\mu^{+\nu'}(1,2)D_{\nu'\nu}^{\gtrless}(2,1') \tag{4.13c}$$

$$+\int_{t_0}^{\infty}d2\Pi_\mu^{\gtrless\nu'}(1,2)D_{\nu'\nu}^{-}(2,1') \tag{4.13d}$$

$$(i\not\partial_1-m_e)S_{\alpha\beta}^{\gtrless}(1,1')=\int_{t_0}^{\infty}d2\Sigma_{\alpha\beta'}^{+}(1,2)S_{\beta'\beta}^{\gtrless}(2,1') \tag{4.13e}$$

$$+\int_{t_0}^{\infty}d2\Sigma_{\alpha\beta'}^{\gtrless}(1,2)S_{\beta'\beta}^{-}(2,1'). \tag{4.13f}$$

If we subtract the $>$ equations from the $<$ equations and multiply the resulting equations by $\pm\theta(\pm(t_1-t_{1'}))$, we get a second set of differential equations:

$$(\partial_1^2+M^2)G^{\pm}(1,1')=\delta^4(1-1')+\int_{t_0}^{\infty}d2Q^{\pm}(1,2)G^{\pm}(2,1') \tag{4.14a}$$

$$\frac{1}{4\pi}\partial_1^2 D_{\mu\nu}^{\pm}(1,1')=\delta^4(1-1')+\int_{t_0}^{\infty}d2\Pi_\mu^{\pm\nu'}(1,2)D_{\nu'\nu}^{\pm}(2,1') \tag{4.14b}$$

$$\begin{aligned}(i\not\partial_1-m_e)S_{\alpha\beta}^{\pm}(1,1') &= \delta^4(1-1')+\int_{t_0}^{\infty}d2\Sigma_{\alpha\beta'}^{\pm}(1,2)S_{\beta'\beta}^{\pm}(2,1').\end{aligned} \tag{4.14c}$$

Solving the initial value problem posed by Eqs. (4.13) using Eqs. (4.14), we find

$$G^{\gtrless}(1,1')$$
$$= \int_{t_0}^{\infty} d2 \int_{t_0}^{\infty} d3 G^{+}(1,2) Q^{\gtrless}(2,3) G^{-}(3,1') + \int d^3x_2 d^3x_3 G^{+}(1,\vec{x}_2,t_0) \times G^{\gtrless}(\vec{x}_2,t_0,\vec{x}_3,t_0) G^{-}(\vec{x}_3,t_0,1') \quad (4.15a)$$

$$D^{\gtrless}_{\mu\nu}(1,1') = \int_{t_0}^{\infty} d2 \int_{t_0}^{\infty} d3 D^{+}_{\mu\mu'}(1,2) \Pi^{\gtrless \mu'\nu'}(2,3) \times D^{-}_{\nu'\nu}(3,1') + \int d^3x_2 d^3x_3 D^{+}_{\mu\mu'}(1,\vec{x}_2,t_0) \times D^{\gtrless \mu'\nu'}(\vec{x}_2,t_0,\vec{x}_3,t_0) D^{-}_{\nu'\nu}(\vec{x}_3,t_0,1') \quad (4.15b)$$

$$S^{\gtrless}_{\alpha\beta}(1,1') = \int_{t_0}^{\infty} d2 \int_{t_0}^{\infty} d3 S^{+}_{\alpha\alpha'}(1,2) \Sigma^{\gtrless}_{\alpha'\beta'}(2,3) S^{-}_{\beta'\beta}(3,1') + \int d^3x_2 d^3x_3 S^{+}_{\alpha\alpha'}(1,\vec{x}_2,t_0) \times S^{\gtrless}_{\alpha'\beta'}(\vec{x}_2,t_0,\vec{x}_3,t_0) S^{-}_{\beta'\beta}(\vec{x}_3,t_0,1'). \quad (4.15c)$$

These equations are the generalized fluctuation-dissipation theorem. They describe the evolution of a density fluctuation (given by the $>$ and $<$ Green's functions) from t_0 to t_1.

C. Phase-space generalized fluctuation-dissipation theorem

We now translate the fluctuation dissipation equations (4.15) into phase-space. We only do so for the scalar equation because the photon and electron equations are similar. First we extend the integration region to cover all time:

$$G^{\gtrless}(x_1,x_{1'}) = \int d^4x_2 d^4x_3 G^{+}(x_1,x_2) Q^{\gtrless}(x_2,x_3) G^{-}(x_3,x_{1'}) + \lim_{t_0 \to -\infty} \int d^4x_2 d^4x_3 \delta(t_0 - x_{20}) \times \delta(t_0 - x_{30}) G^{+}(x_1,x_2) G^{\gtrless}(x_2,x_3) G^{-}(x_3,x_{1'}).$$

Next, we Wigner transform in the relative variable $x_1 - x_{1'}$:

$$G^{\gtrless}(x,p) = \int d^4x' \frac{d^4p'}{(2\pi)^4} \times \tilde{G}^{+}(x,p;x',p') Q^{\gtrless}(x',p') + \lim_{x'_0 \to -\infty} \int d^3x' \frac{d^4p'}{(2\pi)^4} \times \tilde{G}^{+}(x,p;x',p') G^{\gtrless}(x',\vec{p}'). \quad (4.16)$$

We recognize the Wigner transforms of the self-energy and initial particle density:

$$Q^{\gtrless}(x,p) = \int d^4\tilde{x} e^{ip\cdot\tilde{x}} Q^{\gtrless}(x+\tilde{x}/2, x-\tilde{x}/2) \quad (4.17)$$

and

$$\delta(t_0 - x_0) G^{\gtrless}(x,\vec{p}) = \int d^4\tilde{x} e^{ip\cdot\tilde{x}} \delta(t_0 - (x_0 + \tilde{x}_0/2)) \times \delta(t_0 - (x_0 - \tilde{x}_0/2)) \times G^{\gtrless}(x+\tilde{x}/2, x-\tilde{x}/2). \quad (4.18)$$

The delta functions render the initial density independent of p_0. We have also defined the retarded propagator in phase-space:

$$\tilde{G}^{+}(x,p;y,q) = \int d^4x' d^4y' e^{i(p\cdot x' - q\cdot y')} \times G^{+}(x+x'/2, y+y'/2) \times G^{-}(x-x'/2, y-y'/2). \quad (4.19)$$

At this point, one usually applies the gradient approximation to Eq. (4.16), eliminating the d^4x' integral. We do not do this.

Next, we assume the translational invariance of the advanced and retarded propagators. This is reasonable at lowest order in the coupling since the free field advanced and retarded propagators are translationally invariant. Making this approximation, the retarded propagator in phase-space becomes

$$\tilde{G}^{+}(x,p;y,q) = (2\pi)^4 \delta^4(p-q) \int d^4z e^{ip\cdot z} \times G^{+}(x-y+z/2)(G^{+}(x-y-z/2))^* \equiv (2\pi)^4 \delta^4(p-q) G^{+}(x-y,p). \quad (4.20)$$

We will use $G^{+}(x-y,p)$ in all subsequent calculations. In practice, we will only use the lowest order contribution to $G^{+}(x-y,p)$. This means that we dress the $\gtrless$ propagators but not the $\pm$ propagators when we iterate Eq. (4.15). Thus, our particles propagate as though they are in the vacuum. In Appendix G we calculate the lowest order contribution to $G^{+}(x-y,p)$.

Repeating this for the photons and electrons, we arrive at the phase-space generalized fluctuation-dissipation theorem:

$$G^{\gtrless}(x,p) = \int d^4y G^{+}(x-y,p) Q^{\gtrless}(y,p) + \lim_{y_0 \to -\infty} \int d^3y G^{+}(x-y,p) G^{\gtrless}(y,\vec{p}) \quad (4.21a)$$

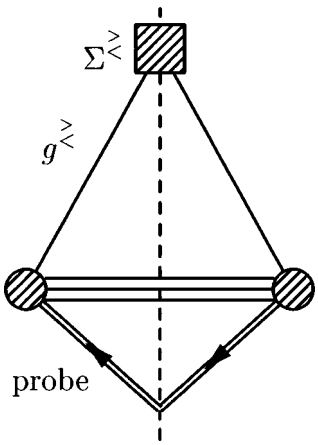

FIG. 12. Cut diagram for probing the particle densities in the generalized fluctuation-dissipation theorem. Time flows downward and, since the the probe interaction is in the future, we leave the nature of the probe unspecified.

$$D^{\gtrless}_{\mu\nu}(x,p)=\int d^4y D^{+}_{\mu\nu\mu'\nu'}(x-y,p)\Pi^{\gtrless\mu'\nu'}(y,p) + \lim_{y_0\to-\infty}\int d^3y D^{+}_{\mu\nu\mu'\nu'}(x-y,p) \times D^{\gtrless\mu'\nu'}(y,\vec{p}) \tag{4.21b}$$

$$S^{\gtrless}_{\alpha\beta}(x,p)=\int d^4y S^{+}_{\alpha\beta\alpha'\beta'}(x-y,p)\Sigma^{\gtrless}_{\alpha'\beta'}(y,p) + \lim_{y_0\to-\infty}\int d^3y S^{+}_{\alpha\beta\alpha'\beta'}(x-y,p) \times S^{\gtrless}_{\alpha'\beta'}(y,\vec{p}). \tag{4.21c}$$

These equations describe the evolution of the particle phase-space densities from $y_0\to-\infty$ to the time x_0, including particle creation and absorption through the particle self-energies. They clearly have the ''source-propagator'' form, but also contain information about the initial particle density. The derivation of these equations does not rely on the form of the self-energies and the general form is shown diagrammatically in Fig. 12. Thus, these equation can be re-applied to QCD. We exploit this fact when we discuss the shape of a nucleon's parton cloud.

D. Phase-space evolution equations

The first step toward getting the phase-space evolution equations from the generalized fluctuation-dissipation theorem is to calculate the self-energies (i.e. the sources). To do this, we insert Eqs. (4.12) and (4.4) into the self-energy equations and keep only the lowest order approximation to the vertex functions. Thus, we assume that the interaction time is much smaller than the other time scales in the problem. So, we arrive at the creation and absorption rates:

$$Q^{\gtrless}(1,1')=i\alpha_{em}Z^2\overleftrightarrow{\partial}_{1\mu}G^{\gtrless}(1,1')\overleftrightarrow{\partial}_{1'\nu}D^{\gtrless\mu\nu}(1,1') + Q^{\gtrless}_{\rm MF}(1)\delta^4(1-1') \tag{4.22a}$$

$$\Pi^{\gtrless}_{\mu\nu}(1,1')=i\alpha_{em}\,{\rm Tr}\{\gamma_\mu S^{\gtrless}(1,1')\gamma_\nu S^{\lessgtr}(1,1')\} + i\alpha_{em}Z^2\overleftrightarrow{\partial}_{1\mu}G^{\gtrless}(1,1')\overleftrightarrow{\partial}_{1'\nu}G^{\lessgtr}(1,1') + \Pi^{\gtrless}_{\rm MF}(1)g_{\mu\nu}\delta^4(1-1') \tag{4.22b}$$

$$\Sigma^{\gtrless}_{\alpha\beta}(1,1')=-i\alpha_{em}(\gamma_\mu)_{\alpha\alpha'}S^{\gtrless}_{\alpha'\beta'}(1,1')(\gamma_\nu)_{\beta'\beta} \times D^{\gtrless\mu\nu}(1,1')+\Sigma^{\gtrless}_{\rm MF}(1)\delta_{\alpha\beta}\delta^4(1-1'). \tag{4.22c}$$

We have neglected the second scalar term in the polarization tensor and the second photon term in the scalar self-energy because they enter with a factor α^2_{em} which is higher order than the other terms we kept.

The self-energies in (4.22) can be Wigner transformed. Taking care to integrate the derivative scalar couplings by parts, we arrive at

$$Q^{\gtrless}(x,p)=i\alpha_{em}Z^2\int\frac{d^4q_1}{(2\pi)^4}\frac{d^4q_2}{(2\pi)^4} \times(q_1+q_2-i\overleftrightarrow{\partial}/2)_\mu G^{\gtrless}(x,q_1) \times(q_1+q_2-i\overleftrightarrow{\partial}/2)_\nu D^{\gtrless\mu\nu}(x,q_2)(2\pi)^4 \times\delta^4(p-(q_1+q_2))+Q^{\gtrless}_{\rm MF}(x) \tag{4.23a}$$

$$\Pi^{\gtrless}_{\mu\nu}(x,p)=i\alpha_{em}\int\frac{d^4q_1}{(2\pi)^4}\frac{d^4q_2}{(2\pi)^4}\,{\rm Tr}\{\gamma_\mu S^{\gtrless}(x,q_1)\gamma_\nu \times S^{\gtrless}(x,q_2)\}(2\pi)^4\delta^4(p-(q_1+q_2)) + i\alpha_{em}Z^2\int\frac{d^4q_1}{(2\pi)^4}\frac{d^4q_2}{(2\pi)^4} \times(q_1+q_2+\overleftrightarrow{\partial}/2)_\mu \times G^{\gtrless}(x,q_1)(q_1+q_2+i\overleftrightarrow{\partial}/2)_\nu \times G^{\gtrless}(x,q_2)(2\pi)^4\delta^4(p-(q_1+q_2)) + \Pi^{\gtrless}_{\rm MF}(x)g_{\mu\nu} \tag{4.23b}$$

$$\Sigma^{\gtrless}_{\alpha\beta}(x,p)=-i\alpha_{em}(\gamma_\mu)_{\alpha\alpha'}\int\frac{d^4q_1}{(2\pi)^4}\frac{d^4q_2}{(2\pi)^4} \times S^{\gtrless}_{\alpha'\beta'}(x,q_1)(\gamma_\nu)_{\beta'\beta}D^{\gtrless\mu\nu}(x,q_2) \times(2\pi)^4\delta^4(p-(q_1+q_2))+\Sigma^{\gtrless}_{\rm MF}(x)\,\delta_{\alpha\beta}. \tag{4.23c}$$

We can rewrite these equations directly in terms of the particle and antiparticle densities[12] to make their structure explicit. In accordance with Eqs. (4.3a)–(4.3f), we define the particle densities as follows:

[12]Also known as the particle and anti-particle Wigner functions.

$$iG^{\gtrless}(x,p)=g^{\gtrless}(x,p)=\text{scalar densities} \quad (4.24a)$$

$$iD^{\gtrless}_{\mu\nu}(x,p)=d^{\gtrless}_{\mu\nu}(x,p)=\text{photon densities} \quad (4.24b)$$

$$\pm iS^{\gtrless}_{\alpha\beta}(x,p)=s^{\gtrless}_{\alpha\beta}(x,p)=\text{lepton densities.} \quad (4.24c)$$

Here the positive energy part of the $>$ Green's functions correspond to the density for emission of $(|p_0|,\vec{p})$ quanta, while the negative energy part corresponds to the density for absorption of $(-|p_0|,\vec{p})$ quanta. Similarly the positive energy part of the $<$ Green's functions correspond to absorbing $(|p_0|,\vec{p})$ quanta and the negative energy part to emission of $(-|p_0|,\vec{p})$ quanta. Thus, $\theta(p_0)g^{<}(x,p)$ is the scalar density and $\theta(-p_0)g^{>}(x,p)$ is the antiscalar density. We can make similar identifications for the photon[13] and lepton densities.

Now, combining (4.21) and (4.23) and inserting the particle densities, we arrive at

$$\begin{aligned} g^{\gtrless}(x,p)=&\int d^4y\,\frac{d^4q_1}{(2\pi)^4}\,\frac{d^4q_2}{(2\pi)^4}\,G^{+}(x-y,p)(2\pi)^4\\ &\times\delta^4(p-(q_1+q_2))\,\alpha_{em}Z^2(q_1+q_2-i\overleftrightarrow{\partial}/2)^{\mu}\\ &\times g^{\gtrless}(y,q_1)(q_1+q_2-i\overleftrightarrow{\partial}/2)^{\nu}d^{\gtrless}_{\mu\nu}(y,q_2)\\ &+\int d^4y G^{+}(x-y,p)iQ^{\gtrless}_{\rm MF}(y)\\ &+\lim_{y_0\to-\infty}\int d^3y G^{+}(x-y,p)g^{\gtrless}(y,\vec{p}) \end{aligned} \quad (4.25a)$$

$$\begin{aligned} d^{\gtrless}_{\mu\nu}(x,p)=&\int d^4y\,\frac{d^4q_1}{(2\pi)^4}\,\frac{d^4q_2}{(2\pi)^4}\,D^{+}_{\mu\nu\mu'\nu'}(x-y,p)\\ &\times(2\pi)^4\delta^4(p-(q_1+q_2))\\ &\times\{\alpha_{em}\,\mathrm{Tr}[\gamma^{\mu'}s^{\gtrless}(y,q_1)\gamma^{\nu'}s^{\gtrless}(y,q_2)]\\ &+\alpha_{em}Z^2(q_1+q_2+i\overleftrightarrow{\partial}/2)^{\mu'}g^{\gtrless}(y,q_1)\\ &\times(q_1+q_2+i\overleftrightarrow{\partial}/2)^{\nu'}g^{\gtrless}(y,q_2)\}\\ &+\int d^4yD^{+}_{\mu\nu\mu'\nu'}(x-y,p)i\Pi^{\gtrless}_{\rm MF}(y)g^{\mu'\nu'}\\ &+\lim_{y_0\to-\infty}\int d^3yD^{+}_{\mu\nu\mu'\nu'}(x-y,p)d^{\gtrless\mu'\nu'}(y,\vec{p}) \end{aligned} \quad (4.25b)$$

$$\begin{aligned} s^{\gtrless}_{\alpha\beta}(x,p)=&\int d^4y\,\frac{d^4q_1}{(2\pi)^4}\,\frac{d^4q_2}{(2\pi)^4}\,S^{+}_{\alpha\beta\alpha'\beta'}(x-y,p)\\ &\times(2\pi)^4\delta^4(p-(q_1+q_2))\,\alpha_{em}(\gamma^{\mu})_{\alpha'\alpha''}\\ &\times s^{\gtrless}_{\alpha''\beta''}(y,q_1)(\gamma^{\nu})_{\beta''\beta'}d^{\gtrless}_{\mu\nu}(y,q_2)\\ &+\int d^4yS^{+}_{\alpha\beta\alpha'\beta'}(x-y,p)(\pm i\Sigma^{\gtrless}_{\rm MF}(y))\,\delta_{\alpha'\beta'}\\ &+\lim_{y_0\to-\infty}\int d^3yS^{+}_{\alpha\beta\alpha'\beta'}(x-y,p)s^{\gtrless}_{\alpha'\beta'}(y,\vec{p}). \end{aligned} \quad (4.25c)$$

These equations are the most important result of this section. They simultaneously describe all ''partonic'' splittings, recombinations and scatterings from the distant past to the present. Note that an implementation of these equations would be very different from the conventional transport approach. First, these splittings and recombinations occur in all cells of coordinate-space. This is very different from the conventional approach where particles interact only when they are within $\sqrt{\sigma_{TOT}}$ of each other [28,21,7]. Second, the particles in our approach do not follow straight-like trajectories. Instead, they have a ''probability'' distribution for propagating to a certain point.

Equations (4.25) are the phase-space QED analog of Makhlin's evolution equations [29]. A QCD version of the phase-space evolution equations should reduce to Makhlin's equations when integrating out the coordinate dependence. Geiger [10] has derived a set of QCD transport equations based on Makhlin's work. While his derivation is very similar to our derivation of the phase-space evolution equation, he does use the gradient approximation to simplify his collision integrals. The QCD version of the transport equations we derive in Sec. IV F would reduce to his semiclassical equations if one applies this approximation.

There are several ways to solve Eq. (4.25) but we propose only two methods in the following subsections. The first method is a perturbative scheme which we will use to derive the time-ordered version of the results of Secs. II–III. The second method is to derive transport equations from Eq. (4.25).

E. Perturbative solution to the phase-space evolution equations

We can perform a perturbative expansion on Eqs. (4.25) and get the leading contributions to the particle densities. We show this for both the photons and electrons surrounding a classical (scalar) point charge.

We begin by stating the initial conditions[14] for the particle densities and listing the other assumptions used here. The initial electron and photon densities (at $y_0\to-\infty$) are $s^{\gtrless}_{\alpha\beta}(-\infty,\vec{y},\vec{p})=d^{\gtrless}_{\mu\nu}(-\infty,\vec{y},\vec{p})=0$. We also take the initial scalar densities to be $g^{>}(-\infty,\vec{y},\vec{p})=0$ and $g^{<}(y_0,\vec{y},\vec{p})=\mathcal{N}\theta(p_0)\,\delta^3(\vec{p}-\vec{p_i})\,\delta(p^2-M^2)\,\delta^3(x_0\vec{p}/p_0-\vec{x})$. To get this form for $g^{<}$, we localize the initial scalar wavepacket in momentum as discussed in Appendix C 3. In addition to as-

[13]The $d^{<}_{\mu\nu}(x,p)$ in this section is the Wigner transform of the vector potential, $A_{\mu\nu}(x,q)$, of Sec. II, as we demonstrate in subsection IV E.

[14]Unlike Feynman perturbation theory, we can only specify the initial particle densities here.

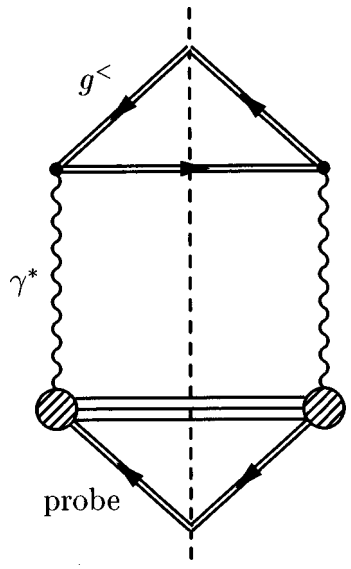

FIG. 13. Cut diagram for the time-ordered (nonequilibrium) photon density. Time flows downward and, since the probe interaction is in the future, we leave the nature of the probe unspecified.

suming these densities, we must also neglect the mean field and drop the gradients in the scalar-photon coupling.

1. Photons

Since the scalar field only couples to the photons, the lowest order contribution to the photon density comes from the photons directly coupling to the initial scalar density. The cut diagram for this process is in Fig. 13. For positive energy photons, the density is

$$d^<_{\mu\nu}(x,p)=\int d^4y\,\frac{d^4q_1}{(2\pi)^4}\frac{d^4q_2}{(2\pi)^4}\,D^+_{\mu\nu\mu'\nu'}(x-y,p)\times(2\pi)^4\delta^4(p-(q_1+q_2))\alpha_{em}Z^2(q_1+q_2)^{\mu'}\times g^<(y,q_1)(q_1+q_2)^{\nu'}g^<(y,q_2).$$

Now, $G^>(x,p)=G^<(x,-p)$ because $\gtrless$ propagators obey the relation $G^>(x,y)=G^<(y,x)$. Thus, we can switch one of the $g^<(y,q)$ to $g^>(y,-q)$, changing it from an initial state antiscalar to a final state scalar. Doing so, we have

$$d^<_{\mu\nu}(x,p)=\int d^4y\,\frac{d^4q_1}{(2\pi)^4}\frac{d^4q_2}{(2\pi)^4}\,D^+_{\mu\nu\mu'\nu'}(x-y,p)\times(2\pi)^4\delta^4(p-(q_1-q_2))\alpha_{em}Z^2(q_1-q_2)^{\mu'}\times g^<(y,q_1)(q_1-q_2)^{\nu'}g^>(y,q_2). \tag{4.26}$$

Now we can bring $\alpha_{em}Z^2(q_1-q_2)^{\mu'}g^<(y,q_1)(q_1-q_2)^{\nu'}g^>(y,q_2)$ into the form of the Wigner transform of the scalar current. To do this, we take the final state scalar to be free and sum over all possible final momentum.[15] Doing so, Eq. (4.26) becomes

[15]We perform this calculation in detail in Appendix D.

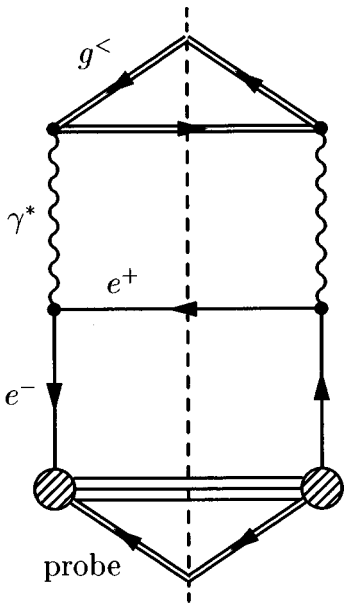

FIG. 14. Cut diagram for the time-ordered (nonequilibrium) electron density. Time flows downward and, since the the probe interaction is in the future, we leave the nature of the probe unspecified.

$$d^<_{\mu\nu}(x,p)=\int d^4y D^+_{\mu\nu\mu'\nu'}(x-y,p)\times J^{\mu'\nu'}_{\text{classical}}(y,p).$$

Thus, $d^<_{\mu\nu}(x,p)$ can be identified with the $A_{\mu\nu}(x,p)$ in Eq. (2.7).

2. Electrons

Since the electrons only couple to the photons, the lowest order contribution to the electron density comes from a photon splitting into electron-positron pairs. The cut diagram for this is shown in Fig. 14. From Eq. (4.25c) we have

$$s^<_{\alpha\beta}(x,p)=\int d^4y\,\frac{d^4q_1}{(2\pi)^4}\frac{d^4q_2}{(2\pi)^4}\,S^+_{\alpha\beta\alpha'\beta'}(x-y,p)\times(2\pi)^4\delta^4(p-(q_1+q_2))\times\alpha_{em}(\gamma^\mu)_{\alpha'\alpha''}s^<_{\alpha''\beta''}(y,q_1)\times(\gamma^\nu)_{\beta''\beta'}d^<_{\mu\nu}(y,q_2).$$

Using $s^<_{\alpha\beta}(x,q)=s^>_{\beta\alpha}(x,-q)$, we find

$$s^<_{\alpha\beta}(x,p)=\int d^4y\,\frac{d^4q_1}{(2\pi)^4}\frac{d^4q_2}{(2\pi)^4}\,S^+_{\alpha\beta\alpha'\beta'}(x-y,p)\times(2\pi)^4\delta^4(p-(-q_1+q_2))\times\alpha_{em}(\gamma^\mu)_{\alpha'\alpha''}s^>_{\beta''\alpha''}(y,q_1)(\gamma^\nu)_{\beta''\beta'}d^<_{\mu\nu}(y,q_2). \tag{4.27}$$

Taking the initial photon density from (4.26) and taking $s^{>}_{\beta'' \alpha''}(y,q_2)$ to be a final state positron, we recover Eq. (3.4). However here all of the propagators are retarded while the electron propagator in Eq. (3.4) is causal.

F. Transport equations

In this section, we find a set of transport equations from the integral equations in (4.25). We write the two equations of motion for the phase-space retarded propagator. Applying these equations to the phase-space evolution equations, we derive two sets of coupled integro-differential equations. The first set of equations are the transport equations and the second set are the ''constraint'' equations of Mrówczyński and Heinz [9,30]. The ''constraint'' equations describe the mass shift of the particles in medium.

The equation of motion for the non-interacting retarded massless scalar propagator is

$$\partial^2 G^+(x) = \delta^4(x).$$

The conjugate equation is

$$\partial^2 (G^+(x))^* = \delta^4(x).$$

Multiplying both sides of the first equation by $(G^+(y))^*$, both sides of the second equation $G^+(y)$ and Wigner transforming in the relative space-time coordinate, we find two equations:

$$(k + i\partial/2)^2 G^+(x,k) = \int d^4x' e^{ix'\cdot k} (G^+(x - x'/2))^* \times \delta^4(x + x'/2) \tag{4.28a}$$

$$(k - i\partial/2)^2 G^+(x,k) = \int d^4x' e^{ix'\cdot k} (G^+(x + x'/2)) \times \delta^4(x - x'/2). \tag{4.28b}$$

Inserting the retarded propagator in the energy-momentum representation (with $m_e = 0$) and adding and subtracting the $+$ and $-$ equations, we find the equations of motion for the retarded propagator:

$$k \cdot \partial G^+(x,k) = \frac{2}{\pi} \theta(x_0)\, \delta(x^2) \sin(2x \cdot k) \tag{4.29a}$$

$$(\partial^2/4 - k^2) G^+(x,k) = \frac{2}{\pi} \theta(x_0)\, \delta(x^2) \cos(2x \cdot k). \tag{4.29b}$$

Taylor series expanding the sine or cosine and keeping only the lowest order is equivalent to performing the gradient expansion.

Now, we apply the $k \cdot \partial$ and $(\partial^2/4 - k^2)$ operators to the particle densities in Eq. (4.25). On the right hand side, these differential operators act on the retarded propagators, so we can use their equations of motion to simplify the results. For scalars we get

$$\begin{aligned} p \cdot \partial g^{\gtrless}(x,p) = & \int d^4y \, \frac{d^4q_1}{(2\pi)^4} \frac{d^4q_2}{(2\pi)^4} \frac{2}{\pi} \, \theta(x_0 - y_0)\, \delta((x-y)^2) \sin(2(x-y)\cdot p)(2\pi)^4 \\ & \times \delta^4(p - (q_1 + q_2))\, \alpha_{em} Z^2 (q_1 + q_2 - i\overleftrightarrow{\partial}/2)^{\mu} g^{\gtrless}(y,q_1)(q_1 + q_2 - i\overleftrightarrow{\partial}/2)^{\nu} d^{\gtrless}_{\mu\nu}(y,q_2) \\ & + \int d^4y \, \frac{2}{\pi} \, \theta(x_0 - y_0)\, \delta((x-y)^2) \sin(2(x-y)\cdot p)\, i Q^{\gtrless}_{\mathrm{MF}}(y) \\ & + \lim_{y_0 \to -\infty} \int d^3y \, \frac{2}{\pi} \, \theta(x_0 - y_0)\, \delta((x-y)^2) \sin(2(x-y)\cdot p)\, g^{\gtrless}(y,\vec{p})(\partial^2/4 - k^2) g^{\gtrless}(x,p) \\ = & \int d^4y \, \frac{d^4q_1}{(2\pi)^4} \frac{d^4q_2}{(2\pi)^4} \frac{2}{\pi} \, (x_0 - y_0)\, \delta((x-y)^2) \cos(2(x-y)\cdot p)(2\pi)^4 \delta^4(p - (q_1 + q_2)) \qquad (4.30a) \\ & \times \alpha_{em} Z^2 (q_1 + q_2 - i\overleftrightarrow{\partial}/2)^{\mu} g^{\gtrless}(y,q_1)(q_1 + q_2 - i\overleftrightarrow{\partial}/2)^{\nu} d^{\gtrless}_{\mu\nu}(y,q_2) + \int d^4y \, \frac{2}{\pi} \, \theta(x_0 - y_0)\, \delta((x-y)^2) \\ & \times \cos(2(x-y)\cdot p)\, i Q^{\gtrless}_{\mathrm{MF}}(y) + \lim_{y_0 \to -\infty} \int d^3y \, \frac{2}{\pi} \, \theta(x_0 - y_0)\, \delta((x-y)^2) \cos(2(x-y)\cdot p)\, g^{\gtrless}(y,\vec{p}) \qquad (4.30b) \end{aligned}$$

Now because of the delta functions, the boundary conditions at $y_0 \to -\infty$ only contribute when $|\vec{x} - \vec{y}|$ goes to ∞, implying that we need $g^{\gtrless}(x,p)$ as $\vec{x} \to \infty$. The densities are zero here, so they drop out from these equations.

The transport equations for the photons and electrons are

$$p\cdot\partial d^{\gtrless}_{\mu\nu}(x,p)=\frac{2}{\pi}\int d^4y\,\theta(x_0-y_0)\,\delta((x-y)^2)\sin(2(x-y)\cdot p)\Bigg\{\int\frac{d^4q_1}{(2\pi)^4}\frac{d^4q_2}{(2\pi)^4}(2\pi)^4\delta^4(p-(q_1+q_2))$$
$$\times\{\alpha_{em}\ \mathrm{Tr}[\gamma^\mu s^{\gtrless}(y,q_1)\gamma^\nu s^{\gtrless}(y,q_2)]+\alpha_{em}Z^2(q_1+q_2+i\overleftrightarrow{\partial}/2)^\mu g^{\gtrless}(y,q_1)(q_1+q_2+i\overleftrightarrow{\partial}/2)^\nu g^{\gtrless}(y,q_2)\}$$
$$+g_{\mu\nu}i\Pi^{\gtrless}_{\mathrm{MF}}(y)\Bigg\} \tag{4.31a}$$

$$p\cdot\partial s^{\gtrless}_{\alpha\beta}(x,p)=\frac{2}{\pi}(\not p+i\not\partial)_{\alpha\alpha'}(\not p-i\not\partial)_{\beta\beta'}\int d^4y\,\theta(x_0-y_0)\,\delta((x-y)^2)\sin(2(x-y)\cdot p)\Bigg\{\int\frac{d^4q_1}{(2\pi)^4}\frac{d^4q_2}{(2\pi)^4}(2\pi)^4$$
$$\times\delta^4(p-(q_1+q_2))\alpha_{em}(\gamma^\mu)_{\alpha'\alpha''}s^{\gtrless}_{\alpha''\beta''}(y,q_1)(\gamma^\nu)_{\beta''\beta'}d^{\gtrless}_{\mu\nu}(y,q_2)+\delta_{\alpha'\beta'}(\pm i\Sigma^{\gtrless}_{\mathrm{MF}}(y))\Bigg\}. \tag{4.31b}$$

These equations almost have the form of the Boltzmann equation: the left side clearly is the Boltzmann transport operator and the right side is almost the collision integrals. If we were to expand the sines in the collision integrals and keep only the lowest term, we would recover the collision integrals. Furthermore, if we were to do this same approximation to the QCD version of (4.31) we would arrive at Geiger's semiclassical QCD transport equations [10].

We also state the constraint equations:

$$(\partial^2/4-k^2)d^{\gtrless}_{\mu\nu}(x,p)=\frac{2}{\pi}\int d^4y\,\theta(x_0-y_0)\,\delta((x-y)^2)\cos(2(x-y)\cdot p)\Bigg\{\int\frac{d^4q_1}{(2\pi)^4}\frac{d^4q_2}{(2\pi)^4}(2\pi)^4\delta^4(p-(q_1+q_2))$$
$$\times\{\alpha_{em}\ \mathrm{Tr}[\gamma^\mu s^{\gtrless}(y,q_1)\gamma^\nu s^{\gtrless}(y,q_2)]+\alpha_{em}Z^2(q_1+q_2+i\overleftrightarrow{\partial}/2)^\mu g^{\gtrless}(y,q_1)(q_1+q_2+i\overleftrightarrow{\partial}/2)^\nu g^{\gtrless}(y,q_2)\}$$
$$+g_{\mu\nu}i\Pi^{\gtrless}_{\mathrm{MF}}(y)\Bigg\} \tag{4.32a}$$

$$(\partial^2/4-k^2)s^{\gtrless}_{\alpha\beta}(x,p)=\frac{2}{\pi}(\not p+i\not\partial)_{\alpha\alpha'}(\not p-i\not\partial)_{\beta\beta'}\int d^4y\,\theta(x_0-y_0)\,\delta((x-y)^2)\cos(2(x-y)\cdot p)\Bigg\{\int\frac{d^4q_1}{(2\pi)^4}\frac{d^4q_2}{(2\pi)^4}(2\pi)^4$$
$$\times\delta^4(p-(q_1+q_2))\alpha_{em}(\gamma^\mu)_{\alpha'\alpha''}s^{\gtrless}_{\alpha''\beta''}(y,q_1)(\gamma^\nu)_{\beta''\beta'}d^{\gtrless}_{\mu\nu}(y,q_2)+\delta_{\alpha'\beta'}(\pm i\Sigma^{\gtrless}_{\mathrm{MF}}(y))\Bigg\}. \tag{4.32b}$$

If we were to derive the constraint equation for massive particles, we would find that $(\partial^2/4-k^2)\rightarrow(\partial^2/4-k^2+m^2)$. Therefore, the constraint equations give rise to the in-medium mass shift for the photons and electrons and thus the RHS of the constraint equations can be interpreted as an ''in-medium'' mass. Note that despite the presence of this ''in-medium'' mass, particles still scatter onto the light-cone. This is not a surprise since the particles are massless. Finally, we have not written the various constants in terms of their renormalized values. Dressing the particle densities by solving the evolution equations (which are nonperturbative) should, to some extent, be equivalent to using renormalized couplings.

G. Implications for QCD parton transport theory

The ''source-propagator'' picture must apply to QCD partons since our derivation of the phase-space generalized fluctuation-dissipation theorem only depends on the form of the Dyson-Schwinger equations for the contour propagators in (4.7). In particular, the specific form of the self-energies is irrelevant. It would then seem that if we find the QCD self-energies and define the parton distributions appropriately, we may construct QCD phase-space parton evolution equations. However, before we could do this we must assess whether we need to dress the phase-space propagators and vertices, implement renormalization and possibly attempt to treat the bound states.

In the present work, we dress the particle densities by iterating the phase-space evolution equations but we do not dress the phase-space propagators or vertices. However, dressing the particle densities may be sufficient to incorporate any needed higher order or many particle effects. One such effect is the mass shift of a particle in-medium. This has been mentioned above and given this, it may prove necessary to give particles an effective mass as a simple form of in-medium dressing of the phase-space propagators. In this event, we would then need the propagators with non-zero mass and we do not know the form of the retarded phase-space propagators for this case. We are currently investigating propagation in this case.

The issue of implementing renormalization will require some work as there is not a well-developed understanding of renormalization in non-equilibrium quantum mechanics. In momentum-space perturbation theory, renormalization is

used to correct some parameters (e.g. a particle's mass) to make them correspond to their observed values. Some of these corrections can be ascribed to many-particle effects that are effectively dealt with by dressing the densities, propagators and/or vertices. Nevertheless, there may be divergencies that need to be removed in our formulation of non-equilibrium perturbation theory but, at the present, we have not yet encountered any. The issue of renormalization brings up one other question. Usually momentum-space renormalization is interpreted as removing physics at one momentum scale in favor of another scale. It is not clear what this means in phase-space. When renormalizing in phase-space, are we removing physics at a certain length scale, a certain momentum scale, both, or neither? Is renormalization a form of smoothing in phase-space, akin to the gradient approximation?

The issue of QCD bound states is very much an open issue. Will we need to introduce higher-order correlations (i.e. four and six point functions) into the Dyson-Schwinger equations? If so, this presumably would require some understanding of hadronization and the role of Λ_{QCD}. Λ_{QCD} is usually interpreted as a momentum cut-off in perturbation theory; as one approaches Λ_{QCD}, nonperturbative effects increase and perturbation treatments break down. This interpretation may not be appropriate in phase-space for several reasons. First, the phase-space evolution equations are nonperturbative objects, so there should be no cut-off in momentum. Second, it is not clear whether Λ_{QCD} should be viewed as a cut-off in momentum or whether $1/\Lambda_{QCD}$ should be viewed as a cut-off in coordinate space. In fact, it may be that $1/\Lambda_{QCD}$ is simply a characteristic length scale for QCD bound states (i.e. hadrons) so that a proper treatment of bound states may lead to a clear identification of the role of $1/\Lambda_{QCD}$.

In any event, these three issues are intricately intertwined and their investigation is beyond the scope of the present work. Nevertheless, in the absence of a phase-space evolution equation, we can still use the generalized fluctuation-dissipation theorem as insight to build models. This is what we do in the next section.

V. PARTON CLOUD OF A NUCLEON

We cannot calculate the phase-space parton distribution functions without a set of QCD phase-space evolution equations. Nevertheless, there is significant work calculating the parton distribution functions in momentum-space and many of these results can be translated into phase-space. In particular, we show that the leading logarithm approximation should work in phase-space. Using the momentum ordering in the leading logarithm approximation and a simple model of the nucleon we estimate the size of the sea parton distribution as a function of parton momentum.

A. QCD parton model and leading logarithm approximation

The QCD parton model rests on two simple assumptions: $\alpha_s \ll 1$ (so perturbation theory is valid) and the parton lifetime is much larger than parton interaction time [25]. Both of these conditions are necessary to factorize a cross section in a momentum-space calculation. Typically the parton distribution functions are calculated using either DGLAP, BFKL, or GLR evolution, all of which are equivalent to applying a leading logarithm approximation (LLA). In the LLA, we assume the parton is produced in a cascade represented by the ladder diagram in Fig. 15. The probability of emitting the nth parton with longitudinal momentum fraction x_n and transverse momentum q_{nT}^2 from this cascade is [26]

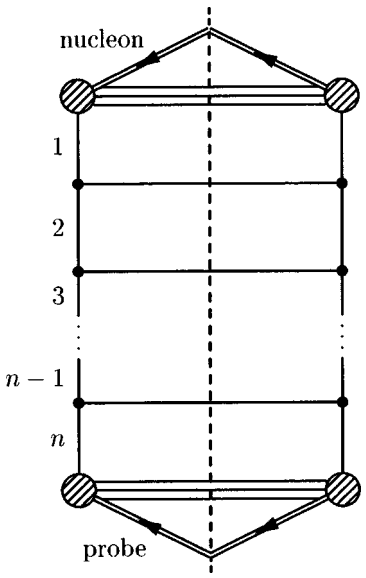

FIG. 15. Cut diagram for probing the nth generation of partons in a typical cascade. Time flows downward in this diagram and the probe, being somewhere in the future, is left unspecified.

$$dP_n = \frac{N_c \alpha_s}{\pi} \frac{dx_n}{x_n} \frac{dq_{nT}^2}{q_{nT}^2}. \tag{5.1}$$

Thus, by ordering the momentum properly as we go down the ladder, we can pick up the largest logarithmic contributions to the nth parton's density.

Most hadron colliders probe regions where the data are well described with parton distribution functions calculated within the Dokshitzer-Gribov-Lipatov-Altarelli-Parisi (DGLAP) evolution scheme. DGLAP evolution is equivalent to the leading logarithm approximation in $1/q^2$ [LLA(Q^2)]. New experiments at the DESY ep collider HERA are beginning to see evidence that Balitskii-Fadin-Kuraev-Lipatov (BFKL) type evolution is necessary to describe the parton distribution functions at small-x [31]. BFKL-type physics is believed to be responsible for the rise in the number of partons as $x \to 0$, however this rise can also be partially described by DGLAP-type physics [26,3,31]. BFKL evolution is equivalent to the leading logarithm approximation in $1/x$ [LLA(x)]. Unlike DGLAP and BFKL evolution, Gribov-Levin-Ryskin (GLR) type evolution does not have a simple momentum ordering because one sums terms with varying powers of $1/x$ and $1/q^2$ [32,26]. Because of the simplicity of the ladder structure and the momentum ordering needed to pick up the largest contributions, we will discuss both DGLAP and BFKL type partons in phase-space.

We can apply the QCD parton model and LLA in phase-space if both are modified appropriately. Assume that we are working in a regime where $\alpha_s \ll 1$, so we can apply phase-space perturbation theory, and assume that all elementary particles are massless. Assume also that the probe is localized on the length scale of the parton cloud. This assumption is equivalent to saying the parton lifetime is large compared to the interaction time.

Now, if we find the same singularities in both phase-space and momentum-space, then we know that the LLA will give the dominant contribution to the particle densities in phase-space. The generalized fluctuation dissipation theorem tells us that the parton density has the form

$$g^{\gtrless}(x,p) = \int d^4y G^{+}(x-y,p)\Sigma^{\gtrless}(y,p). \tag{5.2}$$

The self-energy, $\Sigma^{\gtrless}$, is given by the parton ladder in Fig. 15 and the nth segment of $\Sigma^{\gtrless}$ is shown in Fig. 16. In momentum-space, the cut rung gives a $d^3k/|k_0|$ which leads to the dx/x in Eq. (5.1). To see how the factor of $d^3k/|k_0|$ arises in phase-space, one needs only look at the electron source in Sec. III B 1. The electron source has exactly the form of the segment in Fig. 16 and in that calculation we found exactly this factor of $d^3k/|k_0|$. The fact that we find the same factor of $d^3k/|k_0|$ in both the energy-momentum representation and in phase-space simply reflects the fact that the cut parton density is $\theta(k_0)\delta(k^2)$ in both cases and we sum over final parton states. The factor of dq^2/q^2 occurs in Eq. (5.1) because of the integration over the leg's propagator $1/q^2$. In phase-space, the $1/q^2$ poles are tied up in the Wigner transform of the retarded propagator, but they are still there:

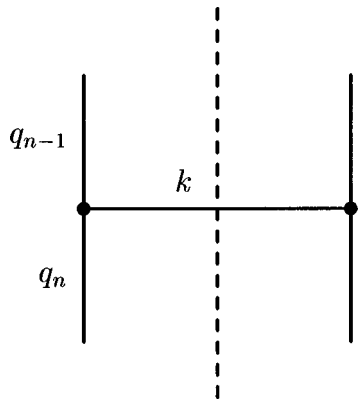

FIG. 16. Typical rung of the LLA ladder.

$$G^{+}(x,q) = \int \frac{d^4q'}{(2\pi)^4} e^{-ix\cdot q'} \frac{1}{(q+q'/2)^2 + i\epsilon(q_0+q_0'/2)} \frac{1}{(q-q'/2)^2 - i\epsilon(q_0-q_0'/2)}.$$

Thus, this segment of the parton ladder produces the same divergencies in phase-space and momentum-space whatever orderings are needed to produce the leading contributions in momentum space will produce the same leading contributions in phase-space.

Our self-energy has the same ladder structure as the electron source in Sec. III, so we know the spatial structure of the nth parton's source is given by the $n-1$th parton's distribution. Iterating back to the 0th parton (a valence quark), we see that the shape of the valence distribution sets the shape of the sea parton source. We take the valence quark wave function to be uniformly spread throughout a bag with radius R_{bag}. Since we are interested in high-energy collisions, we take the nucleon bag to be moving to the right with 4-momentum $p_\mu = (P_0, P_L, \vec{0}_T)$ with $P_0 \approx P_L \gg M_N$. Thus, this nucleon has 4-velocity $v_\mu = (1, v_L, \vec{0}_T)$ and the bag is contracted in the longitudinal direction by a factor of $\gamma = 1/\sqrt{1-v_L^2} \gg 1$. We assume the partons lose memory of the original valence quark momentum as one goes down the ladder. Thus, any momentum-coordinate correlations in the source function should be washed out by the spatial integrations in Eq. (5.2). One might expect that the sea partons forget the shape of the nucleon bag as well, but we show that the partons cannot propagate far enough from the original source for this to happen.

B. Large-Q^2 (DGLAP) partons

In the large-Q^2 regime, the parton density is low but $\alpha_s(Q^2)\ln(Q^2/\Lambda_{QCD}^2) \gtrsim 1$. Here the largest contribution to the leading log ladder comes from large Q^2 logarithms.[16] To get the largest contributions from these logs, we order the momenta as we move down the ladder:

$$-q_n^2 \gg -q_{n-1}^2 \gg \cdots \gg -q_1^2 \gg 1/R_{bag}^2 \approx \Lambda_{QCD}^2.$$

Here q_i^2 is the virtuality of the ith leg. The kinematics at each leg-rung vertex ensure that the momentum fraction carried by each leg is also ordered:

$$1 \geqslant x_1 \geqslant \cdots \geqslant x_{n-1} \geqslant x_n.$$

Whether a rung or leg is a quark or gluon is irrelevant, provided $k^2 = 0$ and the q^2 ordering holds. Now, given that the proton has longitudinal momentum P_L and the rungs and legs are massless, each generation of partons must have energy $q_{n0} \approx x_n P_L$ and transverse momentum of $q_T^2 \approx -q^2 \ll x^2 P_L^2$.

[16] Q^2 can be taken as the typical momentum scale of the process. In the case of a DIS probe, this is the momentum transferred by the probe.

Let us discuss the general features of the parton cloud. The retarded propagator lets the nth parton propagate out to $R_{n\perp}\sim\hbar c/\sqrt{-q_n^2}$ transverse to the parton momentum and to $R_{n\parallel}\sim\hbar c/q_{n0}=\hbar c/x_nP_L$ parallel to the the parton momentum. Since $xP_L\gg p_T$, the parton momentum is approximately parallel to the nucleon momentum. Because $R_{n\perp}\ll R_{bag}$, the partons can never get far from the bag in the transverse direction and transverse spread of the partons will be dominated by the bag size: $\Delta R_T\sim R_{bag}$. On the other hand, the longitudinal spread of the partons is roughly given by $\Delta R_L\sim R_{bag}/\gamma+\hbar c/xP_L$, so can be dominated by the longitudinal propagation distance $R_\parallel$ if $x\ll M_NR_{bag}/\hbar c$. In fact, for very small x (i.e. $x\sim M_NR_{bag}/\gamma\hbar c$) the spread of the partons can meet or exceed the nucleon bag radius. Furthermore, the actual distribution may be somewhat broader due to the propagation of the virtual partons between the subsequent emissions along the ladder.

So, in our picture, the sea quark and gluon large-Q^2 distributions have the same transverse size as the parent nucleon, but the longitudinal size can be significantly bigger than the parent. Furthermore, the drop off in the parton density in the longitudinal direction occurs at the characteristic radius of $\sim\hbar c/xP_L$. This picture of the nucleon is consistent with the uncertainty principle based arguments of Mueller [20], later user by Geiger to initialize the parton distributions in his Parton Cascade Model (PCM) [21].

C. Small-x (BFKL) partons

In the small-x regime, the parton density is high and $\alpha_s(Q^2)\ln(1/x)\gtrsim 1$. The small-$x$ partons are mostly gluons. In this regime, the leading logs come from the $1/x$-type singularities, i.e. from the cut rungs. Since leading logs come from the $1/x$ type singularities, the largest contributions come about by strongly ordering the longitudinal momentum fraction as one moves down the ladder [33]:

$$1\gg x_1\gg\cdots\gg x_{n-1}\gg x_n.$$

BFKL-type evolution has only a weak dependence on the virtuality of the partons as we move down the ladder, so we assume q^2 to be fixed: $q_{n-1}^2\approx q_n^2\gg 1/R_{bag}^2$. This does not significantly effect the results of the analysis [34].

Now we must understand how the transverse momentum and energy of each parton leg changes as we go down the ladder. A well known effect of iterating the BFKL kernel (equivalent to moving down the ladder) is that the transverse momentum undergoes a random walk in $\ln(q_T^2)$ [26,33]. In fact, after iterating through a sufficiently large number of rungs, the spread in the q_T distribution is given by

$$\left\langle\left(\ln\left(\frac{q_{nT}^2}{q_{1T}^2}\right)\right)^2\right\rangle=C\,\ln\left(\frac{1}{x}\right)$$

where $C=(N_c\alpha_s/\pi)28\zeta(3)=32.14\alpha_s$. Thus, q_{nT}^2 can be orders of magnitude larger or smaller than q_{1T}^2. We restate this as

$$q_{nT}^2\sim q_{1T}^2e^{\pm 5.7\sqrt{\alpha_s\ln(1/x)}}. \tag{5.3}$$

We will consider the extreme cases of the transverse momentum and comment on the typical case, $q_{nT}^2\sim q_{1T}^2$.

If the random walk results in a large transverse momentum, we will have $q_{nT}^2\gg q_{1T}^2\sim -q^2\sim(x_nP_L)^2$. Thus, the nth parton will have 3-momentum in the transverse direction. We know that the parton can only propagate to a distance of roughly $R_\parallel\sim\hbar c/|q_0|=\hbar c/\sqrt{q^2+q_T^2+(xP_L)^2}$ in the direction parallel to $\vec{q}$. Since $\hbar c/\sqrt{q^2+q_T^2+(xP_L)^2}\approx\hbar c/|q_T|\ll R_{bag}$, the parton cannot travel far from the original source in the transverse direction. On the other hand, the parton's longitudinal spread can be larger than the longitudinal bag size. The parton can propagate to a distance of $R_\perp\sim\hbar c/\sqrt{-q^2}$ in the direction perpendicular to $\vec{q}$, so we can expect a longitudinal spread of the parton distribution of $\Delta R_L\sim R_{bag}/\gamma+\hbar c/\sqrt{-q^2}$. Since $R_{bag}\gg\hbar c/\sqrt{-q^2}$, this additional spread can not match the spread of the DGLAP partons.

If the random walk results in a small transverse momentum, we will have $q_{nT}^2\ll q_{1T}^2\sim -q^2\sim(x_nP_L)^2$. In this case, the nth parton will have 3-momentum in the longitudinal direction. As in the case of the DGLAP partons the additional transverse spread is $\Delta R_T\sim\hbar c/\sqrt{-q^2}\ll R_{bag}$ and so is negligible. The additional longitudinal spread is $\Delta R_L\sim\hbar c/|q_0|=\hbar c/\sqrt{q^2+(xP_L)^2+q_T^2}$ and may be significantly larger than the bag radius because the parton is space-like.

Summarizing both possibilities, the BFKL parton distributions have the same transverse spread, $\Delta R_T\sim R_{bag}$, but different longitudinal spreads. The longitudinal spread may range from $\Delta R_L\sim R_{bag}/\gamma+\hbar c/\sqrt{-q^2}\ll R_{bag}$ to $\Delta R_L\sim R_{bag}/\gamma+\hbar c/\sqrt{q^2+(xP_L)^2+q_T^2}\gg R_{bag}$ for partons with space-like momentum. The fact that the spatial extent of the BFKL cloud is so large in the longitudinal direction suggests that the small-x partons (which are mostly gluons) can see the color charge of any other nucleon in the longitudinal tube centered on the parent nucleon. This suggests that we should treat the nucleus as a whole as a source of color charge in the spirit of McLerran-Venugopalan model [35].

The large longitudinal extent of the small-x cloud has another consequence: in a zero impact parameter nucleon-nucleon collision, we would find that the soft (BFKL) partons interact much earlier than the harder (DGLAP) partons because of their greater longitudinal spread. This, coupled with the large density of small-x partons, leads to earlier entropy production and stopping of the soft partons.

VI. CONCLUSION

We have made progress toward specifying the initial phase-space parton distributions of a relativistic nuclear collision. Regardless of the kinematical regime, the transverse spread of a parton distribution is dominated by the bag radius ~ 1 fm. The longitudinal spread of a parton distribution varies from roughly $\sim R_{bag}/\gamma+\hbar c/xP_L$ for moderate to large x (i.e. for DGLAP partons) and from $\Delta R_L\sim R_{bag}/\gamma+\hbar c/\sqrt{-q^2}$ to $\Delta R_T\sim R_{bag}/\gamma+\hbar c/\sqrt{q^2+(xP_L)^2+q_T^2}$ for small x (i.e. BFKL partons). Since the small x partons have a large longitudinal spread and a high density, we expect the small x partons to interact much earlier than the large x

partons in a typical nuclear collision. This may cause earlier entropy production and higher stopping than one expects in models that include only DGLAP parton distributions such as the PCM [21], HIJING [4], and others.

Using time-ordered non-equilibrium methods, we derived phase-space evolution equations for QED, illustrating how to find them in QCD. Unlike conventional transport approaches, our calculation does not rely on the gradient approximation. Thus, it should work on all length and momentum scales of interest. These phase-space evolution equations describe the complete evolution of a system from some time in the distant past to the present, including all splittings, recombinations and scatterings of the particles. One can use these evolution equations perturbatively or to derive semiclassical transport equations. These evolution equations rely on the generalized fluctuation-dissipation theorem. This theorem states that a particle's density is the convolution of the Wigner transform of its self-energy and a phase-space propagator. The generalized fluctuation-dissipation theorem is quite general and can be directly applied to QCD.

In conventional Feynman perturbation theory, we found the reaction rates (and hence the cross sections) can be written in a parton model form. In other words, they take the form of a reaction rate density convoluted with a phase-space parton distribution function. This phase-space PDF is the parton number density and has the form of a phase-space source folded with a phase-space propagator. Our work with the Weizsäcker-Williams approximation demonstrates that the parton distribution functions can be defined in phase-space.

In order to illustrate how the propagators and sources work in phase-space, we calculated the effective photon and electron distributions. We found that both the retarded and Feynman propagators propagate particles to distances of $\sim R_{\parallel}=\hbar c/\min(|q_0|,|\vec{q}|)$ parallel to the particle's momentum and to distances of $\sim R_{\perp}=\hbar c/\sqrt{|q^2|}$ perpendicular to the particle's momentum when $q^2\neq 0$. When $q^2=0$, the particles tend to follow their classical paths with deviations from this path being of order $1/|q_0|$. Furthermore, the retarded propagator can only send particles forward in time and inside the light-cone while the Feynman propagator sends particles both forwards and backwards in time and both inside and outside of the light-cone. We also described a phase-space source that included a simple ''partonic'' splitting: the electron distribution of a point charge. These electrons are created when a virtual photon splits into an electron-positron pair; the diagram for this process is the first segment of a parton ladder. We found that shape of the electron's source is controlled by the parent photon's distribution.

We hope that we have provided insight into the behavior and calculation of the phase-space densities. Specifically, we hope the ''source-propagator'' picture of the generalized fluctuation-dissipation theorem and the resulting phase-space evolution equations can be coupled with appropriately defined QCD phase-space parton densities. The resulting theory could describe the various many-particle effects we expect in a nuclear collision at RHIC or the LHC and it could incorporate parton model phenomenology.

ACKNOWLEDGMENTS

The authors acknowledge conversations with the participants of the Institute for Nuclear Theory program, specifically Miklos Gyulassy, Berndt Müller, Alejandro Ayala, Raju Venugopalan, and Alexander Makhlin. They also acknowledge Vladimir Zelevinsky, Scott Pratt, C. P. Yuan, Ed Shuryak and George Bertsch for their valuable discussions. This work was supported by the National Science Foundation under Grant PHY-9605207.

APPENDIX A: ELECTRODYNAMICS WITH FERMIONS AND SCALARS

Throughout this paper we use QED and scalar electrodynamics to describe the interactions between the electrons, photons and scalars. In this appendix, we review the QED Lagrangian, equations of motion, equal time commutation relations and contour Feynman rules. The Lagrangians, etc., for QED and for scalar electrodynamics are given in many places [36,37]. Even so, we restate them here both to keep this work self-contained and to clarify our notation. We do not include the renormalization counterterms nor the gauge fixing terms for the photons although they can be easily included. We work in the Lorentz gauge.

The Lagrangian for scalar QED coupled with spinor QED is

$$\begin{aligned}\mathcal{L}=&\frac{i}{2}\bar{\psi}(x)\overleftrightarrow{\partial}\!\!\!\!/\,\psi(x)-m_e\bar{\psi}(x)\psi(x)-\frac{1}{16\pi}F_{\mu\nu}(x)F^{\mu\nu}(x)\\&+(\partial_\mu\phi^*(x))(\partial^\mu\phi(x))-M^2\phi^*(x)\phi(x)\\&-e\bar{\psi}(x)A\!\!\!/(x)\psi(x)-iZeA^\mu(x)(\phi^*(x)\overleftrightarrow{\partial}_\mu\phi(x))\\&+Z^2\alpha_{em}A^2(x)\phi^*(x)\phi(x).\end{aligned}\tag{A1}$$

Here $\psi_\alpha(x)$ is the fermion field, $\phi(x)$ is the complex scalar field, $A_\mu(x)$ is the photon field, and $F_{\mu\nu}(x)=\partial_\mu A_\nu(x)-\partial_\nu A_\mu(x)$. The masses of the fermion and scalar fields are m_e and M respectively. The electrons couple to the photons with strength e while the scalars couple with Ze.

The Heisenberg field operators satisfy the standard equal time commutation relations at time t:

$$[\hat{A}_\mu(t,\vec{x}),\dot{\hat{A}}_\mu(t,\vec{x}')]_-=4\pi g_{\mu\nu}\delta^3(\vec{x}-\vec{x}')\tag{A2a}$$

$$[\hat{A}_\mu(t,\vec{x}),\hat{A}_\mu(t,\vec{x}')]_-=[\dot{\hat{A}}_\mu(t,\vec{x}),\dot{\hat{A}}_\mu(t,\vec{x}')]_-=0\tag{A2b}$$

$$[\hat{\psi}_\alpha(t,\vec{x}),\hat{\psi}^\dagger_\beta(t,\vec{x}')]_+=\delta_{\alpha\beta}\delta^3(\vec{x}-\vec{x}')\tag{A2c}$$

$$[\hat{\phi}(t,\vec{x}),\dot{\hat{\phi}}(t,\vec{x}')]_-=\delta^3(\vec{x}-\vec{x}')\tag{A2d}$$

$$[\hat{\phi}(t,\vec{x}),\hat{\phi}(t,\vec{x}')]_-=[\dot{\hat{\phi}}(t,\vec{x}),\dot{\hat{\phi}}(t,\vec{x}')]_-=0.\tag{A2e}$$

The Lagrangian (A1) leads to the following equations of motion:

$$4\pi j^\nu(x)=\partial_\mu F^{\mu\nu}(x)\tag{A3a}$$

TABLE I. The vertex Feynman rules for scalar and spinor QED.

3 point photon-scalar vertex	$eZ\overleftrightarrow{\partial}_\mu = eZ(\overleftarrow{\partial}_\mu - \vec{\partial}_\mu)$
4 point photon-scalar vertex	$2ie^2Z^2 g_{\mu\nu}$
fermion-photon vertex	$-ie\gamma_\mu$

$$0 = (i\partial\!\!\!/ - eA\!\!\!/(x))\psi(x) - m_e\psi(x) \tag{A3b}$$

$$0 = (\partial_\mu + ieA_\mu(x))(\partial^\mu + ieA^\mu(x)) \times \phi(x) + M^2\phi(x). \tag{A3c}$$

The electromagnetic current operator is

$$\hat{J}^\mu(x) = e\hat{\bar{\psi}}(x)\gamma^\mu\hat{\psi}(x) + iZe\hat{\phi}^*(x)\overleftrightarrow{\partial}\hat{\phi}(x).$$

These equations are solved by the Green's functions in Sec. IV A in the limit as $e \to 0$.

The contour Feynman rules have been derived previously [5], so we state them for spinor and scalar QED below:

(1) The vertex Feynman rules are summarized in Table I.

(2) The contour propagators are summarized in Table II.

(3) Every closed fermion loop yields a factor of (-1).

(4) Every single particle line that forms a closed loop or is linked by the same interaction line yields a factor of $iG^<$.

Notice that the second scalar coupling has higher order than the rest of the couplings. So we neglect this coupling in the derivation of the evolution equations of Sec. IV D.

APPENDIX B: THE CROSS SECTION IN TERMS OF PHASE-SPACE DENSITIES

In this appendix, we discuss the cross-section in terms of phase-space quantities. Since the cross section is measured by scattering a beam of particles off a target, we define the cross section in terms of the projectile-target reaction rate density and the projectile flux. The beam is uniform in the beam direction and in time on the scale of the projectile-target interaction. Thus, the beam can only directly probe the transverse structure of the interaction region. Even this transverse information is washed out in the typical experiment, since the beam is usually uniform in the transverse direction on the length scale of the interaction. In the limit of a transversely uniform beam, we recover the conventional definition of the cross section. Since we consider only simple scattering problems, we work in Feynman perturbation theory where we can specify both the initial and final states of the reactions.

TABLE II. The contour scalar, photon, and electron propagators.

scalar line	$G(x_1,x_2)$
photon line	$D_{\mu\nu}(x_1,x_2) = 4\pi g_{\mu\nu}G(x_1,x_2)$
fermion line	$S_{\alpha\beta}(x_1,x_2) = -(-i\partial\!\!\!/ + m)_{\alpha\beta}G(x_1,x_2)$

The beam is a collection of single particle wavepackets distributed throughout the transverse area A of the beam. For the sake of illustration, we take these particles to be scalars. The Wigner function of these incident wavepackets is

$$f(x,p) = \frac{1}{2Vp_0}\int \frac{d^4p'}{(2\pi)^4}\, e^{-x\cdot p'} \times f(p+p'/2)f^*(p-p'/2) \tag{B1}$$

where the wave function $f(p)$ is given by[17]

$$|i\rangle = \int \frac{d^4p}{(2\pi)^4}\, f(p)|\vec{p}\rangle. \tag{B2}$$

We will assume the beam to be uniform in the longitudinal direction with length L and to be turned on for macroscopic time T. The quantities A, T, and L are much larger than the projectile-target interaction region.

The projectile-target interaction region is characterized by a reaction rate density $\mathcal{W}_{i\to f}(x)$. We assume the reaction rate density to be localized in both space and time. This reflects the small spatial extent of the target and the short interaction time compared to the beam lifetime. The reaction rate is trivially related to the reaction probability:

$$|S_{i\to f}|^2 = \int d^4x \mathcal{W}_{i\to f}(x). \tag{B3}$$

Thus, the reaction rate is easily identifiable in the calculations in Secs. II, III. For example, in the process $\gamma B \to B'$ in Fig. 1(b), the reaction rate density is $\mathcal{W}_{\gamma B\to B'}(x,q)$. For the process $AB \to A'B'$ in Fig. 1(a), it is

$$\mathcal{W}_{AB\to A'B'}(x) = \int d^4r \frac{d^4q}{(2\pi)^4} J_A^{\mu\nu}(x+r/2) \times D^c_{\mu\nu\mu'\nu'}(r,q)J_B^{\mu'\nu'}(x-r/2). \tag{B4}$$

Note that the reaction rate density is a function of the average space-time location of all the vertices in the process.

The cross section is the effective area of the target, so we define the cross section as the integral over the beam face of the fraction of incident particles that interact with the target per unit area:

$$\sigma = \int_A d^2x_T \left(\frac{\text{no. scattered particles}}{\text{unit area}}\right) \Big/ \left(\frac{\text{no. incident particles}}{\text{unit area}}\right). \tag{B5}$$

[17]The delta function that puts the particle on-shell is absorbed into $f(p)$.

The number of incident particles per unit area crossing the target plane is the particle flux:

$$\frac{\text{no. incident particles}}{\text{unit area}} = \mathcal{N}_{inc} \int_{-L/2}^{L/2} dx_L \hat{n} \cdot \vec{j}(x) \equiv \mathcal{F}(\vec{x}_T). \tag{B6}$$

Here $\hat{n}$ is a unit normal to the target plane and $\mathcal{N}_{inc}$ is the number of particles in the beam. The single particle current is given in terms of the incident particle Wigner function by [23]

$$\vec{j}(\vec{x}) = \int d^3p dp^2 \vec{v} f(x,p). \tag{B7}$$

We need not average over time because the beam is uniform on the time scale of the reaction. The number of scattered particles per unit area is found by multiplying the number of incident particles by the reaction probability per unit area:

$$\frac{\text{no. scattered particles}}{\text{unit area}} = \mathcal{N}_{inc} \int_{-L/2}^{L/2} dx_L \int_{-T/2}^{T/2} dx_0 \mathcal{W}_{i\to f}(x) \equiv \mathcal{N}_{inc} \overline{\mathcal{W}}_{i\to f}(\vec{x}_T). \tag{B8}$$

Thus, the cross section is

$$\sigma = \int_A d^2x_T \frac{\mathcal{N}_{inc} \overline{\mathcal{W}}_{i\to f}(\vec{x}_T)}{\mathcal{F}(\vec{x}_T)}. \tag{B9}$$

In Eq. (B9), all longitudinal and temporal structure of the interaction is washed out by the beam. Furthermore, in any practical experiment, the wavepackets are delocalized in the transverse direction on the length scale of the interaction region. Thus, the transverse structure of $\mathcal{F}(\vec{x}_T)$ is gone and the flux reduces to $\mathcal{F} = \mathcal{N}_{inc}|\vec{v}|/A$, where $|\vec{v}|$ is the mean projectile velocity. The flux can then be pulled out of the transverse integral in Eq. (B9). The transverse integral of the reaction probability per unit area is $\mathcal{N}_{inc}|S_{i\to f}|^2$, so the cross section becomes

$$\sigma = \frac{A|S_{i\to f}|^2}{|\vec{v}|}. \tag{B10}$$

This is the conventional momentum space cross section in our choice of normalization.

APPENDIX C: WAVEPACKETS

Throughout this paper, we use wavepackets in the initial and final states of a reaction to provide spatial localization or delocalization. In this appendix, we detail the construction of an initial or final state wavepacket and discuss the limits of either a completely localized or delocalized wavepacket.

1. On-shell Gaussian wavepacket

An initial (or final) state ket can be written with wavepackets:

$$|i\rangle = \int \frac{d^4p}{(2\pi)^4} f(p) |\vec{p}\rangle. \tag{C1}$$

The corresponding Wigner function of the particles is

$$\begin{aligned} f(x,p) &= \int \frac{d^4p'}{(2\pi)^4} e^{-ix\cdot p'} \langle i| \hat{\phi}^*(p-p'/2) \\ &\quad \times \hat{\phi}(p+p'/2)|i\rangle \\ &= \frac{1}{2Vp_0} \int \frac{d^4p'}{(2\pi)^4} e^{-x\cdot p'} \\ &\quad \times f(p+p'/2) f^*(p-p'/2). \end{aligned} \tag{C2}$$

Particles in either the initial or final states are on-shell, so they can be expanded in momentum eigenstates. We choose our wavepacket to be a Gaussian superposition of momentum eigenstates with a momentum spread σ:

$$\phi(p) = \mathcal{N}\delta(p^2 - M^2) \exp[-(\vec{p} - \vec{p}_i)^2/2\sigma^2].$$

The Wigner transform of this wavepacket can not be done analytically except in the limit when $|\vec{p}_i| \gg \sigma$. In this limit, $\vec{p}_i \approx \vec{p} \gg \vec{p'}$ so our wavepacket is localized in momentum giving the following Wigner density of particles:

$$\begin{aligned} f(x,p) &= \frac{|\mathcal{M}|^2}{8\pi p_0^2} \delta(p^2 - M^2) \exp\left[-\frac{(\vec{p} - \vec{p}_i)^2}{2\sigma^2} \right] (2\sigma\sqrt{2\pi})^3 \\ &\quad \times \exp[-2\sigma^2(\vec{v}x_0 - \vec{x})^2]. \end{aligned} \tag{C3}$$

Here $\vec{v} = \vec{p}/p_0$ is the velocity of the wavepacket. Thus, the particle's Wigner function is a Gaussian in both momentum and space. The spread in momentum is the inverse spread in space. The centroid of the Gaussian follows the particle's classical trajectory. The energy of the packet is set by the delta function out front. We have not constrained the particle in energy so this density contains both positive and negative energy contributions.

2. Delocalizing the wavepacket in space: Free wavepacket

In accordance with the uncertainty principle, the wavepacket becomes completely delocalized in space in the limit of complete localization in momentum (i.e. $\sigma \to 0$). In this limit, the spatial Gaussian approaches unity and the momentum Gaussian becomes a delta function. After working out the normalization, we find

$$f^{\text{free}}(x,p) = \frac{1}{2Vp_0} (2\pi)^4 \delta^4(p - p_i). \tag{C4}$$

This is no surprise since we squeezed the state into a momentum eigenstate.

3. Localizing the wavepacket in space: Classical wavepacket

A classical particle is localized in both space and momentum, a seeming violation of the uncertainty principle. In real life, this is not a problem since the reason classical particles appear localized is that we probe them on length (or momentum) scales too coarse to resolve the interesting quantum features. In the case of our Gaussian wavepacket, this amounts to probing the distribution on length scales much larger than $1/\sigma$. In this case, the space Gaussian is too localized to resolve and we can replace it with a delta function. Additionally, we assume that σ is large, so we can replace the momentum Gaussian with a delta function as well.

Making these approximations, we find the Wigner density of a classical particle:

$$f^{\text{classical}}(x,p)=\frac{1}{2}(2\pi)^4\delta^3(\vec{p}-\vec{p}_i)\times\delta(p^2-M^2)\,\delta^3(\vec{v}x_0-\vec{x}). \tag{C5}$$

Here we have inserted the correct normalization for the wavepacket. This density corresponds to an on-mass-shell particle that follows its classical trajectory $\vec{v}x_0=\vec{x}$. Again, we left in both positive and negative energy contributions.

APPENDIX D: THE CLASSICAL CURRENT

In this appendix, we derive the classical current used in the effective photon distribution calculation. For the sake of illustration, we take our point particle to be a scalar particle. The derivation goes in three steps: first we define the Wigner current of a scalar particle, then we derive the photon-scalar interaction vertex in phase-space, and finally we localize the initial and final states of the scalar to give the classical current.

1. Wigner current

We begin by restating Eq. (2.3):

$$J^{\mu\nu}_{\rm A}(x,q)=\int\frac{d^4\tilde{q}}{(2\pi)^4}\,e^{-i\tilde{q}\cdot x}\langle A'|j^{\mu}(q+\tilde{q}/2)|A\rangle\times\langle A|j^{\dagger\nu}(q-\tilde{q}/2)|A'\rangle. \tag{D1}$$

We write the initial and final state bra's and ket's according to Eq. (B2). Rewriting Eq. (D1) in terms of initial and final Wigner densities,

$$J^{\mu\nu}_{\rm A}(x,q)=\int\frac{d^4p_i}{(2\pi)^4}\frac{d^4p_f}{(2\pi)^4}\,f_A(x,p_i)f^*_{A'}(x,p_f)(2\pi)^4\times\delta^4(p_i-p_f-q)\Gamma_{\mu\nu}(q,p_i,p_f). \tag{D2}$$

We assume that the initial and final wavepackets are localized in momentum and somewhat delocalized in space. Shortly, we assume that we probe this current on length scales much larger than even this delocalized space distribution.

2. Scalar vertex

$\Gamma_{\mu\nu}(q,p_i,p_f)$ is not quite the Wigner transform of the $\gamma AA'$ vertex, although it does arise from performing the Wigner transform in Eq. (D1). It is defined by

$$(2\pi)^4\delta^4(p_i-p_f-q)\Gamma_{\mu\nu}(q,p_i,p_f)=4V^2p_f^0p_i^0\int\frac{d^4\tilde{q}}{(2\pi)^4}\,\langle\vec{p}_f|j_\mu(q+\tilde{q}/2)|\vec{p}_i\rangle\times\langle\vec{p}_i|j^\dagger_\nu(q-\tilde{q}/2)|\vec{p}_f\rangle. \tag{D3}$$

Using the matrix element

$$\langle\vec{p}_f|j_\mu(q)|\vec{p}_i\rangle=eZ(2\pi)^4\delta^4(p_i-p_f-q)\frac{(p_i+p_f)_\mu}{2V\sqrt{p_f^0p_i^0}},$$

we get

$$\Gamma_{\mu\nu}(q,p_i,p_f)=\alpha_{em}Z^2\left(p_i+p_f+\frac{1}{2}(\tilde{p}_i+\tilde{p}_f)\right)_\mu\times\left(p_i+p_f-\frac{1}{2}(\tilde{p}_i+\tilde{p}_f)\right)_\nu. \tag{D4}$$

The relative momenta, $\tilde{p}_i$ and $\tilde{p}_f$, become derivatives on x in the current (D2). We assume the wavepackets to be uniform to reaction's length scales, so we ignore the derivatives and arrive at the phase-space scalar vertex

$$\Gamma_{\mu\nu}(q,p_i,p_f)=\alpha_{em}Z^2(p_i+p_f)_\mu(p_i+p_f)_\nu. \tag{D5}$$

3. Classical current

We are now in a position to derive Eq. (2.19) for the classical current density in phase-space. First, we take the final state to be a momentum eigenstate and sum over it. Since the final state is localized in momentum around p_f, this is not a bad approximation. Second, we take the initial state to be a classical wavepacket. In other words, we assume that the initial state is localized in momentum and delocalized in space but we probe it on such large length scales that we still see a spatially localized wavepacket. So, putting Eqs. (C4), (C5) and (D5) into (D2) and summing over final states, we get

$$J^{\mu\nu}(x,q)=2\pi\alpha_{em}Z^2v_\mu v_\nu\delta^3(\vec{x}-x_0\vec{v})p_{i0}\times\delta((p_f+q)^2-M^2).$$

Using $p_f^2=M^2$ and $v_\mu\approx p_{f\mu}/p_{i0}$ and assuming $q^2/p_{i0}\ll q\cdot v$, we get the classical current:

$$J^{\mu\nu}_{\text{classical}}(x,q)=2\pi\alpha_{em}Z^2v_\mu v_\nu\delta(q\cdot v)\,\delta^3(\vec{x}-x_0\vec{v}). \tag{D6}$$

Note that this current allows for emission of both positive and negative energy photons. To use the retarded propagators in Sec. II, we need a $\theta(q_0)$ in Eq. (D6). We can do this

by suitable choosing $\vec{p}_f$ and $\vec{p}_i$ and restricting the initial and final states to have only positive energy.

APPENDIX E: PHASE-SPACE EFFECTIVE PHOTON DISTRIBUTION OF A STATIONARY POINT CHARGE

In this appendix, we describe limit of $\vec{v}=0$ of the photon distribution of the point charge in subsection II D. Since the spatial dependence of the effective photon distribution is controlled by the Wigner transform of the vector potential, $A_\mu(x)$, we only discuss $A_{\mu\nu}(x,q)$ here. When $\vec{v}=0$, the photon vector potential becomes $A_\mu(x)=(e/|\vec{x}|,\vec{0})$ so $A_{\mu\nu}(x,q)$ is the Wigner transform of the Coulomb potential.

We take the point charge to be resting at the origin and emitting photons with four-momentum $q_\mu=(q_0,\vec{q})$. Putting $\vec{v}=0$ in Eq. (2.27), we find

$$A_{00}(x,q)=32\pi^2\alpha_{em}\delta(q_0)\,\frac{1}{|\vec{q}|}\times\mathcal{A}(2|\vec{x}||\vec{q}|\cos(\theta),2|\vec{x}||\vec{q}|\sin(\theta))$$

$$A_{ij}=0 \tag{E1}$$

where θ is the angle between $\vec{x}$ and $\vec{q}$ and the dimensionless function $\mathcal{A}$ is given in Eq. (2.28). Clearly the photon field is time independent and is composed entirely of zero energy photons. Furthermore, by virtue of the $1/|\vec{q}|$ singularity, the photon field is mostly composed of low momentum photons.

In Fig. 17, we plot the dimensionless function $\mathcal{A}$ as a function of $\vec{x}$ for $\vec{q}=(0,0.788,\vec{0}_T)$ MeV/c in the plane defined by $\vec{x}$ and $\vec{q}$. Note that the central region of the distribution is circular, but becomes elliptical as one moves away from the center. In the transverse direction (i.e. the direction perpendicular to the photon three-momentum), the distribution approaches zero, but never goes negative. The width in the transverse direction is approximately 250 fm. In the longitudinal direction, the distribution drops to zero at about $x_L\approx 250$ fm and oscillates about zero for larger distances. These oscillations are expected for a Wigner transformed quantity and simply reflect the fact that x_L and q_L are Fourier conjugate variables.

Because the photon source is a point source, the shape of the Coulomb distribution comes directly from the shape of the retarded propagator in subsection II D 2. Thus, we can estimate the width of the photon distribution using the estimates of the retarded propagator in subsection II D 2. In both the longitudinal and transverse directions, the propagator width is $\sim\hbar c/|q_L|=250$ fm, which is the width we measure from the plots.

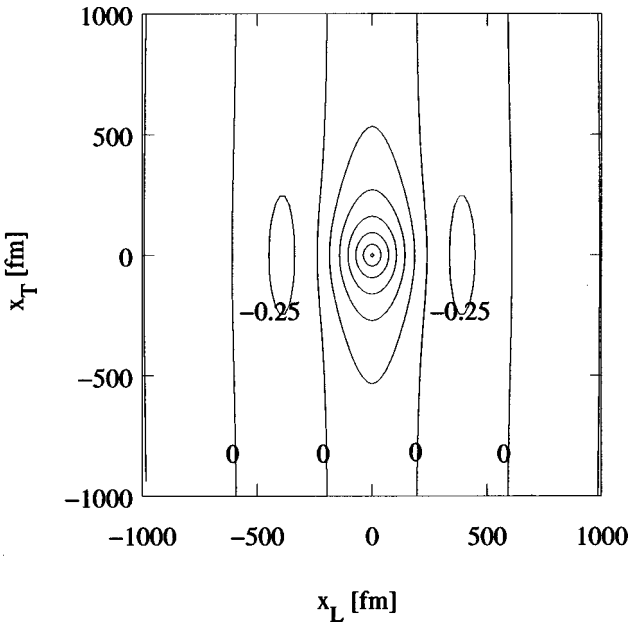

FIG. 17. Plot of the dimensionless function $\mathcal{A}$ corresponding to the Wigner transform of the Coulomb field of a static point charge. The photons in this plot have $q_\mu=(0,0.788,\vec{0}_T)$ MeV/c. The longitudinal axis is defined by the photon three-momentum.

APPENDIX F: EFFECTIVE ELECTRON PHASE-SPACE DISTRIBUTION WITH $M_E\neq 0$

In this appendix, we calculate the effective electron distribution for electrons with a mass much larger than their momentum. This calculation is not included in Sec. III because it is not relevant for QCD partons.

When the electron momentum is much smaller than its mass, we can use Remler's propagators for massive particle [13]. His propagator takes one of two forms depending on whether the electron momentum is space-like or time-like. His propagator is discussed in Appendix G. We show a sample electron density for both the time-like momentum and space-like momentum cases. The momenta of the electrons are chosen to satisfy the requirements that $p\cdot v>0$ and $k_{T\,\max}$ be real. These requirements are equivalent to the requirement that $p\cdot v\geqslant m_e/\gamma$. Since $p\ll m_e$, we must also have $\gamma\gg 1$.

In Sec. III B 1 we show that the electron's source is controlled by the parent photon distribution so we show the parent photon distributions next to the electron distributions in all subsequent plots. We do not restrain the photons to have $q_0>0$ as in Sec. III, so our sources include negative energy contributions. Because we use retarded photon propagators in our source, these calculations only serve to illustrate how Remler's propagators function. In fact, had we restricted $q_0>0$, there would not be enough momentum-space to perform the $\vec{k}_T$ integrals and the electron distribution would be zero.

1. Feynman propagator for particles with space-like momentum

The propagator for electrons with space-like momentum is

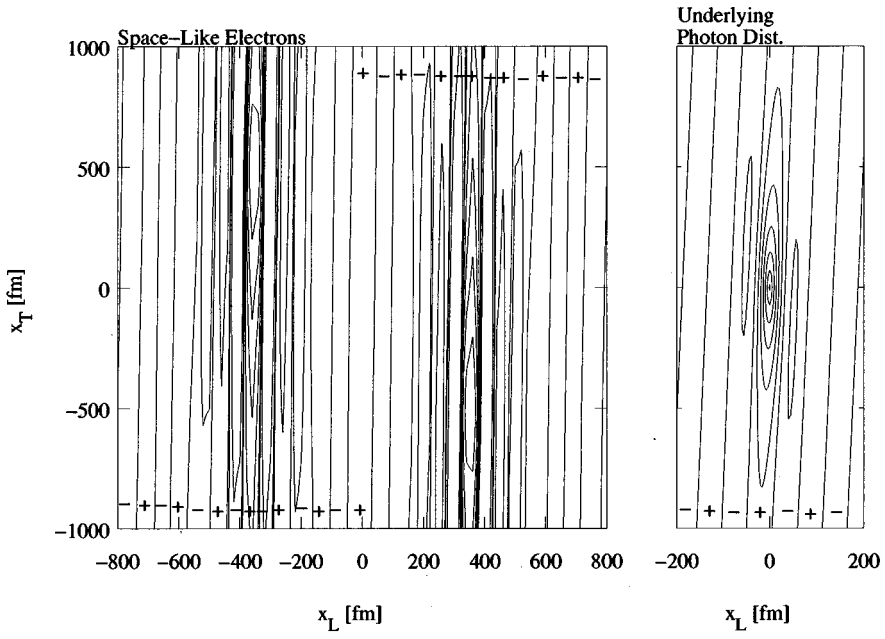

FIG. 18. On the left: coordinate space distribution of space-like $[p_\mu=(0.05,0.008,0.06,0)\ \mathrm{MeV}/c]$ electrons. The $\pm$'s indicate the sign of the function in a particular region. The contours go in steps of 25 (in arbitrary units). On the right: the photon distribution for photons with $q_{+\mu}=(-6.63,-6.65,0.0648,0.00478)\ \mathrm{MeV}/c$. The other root has $q_{-\mu}=(-6.33,-6.36,0.0648,0.00478)\ \mathrm{MeV}/c$ and its distribution is similar. Again, the $\pm$'s indicate the sign of the function in a particular region. Here, the contours go in steps of 0.25 (in arbitrary units).

$$G^c(\Delta x,p)=\int_{-\infty}^{\infty} d\tau\,\delta^4\left(\Delta x-\frac{p}{\sqrt{-p^2}}\tau\right)\times e^{-2m_e|\tau|}\frac{1}{2m_e\sqrt{-p^2}(m_e^2-p^2)}\times\{\sqrt{-p^2}\,\cos(2\tau\sqrt{-p^2})+m_e\,\sin(2|\tau|\sqrt{-p^2})\}.$$

Remler's propagator for space-like electrons has a very simple interpretation. First, the delta function forces the electron to follow its classical trajectory, but with the electron velocity defined as $v_\mu=p_\mu/\sqrt{-p^2}$. The exponential in proper time strongly damps propagation that extends farther in time than $1/2m_e$ along the classical trajectory. The fact that the proper time can extend forward or backwards in time simply reflects the boundary conditions of the Feynman propagator. Next, the sine and cosine cause the expected Wigner oscillations. The rest of the terms simply give normalization. Finally, this propagator allows propagation outside of the light-cone, but such propagation is strongly damped. This may seem strange, but should come as no surprise: the coordinate space propagator for massive particles will propagate a particle outside the light-cone [37].

2. Massive electrons distribution for electrons with space-like momentum

We now perform the integrals over d^2k_T and d^4x in Eq. (3.4). The d^4x is a trivial delta function integral and the integral over d^2k_T can be done numerically. On the left in Fig. 18 we have a sample cut through the phase-space density for electrons with a typical space-like 4-momentum $[p_\mu=(0.05,0.008,0.06,0.0)\ \mathrm{MeV}/c]$. On the right is one of the underlying photon distributions. We chose the source velocity so that $\gamma=12.47$. This velocity is a compromise between having enough momentum space available for the electron and rendering the plot unreadable because of the Lorentz contraction.

Now we examine these plots. First, we see the contributions from retarded emission and propagation (upper left electron pancake) and from advanced propagation (lower right pancake). Let us concentrate on the retarded electrons. At some time in the past, the photons split into the electrons and the positrons. The electrons then propagate forward along their classical trajectory until they reach the location of the left pancake. Notice that this pancake has nearly the same size as the photon distribution on the right. The other photon distribution, corresponding to the other root of positron momentum, has a slightly different tilt and width, but the difference in the plots is not noticeable. The electron pancakes are slightly larger than the photon pancake, presumably because of momentum broadening from the emitted positron. The advanced electrons have exactly the same shape and size as their retarded brethren, but they followed a time-reversed classical trajectory, coming from some time in the future.

3. Feynman propagator for particles with time-like momentum

Remler's propagator for massive particles with time-like momentum is

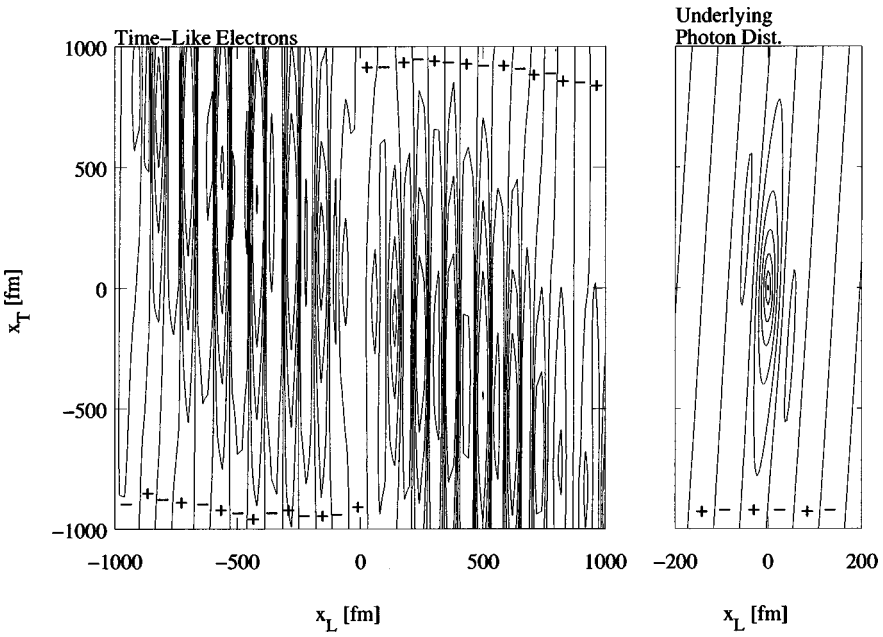

FIG. 19. Coordinate space distribution of time-like $[p_\mu=(0.05,0.005,0.04,0)\ \mathrm{MeV}/c]$ electrons. The $\pm$'s indicate the sign of the function in a particular region. The contours are (in arbitrary units) 150, 10, 5, 1, 0.2, 0, -1, -5, -10, and -150. One of the roots of the underlying photon distribution is shown at the right. These photons have momentum $q_\mu=(-8.39,-8.42,0.182,0.142)\ \mathrm{MeV}/c$. Here, the $\pm$'s indicate the sign of the function in a particular region and the contours go in steps of 0.25 (in arbitrary units).

$$G^{\mathrm{c}}(\Delta x,p)=\int_0^\infty d\tau\,\frac{1}{2m_e\sqrt{p^2}}\times\left\{\frac{\sin(2\tau(\sqrt{p^2}-m_e))}{(\sqrt{p^2}-m_e)}\,\delta^4\left(\Delta x-\frac{p}{\sqrt{p^2}}\tau\right)-\frac{\sin(2\tau(\sqrt{p^2}+m_e))}{(\sqrt{p^2}+m_e)}\delta^4\left(\Delta x+\frac{p}{\sqrt{p^2}}\tau\right)\right\}.$$

Remler's time-like propagator does not have as simple an interpretation as his space-like propagator. Delta functions still keep the particle on its classical trajectory, but the integrals in ''proper time'' are Fourier sine transformed along this classical trajectory. Thus, a simple peak in the underlying photon distribution will get Fourier transformed into a series of peaks and valleys in the electron distribution. Furthermore, the advanced and retarded branches enter with different signs, so we have large *negative* contributions from the advanced branch.

4. Massive electrons distribution for electrons with time-like momentum

Despite the difficulty in interpreting the propagator, the d^4x and d^2k_T integrals can be done. A sample cut through the phase-space distribution is shown in Fig. 19. These electrons have a typical time-like 4-momentum $[p_\mu=(0.05,0.005,0.04,0)\ \mathrm{MeV}/c]$ and the source has a $\gamma=12.47$ and is moving to the right. Again, the source velocity was picked as a compromise between readability of the plot and available momentum space for the electron.

We see the difficulty in interpreting the electron distribution. The Fourier transform took a simple photon peak and produced a series of large electron peaks. The retarded branch corresponds to the envelope of large positive peaks on the upper left. The advanced branch corresponds to the envelope of large negative peaks in the lower right. Each peak in the pair of envelopes appears to be a Lorentz pancake, but the envelope as a whole is significantly broader than the underlying photon peak. Presumably, averaging the distribution over unit areas in phase-space would result in a much tighter average distribution.

APPENDIX G: FREE SCALAR PROPAGATORS IN PHASE-SPACE

In this section, we state all of our phase-space propagators, discuss the symmetries of the massless propagators and outline the derivation of the retarded and Feynman scalar propagators. The massive Feynman propagator is discussed by Remler [13] so our discussion here is brief. The Dirac and vector propagators differ from the scalar propagators by the inclusion of either spin projectors (in the case of Dirac particles) or polarization projectors (in the case of vector particles) so we do not need to discuss them.

We define the Wigner transform of any translationally invariant propagator as

$$G(x,p)=\int\frac{d^4p'}{(2\pi)^4}\,e^{-ix\cdot p'}G(p+p'/2)G^\dagger(p-p'/2)=\int d^4x'\;e^{ix'\cdot p}G(x+x'/2)G^\dagger(x-x'/2). \tag{G1}$$

The vacuum propagators that we use are [37]

$$G^{\pm}(p) = -(p^2 - m^2 \pm i\epsilon p_0)^{-1} \tag{G2a}$$

$$G^{c}_{a}(p) = -(p^2 - m^2 \pm i\epsilon)^{-1}. \tag{G2b}$$

1. Massless scalar propagators

a. Symmetries

A time reversal transform in coordinate space is equivalent to a simultaneous reflection in time and energy in phase-space. Under time reversal the + and − propagators change into one another while the Feynman and anti-Feynman propagators remain unchanged:

$$G^{+}(x_0,\vec{x},p_0,\vec{p}) = G^{-}(-x_0,\vec{x},-p_0,\vec{p}) \tag{G3a}$$

$$G^{a}_{c}(x_0,\vec{x},p_0,\vec{p}) = G^{a}_{c}(-x_0,\vec{x},-p_0,\vec{p}). \tag{G3b}$$

A parity transform in coordinate space is equivalent to a simultaneous reflection in a space coordinate and the corresponding momentum coordinate. Under a parity transformation, all of the propagators remain unchanged:

$$G^{\pm}(x_0,\vec{x},p_0,\vec{p}) = G^{\pm}(x_0,-\vec{x},p_0,-\vec{p}) \tag{G3c}$$

$$G^{a}_{c}(x_0,\vec{x},p_0,\vec{p}) = G^{a}_{c}(x_0,-\vec{x},p_0,-\vec{p}). \tag{G3d}$$

The Feynman propagators have another (rather amusing) *argument switching* symmetry. Here all the space-time components are switched with the the corresponding momentum-energy components:

$$G^{a}_{c}(x,p) = G^{a}_{c}(p,x). \tag{G3e}$$

Finally, the Feynman and anti-Feynman propagator are related through a complete reflection of all of the space or momentum coordinates:

$$G^{c}(x,p) = G^{a}(-x,p) \tag{G3f}$$

$$G^{c}(x,p) = G^{a}(x,-p). \tag{G3g}$$

b. Propagators

We now present the massless Feynman and retarded propagators. The advanced and anti-Feynman propagators can be recovered using the symmetry relations above. Since all of the massless scalar propagators are dimensionless and Lorentz invariant, we expect that they will be functions of $x\cdot p$ and x^2p^2 and possibly theta functions in energy or time. In fact, the propagators are

$$G^{c}(x,p) = \frac{1}{4\pi}[\mathrm{sgn}(x^2) + \mathrm{sgn}(p^2) + 2\,\mathrm{sgn}(x\cdot p)] \times \left\{ \theta(\lambda^2)\,\frac{\sin(2\sqrt{\lambda^2})}{\sqrt{\lambda^2}} - \theta(-\lambda^2)\,\frac{\exp(-2\sqrt{-\lambda^2})}{\sqrt{-\lambda^2}} \right\} \tag{G4a}$$

$$G^{+}(x,p) = \frac{1}{\pi}\,\theta(x_0)\,\theta(x^2)\,\theta(\lambda^2) \times \frac{\sin(2\sqrt{\lambda^2})}{\sqrt{\lambda^2}}. \tag{G4b}$$

Here the Lorentz invariant λ^2 is given by $\lambda^2 = (x\cdot p)^2 - x^2p^2$. Since we discuss how the propagators work in the Secs. II D 2 and III B 3, we do not do so here.

c. Derivation of G^+

The Wigner transform of G^+ is easiest to do in coordinate space. In coordinate space, $G^+(x) = (1/2\pi)\,\theta(x_0)\,\delta(x^2)$, so the Wigner transform integral is a series of delta function integrals. Performing the first delta function integral in (G1), and simplifying the theta functions, we find

$$G^{+}(x,p) = \frac{\theta(x_0)}{(2\pi)^2}\int_{-2x_0}^{2x_0} dx_0'\sqrt{4x^2 + x_0'^2} \times \int_{4\pi} d\Omega_{\vec{x}'} e^{ix'\cdot p}\,\delta(x'\cdot x).$$

Using $2\pi\delta(x) = \int_{-\infty}^{\infty} d\alpha e^{ix\alpha}$, we can do the angular integral, giving us a Bessel function:

$$G^{+}(x,p) = 4\pi\,\theta(x_0)\,\theta(x^2)\int_{-1}^{1} d\alpha e^{i\alpha\eta} J_0(\xi\sqrt{1-\alpha^2}).$$

Here $\eta = 2(p_0|\vec{x}| - x_0\hat{x}\cdot\vec{p})$ and $\xi = 2\sqrt{x^2(\vec{p}^2 - (\vec{p}\cdot\hat{x})^2)}$. This integral is in any standard integral table [38]. After a bit of simplification, one gets the result (G4b). This result can be checked by performing the Wigner transforms in momentum space, but the contour integrals needed for this calculation are quite tedious.

d. Derivation of G^c

The simplest derivation of $G^c(x,p)$ is far more complicated than the derivation of $G^+(x,p)$. We start by finding the transport-like equation of motion for the Wigner propagator.[18] The derivation is simple and very similar to the derivation for the retarded equation of motion in Sec. IV F. So we only state the result:

[18]The constraint-like equation could also be used, but G^c is easier to derive using the transport-like equation.

$$p\cdot\partial G^c(x,p)=\frac{1}{\pi^2}\left[\pi\delta(x^2)\sin(2x\cdot p)-\mathcal{P}\,\frac{1}{x^2}\cos(2x\cdot p)\right].$$

Now we define a projector onto the space perpendicular to the particle's momentum, $g_{\perp\mu\nu}=g_{\mu\nu}-p_\mu p_\nu/p^2$. This allows us to change variables to $x_{\perp\mu}=g_{\perp\mu\nu}x^\nu$ and $\tau=x\cdot p/\sqrt{|p^2|}\ \mathrm{sgn}(p^2)$. In terms of these variables, we find $\lambda^2=-p^2x_\perp^2$ and the equation of motion becomes

$$\partial_\tau G^c(\tau,x_\perp,p)=\frac{\mathrm{sgn}(p^2)\sqrt{|p^2|}}{\pi^2}\left[\pi\delta(|k^2|\tau^2-\lambda^2)\sin(2\sqrt{|k^2|}\tau)-\mathcal{P}\,\frac{\cos(2\sqrt{|k^2|}\tau)}{|k^2|\tau^2-\lambda^2}\right].$$

So, instead of doing the Wigner transform directly, we only have to solve this ordinary differential equation.

We find the solution by integrating this differential equation. The delta function integral is simple and the principle value integral can be done by contour integration. We find

$$G^c(\tau,x_\perp,p)=G^c(\infty,x_\perp,p)-\frac{1}{\pi}\left\{\theta(\lambda^2)\,\frac{\sin(2\sqrt{\lambda^2})}{\sqrt{\lambda^2}}\left[\frac{1}{2}(\theta(p^2)-\theta(x^2))+\mathrm{sgn}(p^2)\,\theta(-\tau)\right]-\mathrm{sgn}(p^2)\,\theta(-\tau)\,\frac{e^{-2\sqrt{-\lambda^2}}}{\sqrt{-\lambda^2}}\right\}.$$

We must now divine the boundary condition at $\tau\to\infty$.

To find the boundary condition, we actually have to go back to the Wigner transform of the propagator starting from momentum-space version of Eq. (G1). We again change variable from x to τ and $x_\perp$. We also change from p' to $p'_\perp=g_{\perp\mu\nu}p'^\nu$ and $p\cdot p'=\mathrm{sgn}(p^2)\sqrt{|p^2|}k$. With this, we perform the k contour integral. The integral is straightforward, but tedious. However, when we take the limit as $\tau\to\infty$, the result simplifies dramatically:

$$G^c(\infty,x_\perp,p)=\frac{1}{\pi^2\sqrt{|p^2|}}\int d^3p_\perp\,\cos(2x_\perp\cdot p_\perp)\,\delta(p^2+p_\perp^2).$$

The delta function integral is trivial and the last pair of integrals requires integral tables, but in the end we find

$$G^c(\infty,x_\perp,p)=\frac{1}{\pi}\left\{\theta(\lambda^2)\mathrm{sgn}(p^2)\,\frac{\sin(2\sqrt{\lambda^2})}{\sqrt{\lambda^2}}+\theta(-\lambda^2)\,\theta(-p^2)\,\frac{e^{-2\sqrt{-\lambda^2}}}{\sqrt{-\lambda^2}}\right\}.$$

Plugging this into the solution of our differential equation, we find Eq. (G4b). This result can be checked by performing a series of contour integrals in momentum or coordinate space.

2. Massive scalar Feynman propagator

Remler [13] has found the Wigner transform of the massive Feynman propagator. This transform is difficult but, when one uses the approximation $p'^2\approx(p\cdot p')^2/p^2$, where p is the average momentum and p' is the relative momentum, the integrals become simple contour integrals. We state Remler's result here:

$$G^c(x,p)=\begin{cases}\displaystyle\int_{-\infty}^{\infty}d\tau\,\delta^4\!\left(x-\frac{p}{\sqrt{-p^2}}\tau\right)e^{-2m|\tau|}\,\frac{1}{2m\sqrt{-p^2}(m^2-p^2)}\,\{\sqrt{-p^2}\,\cos(2\tau\sqrt{-p^2})+m\,\sin(2|\tau|\sqrt{-p^2})\} & \text{for } p^2<0,\\ \displaystyle\int_0^{\infty}d\tau\,\frac{1}{2m\sqrt{p^2}}\left\{\frac{\sin(2\tau(\sqrt{p^2}-m))}{(\sqrt{p^2}-m)}\,\delta^4\!\left(x-\frac{p}{\sqrt{p^2}}\tau\right)-\frac{\sin(2\tau(\sqrt{p^2}+m))}{(\sqrt{p^2}+m)}\,\delta^4\!\left(x+\frac{p}{\sqrt{p^2}}\tau\right)\right\} & \text{for } p^2>0.\end{cases}\tag{G5}$$

Note that, because of the approximation made, this propagator is oversmoothed in the direction transverse to the particle's momentum and we expect these propagators to be accurate only for length scales much larger than the size of the smoothing. Since the resulting propagators vary on length scales of order $1/m$, we should only use these propagators for momenta with $p\ll m$. Note also that the sine and exponential functions in the two terms in (G5) have the property that they become proportional to $\delta(p^2-m^2)$ as $\tau\to\infty$. Thus, this propagator reduces to the classical propagator [13]. Finally, we note that the δ-functions constrain the particle to move along its classical trajectory, even though its four-momentum (and hence its four-velocity) is being modulated by the sine and exponential functions.

[1] K. J. Eskola and X.-N. Wang, ''Proceedings of the Workshop on Pre-Equilibrium Parton Dynamics,'' Berkeley, CA (1993).
[2] J. Harris and B. Müller, Annu. Rev. Nucl. Part. Sci. **46**, 71 (1996).
[3] Y. P. Nikitin and I. L. Rozental, *High Energy Physics with Nuclei* (Harwood Academic, New York, 1986), pp. 35–40.
[4] X.-N. Wang and M. Gyulassy, Phys. Rev. D **44**, 3501 (1991); **45**, 844 (1992); X.-N. Wang, Nucl. Phys. **A590**, 47c (1995).
[5] P. Danielewicz, Ann. Phys. (N.Y.) **152**, 239 (1984).
[6] B. Bezzerides and D. F. DuBois, Ann. Phys. (N.Y.) **70**, 10 (1972).
[7] S. Klevansky, A. Ogura, and J. Hüfner, Ann. Phys. (N.Y.) **261**, 37 (1997).
[8] S. Mrówczyński and P. Danielewicz, Nucl. Phys. **B342**, 345 (1990).
[9] S. Mrówczyński and U. Heinz, Ann. Phys. (N.Y.) **229**, 1 (1994).
[10] K. Geiger, Phys. Rev. D **54**, 949 (1996).
[11] P. A. Henning, ''Proceedings of the 4th International Workshop on Thermal Field Theories,'' Dalian, China (1995); P. A. Henning, M. Blasone, R. Fauser, and P. Zhuang, GSI report GSI-96-57, 1996.
[12] J. P. Blaizot and E. Iancu, Nucl. Phys. **B417**, 608 (1994).
[13] E. A. Remler, Ann. Phys. (N.Y.) **202**, 351 (1990).
[14] C. F. von Weizsäcker, Z. Phys. **88**, 612 (1934); E. J. Williams, Phys. Rev. **45**, 729 (1934).
[15] J. D. Jackson, *Classical Electrodynamics* (Wiley, New York, 1975), pp. 668–669, 719–725.
[16] C. A. Bertulani and G. Baur, Phys. Rep. **163**, 299 (1988).
[17] H. Lehmann, Nuovo Cimento Suppl. **14**, 153 (1959).
[18] G. Altarelli and G. Parisi, Nucl. Phys. **B126**, 298 (1977).
[19] C. Quigg, *Gauge Theories of the Strong, Weak and Electromagnetic Interactions* (Addison-Wesley, New York, 1983).
[20] A. H. Mueller, Nucl. Phys. **A498**, 41c (1989).
[21] K. Geiger, Phys. Rev. D **46**, 4965 (1992); **46**, 4986 (1992); **49**, 3234 (1994); K. Geiger and J. Kapusta, *ibid.* **47**, 4905 (1993); K. Geiger, Phys. Rep. **237**, (1995).
[22] V. I. Tatarskii, Sov. Phys. Usp. **26**, 311 (1983); H. W. Lee, Phys. Rep. **259**, 147 (1995).
[23] P. Carruthers and F. Zachariasen, Rev. Mod. Phys. **55**, 245 (1983).
[24] V. M. Budnev *et al.*, Phys. Rep., Phys. Lett. **15C**, 181 (1975).
[25] R. D. Field, *Applications of Perturbative QCD* (Addison-Wesley, New York, 1989); Y. L. Dokshitzer *et al.*, *Basics of Perturbative QCD* (Editions Frontières, Gif-sur-Yvette, France, 1991); W. K. Tung and H. Weerts, ''Summer School on QCD Analysis and Phenomenology,'' Lake Ozark, Missouri, 1994 (unpublished); CTEQ Collaboration, Rev. Mod. Phys. **67**, 157 (1995).
[26] E. Laenen and E. Levin, Annu. Rev. Nucl. Part. Sci. **44**, 199 (1994).
[27] W. H. Press *et al.*, *Numerical Recipes: The Art of Scientific Computation* (Cambridge University Press, Cambridge, 1989).
[28] C. M. Ko, Q. Li, R. Wang, Phys. Rev. Lett. **59**, 1084 (1987).
[29] A. Makhlin, Phys. Rev. C **51**, 3454 (1995); **52**, 995 (1995).
[30] P. Zhuang and U. Heinz, Ann. Phys. (N.Y.) **245**, 311 (1996).
[31] S. Aid *et al.*, Phys. Lett. B **356**, 118 (1995).
[32] L. V. Gribov, E. M. Levin, and M. G. Ryskin, Phys. Rep. **100**, 1 (1983).
[33] Ya. Ya. Balitsky and L. N. Lipatov, Yad. Fiz. **28**, 1597 (1978) [Sov. J. Nucl. Phys. **28**, 822 (1978)]; E. A. Kuraev and V. S. Fadin, Zh. Eksp. Teor. Fiz. **71**, 840 (1976) [Sov. Phys. JETP **44**, 443 (1976)]; Zh. Eksp. Teor. Fiz. **72**, 377 (1977) [Sov. Phys. JETP **45**, 199 (1977)]; L. N. Lipatov, Yad. Fiz. **23**, 642 (1976) [Sov. J. Nucl. Phys. **23**, 338 (1976)].
[34] J. Bartels and H. Lotter, Phys. Lett. B **309**, 400 (1993).
[35] R. Venugopalan, Nucl. Phys. **A590**, 147c (1995).
[36] A. I. Akhiezer and V. B. Berestetskii, *Quantum Electrodynamics* (Wiley Interscience, New York, 1965); C. Itzykson and J.-B. Zuber, *Quantum Field Theory* (McGraw-Hill, Inc., New York, 1980).
[37] N. N. Bogoliubov and D. V. Shirkov, *Introduction to the Theory of Quantized Fields* (Wiley, New York, 1979).
[38] I. S. Gradsteyn and I. M. Ryzhik, *Table of Integrals, Series and Products* (Academic Press, New York, 1980).